UNIVERSITY OF RIJEKA

FACULTY OF MEDICINE

Vedrana Krušić Alić

SEPARATION AND PROPERTIES OF EXOSOMES FROM CEREBROSPINAL FLUID OF PATIENTS WITH TRAUMATIC BRAIN INJURY

Doctoral thesis

Rijeka, 2024

UNIVERSITY OF RIJEKA

FACULTY OF MEDICINE

Vedrana Krušić Alić

SEPARATION AND PROPERTIES OF EXOSOMES FROM CEREBROSPINAL FLUID OF PATIENTS WITH TRAUMATIC BRAIN INJURY

Doctoral thesis

Rijeka, 2024

Mentor: Assoc. Prof. Kristina Grabušić
Co-mentor: Prof. Mladenka Malenica

SVEUČILIŠTE U RIJECI

MEDICINSKI FAKULTET

Vedrana Krušić Alić

SEPARACIJA I SVOJSTVA EGZOSOMA IZ CEREBROSPINALNE TEKUĆINE BOLESNIKA S TRAUMATSKOM OZLJEDOM MOZGA

Doktorski rad

Rijeka, 2024.

Mentorica: izv. prof. dr. sc. Kristina Grabušić
Komentorica: prof. dr. sc. Mladenka Malenica

Mentorica: izv. prof. dr. sc. Kristina Grabušić

Komentorica: prof. dr. sc. Mladenka Malenica

Doktorski rad obranjen je dana _____ u/na _____ _____, pred povjerenstvom u sastavu:

1. _____ (titula, ime i prezime)

2. _____ (titula, ime i prezime)

3. _____ (titula, ime i prezime)

4. _____ (titula, ime i prezime)

5. _____ (titula, ime i prezime)

Rad ima _____ listova.

UDK: _____ (UDK broj dodjeljuje Knjižnica Medicinskog fakulteta u Rijeci)

Predgovor

Ova doktorska disertacija izrađena je na Zavodu za fiziologiju, patofiziologiju I imunologiju Medicinskog fakulteta Sveučilišta u Rijeci, u suradnji s kolegama Klinike za anesteziologiju, intenzivnu medicinu i liječenje boli Kliničkog bolničkog centra Rijeka te Odjelom za anesteziju, reanimatologiju, intenzivnu medicinu i liječenje boli Opće bolnice Pula.

Istraživanje je izvršeno u sklopu projekta Hrvatske zaklade za znanost „Identifikacija cirkulirajućih biomarkera neurološkog oporavka u bolesnika s ozljedom mozga“ (IP-2019-04-1511) pod voditeljstvom izv. prof. dr. sc. Kristine Grabušić te projekata „Izvanstanične vezikule kao klinički markeri neuroregeneracije nakon teške ozljede mozga“ (UNIRI uniri-biomed-18-5) pod voditeljstvom izv. prof. dr. sc Kristine Grabušić i „Uspostava protokola na Sveučilištu u Rijeci za primjenu nanotehnoloških metoda: mikroskopije atomskih sila i skenirajućeg elektronskog mikroskopa prilikom vizualizacije i karakterizacije egzosoma“ (UNIRI uniri-biomed-18-279) pod voditeljstvom prof. dr. sc. Mladenke Malenice, financiranih od strane Sveučilišta u Rijeci.

Zahvale

Zahvaljujem svojoj mentorici izv. prof. dr. sc. Kristini Grabušić na pruženoj prilici, ukazanom povjerenju, vodstvu, podršci i konstruktivnim kritikama za vrijeme istraživanja i izrade ovog rada. Hvala za svu pomoć i savjete tijekom ovog iskustva koje mi je pomogla oblikovati se u osobu koja sada jesam, kao i na prenesenom znanju koje ipak, na kraju dana, nosi najveću vrijednost čitavog ovog procesa.

Želim se zahvaliti i svojoj komentorici prof. dr. sc. Mladenki Malenici na vječito pozitivnom stavu, korisnim savjetima te pomoći i podršci prilikom istraživanja i pisanja ove doktorske disertacije.

Zahvaljujem se kolegama i kolegicama sa Zavoda za fiziologiju, patofiziologiju i imunologiju Medicinskog fakulteta u Rijeci, a posebice našoj „petkom zajedno“ ekipi - Kseniji, Maji, Tatjani, Tihani, Sanji, Igoru, Hrvoju, Ljerki, Silviji, Nataliji, Marini, Ivoni, Barbari i Alenu, koji su mi iznimno uljepšali ovo iskustvo i pružili toplo prijateljsko okruženje u koje sam se svaki dan bila sretna vratiti. Posebno hvala mojim kolegicama iz novačke sobe Ivoni i Barbari na smijehu, prijateljstvu i zajedničkim trenutcima kojih ću se uvijek rado sjećati.

Neizmjerno hvala mojoj mami i mom tati što su cijeli moj život vjerovali u mene i pružali mi neizmjernu podršku u svim mojim odlukama, kakve god one bile. Hvala na bezuvjetnoj ljubavi koju ste mi uvijek pružali.

Mojoj boljoj polovici beskrajno hvala na vječitoj podršci, ljubavi i bezgraničnom strpljenju koje si imao za mene tijekom svih ovih godina. Ti i Aleksandra dajete mi snagu da budem bolja svaki dan iznova.

Summary

Objectives: Severe traumatic brain injury (sTBI) is a complex, life-threatening condition requiring emergent treatment with no known biomarkers to guide clinical interventions. A promising source of such biomarkers are intracranial exosomes. However, isolation of exosomes is still challenging with size exclusion chromatography (SEC) emerging as a favourable tool to isolate total and intact exosomes. This study aims to compare the efficiency of different SEC solutions for exosome isolation from cerebrospinal fluid (CSF) of sTBI patients.

Patients and methods: Nine CSF samples from three patients requiring external CSF drainage during the first three days post-sTBI were collected, pooled, and screened by western blot for exosomal makers CD81 and CD9, lipoprotein markers apolipoprotein AI (ApoAI) and E (ApoE), and albumin. The pooled sample was separated by four gravity flow-based SECs with either a commercial prepacked column or an in-house column packed with Sepharose CL-6B, Sephacryl S-400 or Superose 6 PG. A total of 46 fractions were collected per SEC and analysed by slot blot followed by Ponceau staining. Immunodetection was performed on selected SEC fractions for albumin, CD81, CD9, flotillin-1, ApoAI, and ApoE. Tunable resistive pulse sensing (TRPS) was utilised for exosome size, concentration and surface charge measurement, while transmission electron microscopy (TEM) was used for exosome visualisation.

Results: Post-sTBI CSFs contain exosomes, along with lipoproteins and albumin, as shown by western blot, confirming the complexity of clinical samples. All four tested SECs provided separation of exosomes but differed in efficiency. Sepharose CL-6B SEC yielded the highest quantity of exosomes in TRPS measurement and resulted in clear separation from lipoproteins and free proteins, as shown by exosome visualisation by TEM and immunodetection of exosomal (CD9, CD81 and flotillin-1), lipoprotein (ApoA1 and ApoE) and free protein (albumin) markers.

Conclusion: Intracranial CSF after sTBI has a complex composition encompassing exosomes, lipoproteins and free proteins, which can be separated by SEC. However, SEC designs vary and impact the exosome isolation efficiency. Sepharose CL-6B stands out as an effective SEC resin to isolate exosomes from clinical samples.

Key words: Exosomes; Chromatography, Gel; Brain Injuries, Traumatic; Cerebrospinal Fluid

Prošireni sažetak

Cilj istraživanja: Teška traumatska ozljeda mozga (tTOM) je kompleksno životno ugrožavajuće stanje koje zahtjeva hitno liječenje, ali nema poznatih biomarkera koji bi pomogli u odlučivanju o kliničkim intervencijama. Intrakranijalni egzosomi predstavljaju obećavajući izvor takvih biomarkera. Međutim, izolacija egzosoma je i dalje izazovna, a kromatografija isključenjem po veličini (eng. *Size Exclusion Chromatography*, SEC) pojavljuje se kao prikladan alat za izolaciju ukupnih i intaktnih egzosoma. Cilj ovog istraživanja je usporediti učinkovitost različitih rješenja SEC-a za izolaciju egzosoma iz CSF-a pacijenata s TBI.

Ispitanici i metode: Devet uzoraka CST-a od triju pacijenata kojima je uspostavljena vanjska drenaža CST-a tijekom prva tri dana nakon tTOM-a prikupljeno je, objedinjeno i ispitano western blot metodom na egzosomalne markere CD81 i CD9, lipoproteinske markere apolipoprotein AI (ApoAI) i E (ApoE) te albumin. Skupni uzorak CST-a odvojen je pomoću četiri metode SEC-a temeljene na gravitacijskom protoku, pomoću komercijalne kolone za izolaciju egzosoma ili interno pakiranim kolonama napunjenim punilima Sepharose CL-6B, Sephacryl S-400 i Superose 6 PG. Prilikom svake separacije prikupljeno je ukupno 46 frakcija, nakon čega je uslijedila slot blot analiza i bojanje Ponceau S. Imunodetekcija na odabranim frakcijama SEC-a provedena je na albumin, CD81, CD9, flotillin-1, ApoAI i ApoE. Za mjerenje veličine, koncentracije i površinskog naboja egzosoma korištena je metoda opažanja pomoću podesivog otpornog pulsa (eng. *Tunable Resistive Pulse Sensing*, TRPS), dok je transmisijska elektronska mikroskopija (TEM) korištena za vizualizaciju egzosoma.

Rezultati: CST nakon tTOM sadrži egzosome, lipoproteine i albumin, kao što je prikazano western blotom, što govori u prilog kompleksnosti kliničkih uzoraka. Sve četiri SEC metode omogućile su odvajanje egzosoma, ali su pritom pokazale različitu učinkovitost. Prema mjerenjima pomoću TRPS, razdvajanje punilom Sepharose-CL-6B dovelo je do najvećeg prinosa egzosoma i rezultiralo jasnim odvajanjem od lipoproteina i slobodnih proteina, kao što je prikazano vizualizacijom egzosoma pomoću TEM-a i imunodetekcijom egzosoma (CD9, CD81 i Flotillin-1), lipoproteina (ApoA1 i ApoE) i markera slobodnih proteina (albumin).

Zaključak: Intrakranijalni CST nakon tTOM složenog je sastava te sadrži egzosome, lipoproteine i slobodne proteine, koji se mogu razdvojiti SEC-om. Međutim, dizajn

SEC-a može značajno varirati i utjecati na učinkovitost izolacije egzosoma. Sepharose CL-6B ističe se kao učinkovito punilo za kromatografsku izolaciju egzosoma iz kliničkih uzoraka.

Ključne riječi: cerebrospinalna tekućina; egzosomi; kromatografija, gel-filtracijska; traumatska ozljeda mozga

CONTENTS

1. INTRODUCTION AND LITERATURE REVIEW 1
1.1. Traumatic Brain Injury 1
1.1.1. Epidemiology of Traumatic Brain Injury 2
1.1.2. Classifications of Traumatic Brain Injury 3
1.1.3. Biophysical Mechanisms of Brain Damage in Traumatic Brain Injury 4
1.1.4. Pathophysiology of Traumatic Brain Injury 6
1.1.5. Current Management of Traumatic Brain Injury Patients 7
1.2. Extracellular Vesicles 9
1.2.1. A Brief History of Extracellular Vesicles – from „Garbage Bags“ to Intercellular Messengers 9
1.2.2. Classification and Biogenesis of Extracellular Vesicles 11
1.2.3. Extracellular Vesicles as Potential Biomarkers in TBI 15
1.3. Methods of Extracellular Vesicles Isolation 17
1.3.1. Ultracentrifugation 19
1.3.2. Ultrafiltration 20
1.3.3. Precipitation-Based Methods 21
1.3.4. Immunoaffinity-Based Isolation 22
1.3.5. Size-Exclusion Chromatography 23
1.4. Techniques for EV Characterisation and Analysis 26
1.4.1. Methods for Measuring EV Concentration and Size 26
1.4.2. Methods for Analysing EV Protein Composition 30
1.4.3. Methods of EV Visualisation and Morphology Analysis 31
2. RESEARCH GOAL 33
3. PATIENTS, MATERIALS AND METHODS 34
3.1. Patients 34
3.2. Materials 34
3.2.1. Chemicals 34
3.2.2. Solutions 35
3.2.3. Reagents and Materials 37
3.2.4. Antibodies 38
3.3. Methods 39
3.3.1. Cerebrospinal Fluid Sampling and Storing 39

3.3.2. Size-Exclusion Chromatography 39
3.3.3. Western Blot 40
3.3.4. Slot Blot 41
3.3.5. Tunable Resistive Pulse Sensing 41
3.3.6. Zeta Potential Measurement 44
3.3.7. Transmission Electron Microscopy 45
3.3.8. Statistical and data analysis 45
4. RESULTS 46
4.1. Clinical Features of Severe Traumatic Brain Injury Patients 46
4.2. Extracellular Vesicles and Lipoproteins Are Found in Intracranial Cerebrospinal Fluid Three Days After Traumatic Brain Injury 47
4.3. Establishing In-House Protocols for Size-Exclusion Chromatography and Nanoparticle Quantification 49
4.4. Sepharose CL-6B Outperforms Other Tested Size Exclusion Chromatography Methods in Isolation of Nanoparticles 54
4.5. Nanoparticles of Comparable Size and Negative Charge Are Isolated in Similar Proportions by the Applied SEC Methods 58
4.6. Sepharose CL-6B Separates Exosomes from Lipoproteins and Free Proteins 62
5. DISCUSSION 67
6. CONCLUSION 73
7. LITERATURE 74
ILLUSTRATIONS 85
LIST OF FIGURES 85
LIST OF TABLES 87
LIST OF ABBREVIATIONS 88
CURRICULUM VITAE 91

1. INTRODUCTION AND LITERATURE REVIEW

1.1. Traumatic Brain Injury

Traumatic brain injury (TBI) is an acquired condition in which the brain's normal function or structure is disrupted due to external insult to the brain tissue. It is one of the leading causes of mortality among the young and elderly population, often associated with long-term disability and cognitive impairments among survivors [1,2]. The symptoms of TBI vary drastically depending on the severity of the injury, ranging from temporary disorientation and confusion to deep coma and death. In most patients with mild TBI, symptoms resolve in a matter of few weeks. However, the road to recovery for those with moderate and severe cases of TBI can take months or years with long-lasting physical, behavioural and cognitive issues [1,3,4].

Besides the immediate damage of brain parenchyma, initial head trauma can trigger a series of harmful intracellular and extracellular pathological processes, leading to additional intracranial or systemic complications. Apart from impairments that occur in the early post-injury period, an association has been revealed between severe TBI and the risk of developing neurodegenerative diseases, epilepsy, endocrinopathies, psychiatric diseases and sleep disorders in months or years after the accident [4,5]. Consequently, TBI is starting to be acknowledged as a chronic condition, where intrinsic pathophysiologic processes and secondary insults worsen the primary injury, resulting in lower quality of life and reduced life expectancy [4–6].

Current management of TBI is mainly supportive and focuses on preventing further brain damage following the initial injury, primarily through surgical interventions, intensive care treatment, and intracranial pressure (ICP) monitoring. However, treatments that would promote neuroprotection are still lacking. Although tremendous efforts have been made to identify potential neuroprotective agents that would facilitate recovery in TBI patients with many promising pre-clinical candidates, none so far proved effective in phase III clinical trials [7,8].

1.1.1. Epidemiology of Traumatic Brain Injury

TBI poses a substantial burden on affected individuals, the public health system and society. It is estimated that 2.5 million people in the EU annually suffer from TBI, out of which 1.5 million require hospital admission and 57,000 die [2]. Considering the length and complexity of treatment, as well as the high prevalence of debilitating life-changing implications for survivors, it is clear that the consequences of TBI present a major public health and socioeconomic issue and expand well beyond the acute phase of the recovery [2,9].

According to Global Burden of Disease Study 2016 estimations, 27.08 million people suffered TBI globally, with age-standardised incidence rates of 369 per 100,000 population, presenting a 3.6% increase from 1990 to 2016 [9]. In the same time period, the observed global prevalence for TBI was 759 per 100,000 and years of life with disability was 111 per 100,000, presenting an increase of 8.4% and 8.5%, respectively [9]. Out of all reported TBI cases, it is estimated that 70-90% fall under mild TBI diagnosis. However, those numbers are probably an understatement, given the fact that most patients with mild TBI never seek out medical help [10]. Additionally, incidence and prevalence rates vary drastically among different geographic regions and income groups. Available studies suggest a higher incidence of TBI in low-income countries [9,11]. Since low-income countries often provide only limited data for larger epidemiological studies, the overall number of TBI cases could be much more substantial, with one study estimating a global incidence of 69 million a year [11,12].

Though TBI can affect people of all ages, three age groups are particularly susceptible to TBI, with older adults being most at risk (≥75 years), followed by young children (0 to 4 years), and adolescents and young adults (15 to 24 years) [1]. In both older adults and young children, falls were the main mechanism of injury, while road traffic accidents present the leading cause of TBI for the adolescents and young adults age group [1,2,12]. Gender also presents a risk factor. In the general adult population, men are 2.22 times more likely to suffer TBI than women, with the exception of the elderly population, where women show a greater incidence of TBI-related hospitalisations [1,13,14].

Albeit being a life-threatening condition that accounts for over 30% of all fatalities resulting from an injury, overall fatality rates are low since most cases fall into

mild TBI [2,15]. In a cross-sectional study on population mortality from 25 European countries conducted in 2012, the reported mortality rate was about 12 per 100,000 people [2]. Yet, the prognosis varies drastically depending on the severity of the injury, with Roozenbeek et al. reporting a mortality rate of 23% among patients with severe TBI within 14 days of the injury [16].

1.1.2. Classifications of Traumatic Brain Injury

TBI is considered “the most complex disease of the most complex organ”, thus obtaining a singular satisfying TBI classification proved challenging [17]. Efforts have been made to systematically categorise TBIs and multiple classification systems have been proposed based on TBI severity, type of pathoanatomic lesions and physical mechanism of the injury [8,18].

Classification most commonly used in the clinical setting is based on TBI severity, measuring the patient’s level of consciousness through the Glasgow coma scale (GCS). A series of tests are performed to assess patients’ best eye, motor and verbal responses, with each response being assigned a numerical value, as shown in Table 1. GCS score represents the sum of those values, which then classifies a TBI as mild, moderate or severe with scores of 13 or more, 8-12 and less than 8, respectively. The lowest score of 3 corresponds to deep coma, and the highest score of 15 indicates full consciousness [1,19]. Additionally, a non-contrast computed tomography (CT) head scan is used for evaluation of the TBI, as well as for monitoring the potential progression of the injury [1].

Brain injuries can also be characterised through their pathoanatomical description, identifying the anatomical location and features of injuries to their dysfunction for acute management of TBI patients. Pathoanatomic lesions can be broadly categorised as focal or diffuse. Focal injuries typically emerge from direct impact and result in localized lesions, while diffuse injuries refer to widespread damage that occurs from rapid acceleration and deceleration forces to the brain. Focal injuries include contusions and lacerations, skull fractures and intracranial haemorrhages and haematoma formations, whereas diffuse injuries include diffuse axonal injury, hypoxic-ischemic injury, diffuse cerebral oedema and diffuse vascular injuries [8,18,20]. In

patients with severe injuries multiple lesions are frequently present, varying in severity, size and location, thus limiting this classification as a standalone classification system.

Table 1. Glasgow coma scale. Adapted from [19].

	Response	Score
Eye response	Spontaneous	4
	To speech	3
	To pain	2
	None	1
Best verbal response	Oriented	5
	Confused	4
	Inappropriate words	3
	Incomprehensible sounds	2
	None	1
Best motor response	Obeying	6
	Localizing	5
	Withdrawal from pain	4
	Flexion response to pain	3
	Extension response to pain	2
	None	1

1.1.3. Biophysical Mechanisms of Brain Damage in Traumatic Brain Injury

TBI occurs when physical energy is transferred to the head through impact or sudden changes in motion. Depending on the duration, that transfer of energy can be defined as static loading, when the force is applied gradually in time intervals longer than 200 milliseconds, or dynamic loading, when the force is exerted more rapidly, typically lasting less than 20 milliseconds [21,22]. Injuries caused by static loading are relatively rare and usually happen during natural disasters when the person's head is entrapped by heavy debris. Dynamic loading is much more common and can be further

characterised as impact loading, impulse loading or blast overpressure. Most TBIs are caused by a combination of impact loading forces arising from a collision of the head with a blunt object and impulse loading forces exerted by head acceleration and deceleration, as depicted in Figure 1. Understanding the nature of those forces is important for anticipating brain regions most vulnerable to damage from these forces, and subsequent neurobehavioral challenges in individuals with TBI [21,23,24].

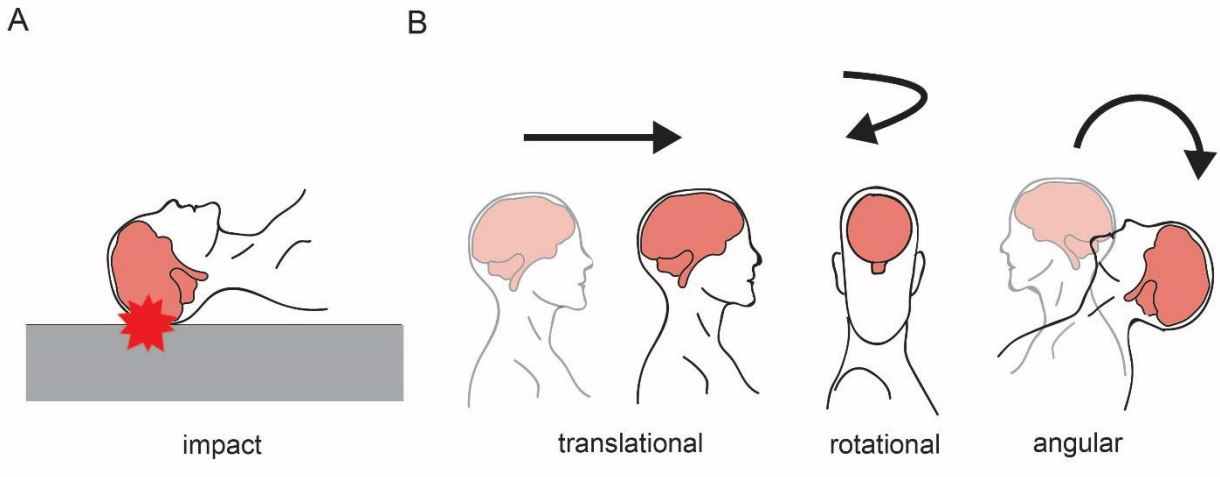

Figure 1. Typical biophysical mechanisms of traumatic brain injury. A. Impact loading injury occurs when the head is struck by a blunt object. During impact loading, contact forces can often lead to abrupt unrestricted movement of the head, triggering a subsequent impulsive loading event. B. In impulsive loading, injury occurs from acceleration/deceleration caused by sudden head movement without a direct blow to the head. Resulting inertial forces lead to translational, rotational and angular acceleration of the head, with the latter, being the combination of the elements from the other two, causing the most damage.

Under the influence of these forces, the resulting TBI can be categorised as closed head, penetrative and blast injury [21,24]. Closed head injuries account for the majority of TBIs, and usually happen as a result of traffic road accidents, falls and sports injuries. In injuries caused by a non-penetrating impact-loading blow to the head, shock waves radiate from the point of contact causing rapid movements of the brain within the skull and bruising, stretching and tearing of neuronal and vascular cells. Additionally, impulsive loading acceleration and deceleration forces applied to the skull can lead to further damage [1,6,20,22]. Furthermore, TBIs can occur from the head being abruptly set in motion or coming to a stop without hitting an object. In these

cases, the injury is caused solely by impulsive loading inertial forces that strain the tissue and lead to diffuse damage within the brain [21,22].

In penetrating TBIs, often from a bullet or a knife wound, damage to the brain is primarily focal, occurring along the route the foreign object travelled throughout the brain. Penetrating TBI carries the worst prognosis and highest mortality rate, with 70-90% of the victims succumbing before arriving at the hospital, and 50% passing away in the emergency department during resuscitation [6,25].

Blast TBI is a distinctive type of brain injury caused by exposure to explosive blast. Explosion victims can sustain brain damage through multiple injury mechanisms, including straining and stretching of brain tissue from rapid changes in pressure caused by the blast overpressure wave, impact loading injuries from propelled debris or fragments and impulse loading injuries from being thrown away by the explosion [6,21]. Unlike the aforementioned types, blast TBI stands out for its unique mechanism of injury, complex injury profile and widespread damage, which may not be as apparent in other types of TBIs.

1.1.4. Pathophysiology of Traumatic Brain Injury

TBI encompasses a wide variety of heterogeneous pathological processes, which can typically be divided into two phases. The initial phase, known as the primary injury, refers to a physical mechanical disruption of tissues and blood vessels in the brain at the moment of the impact. The second phase occurs in hours, days and weeks following the initial trauma when a series of cellular and metabolic processes triggered by biochemical changes from the primary injury lead to further neurological damage and the development of secondary injury to the brain tissue [1,6].

The primary injury results in direct damage to neurons, glial cells and cerebral blood vessels. Once sustained, the immediate neurological damage caused by the initial forces is typically not reversible. Primary injuries can result in focal, multifocal and diffuse damage to the brain. Focal injuries occur as a direct result of direct mechanical force, and the neurological damage is localized to the site of the impact. Frontal and temporal lobes are most commonly affected due to being at frequent sites of impact, but also because of their anatomical positioning and the structure of the skull [1,6,26].

One specific type of focal injury that often leads to simultaneous damage in both frontal and temporal lobes is coup/contrecoup injury. However, depending on the direction of impact, other brain areas can also be affected. The main characteristic of a coup/contrecoup injury are contusions that appear both at the site of the impact (coup) and on the opposite side (contrecoup) of the brain, which usually occurs in acceleration/deceleration associated injuries with or without the direct impact [20,26].

The pathophysiological response to the sustained insult to the brain tissue can trigger a series of complex mechanisms that exacerbate cerebral damage and lead to the development of secondary injury. Secondary injury is caused by several processes, including ischemia, excitotoxicity, calcium-mediated damage, mitochondrial dysfunction, oxidative stress and neuroinflammation [6,20]. Some secondary injuries, including an increase in intracranial pressure, development of cerebral oedema, ischemia, hypoxia, haemorrhages and seizures, can occur shortly after the head injury. However, some delayed complications like cognitive impairments, emotional and behavioural changes, and the onset of neurological and neurodegenerative disorders present long-term effects of the initial TBI. Since these processes take place in days and weeks following the primary injury and can significantly affect the patient's outcome, they present a key target for medical intervention to prevent further neurological decline [4,5,20].

1.1.5. Current Management of Traumatic Brain Injury Patients

Determining an initial GCS score in a TBI patient is the crucial first step in deciding on further treatment options. Since patients' neurological status can deteriorate quickly requiring rapid measures of care, the GCS score should be frequently re-assessed to guide timely interventions and improve outcomes. The management of TBI patients varies greatly depending on the severity of the injury. While most mild TBI cases do not require specific treatments other than rest and symptom management, treatment of moderate and severe TBI usually requires a combination of medical and surgical approaches [1,27].

Critical care management of moderate and severe TBI centres on minimizing further brain damage by preventing intracranial hypertension and the progression of secondary brain injury. Due to the higher risk of poor outcomes and mortality linked to

intracranial hypertension, ICP measurement is advisable in TBI patients with a GCS score of 3–8 and an abnormal CT scan after resuscitation. The gold standard for ICP monitoring is the placement of an external ventricular drainage device into the lateral cerebral ventricle, as depicted in Figure 2 [27–29]. Depending on the injury, additional surgical interventions like the evacuation of intracranial haematomas or decompressive craniectomy may be necessary. Other key components can also include analgosedation, mechanical ventilation, maintaining adequate oxygenation and cerebral haemodynamic stability, hyperosmolar therapy, nutritional support, and prevention of thrombosis and seizures [27,28].

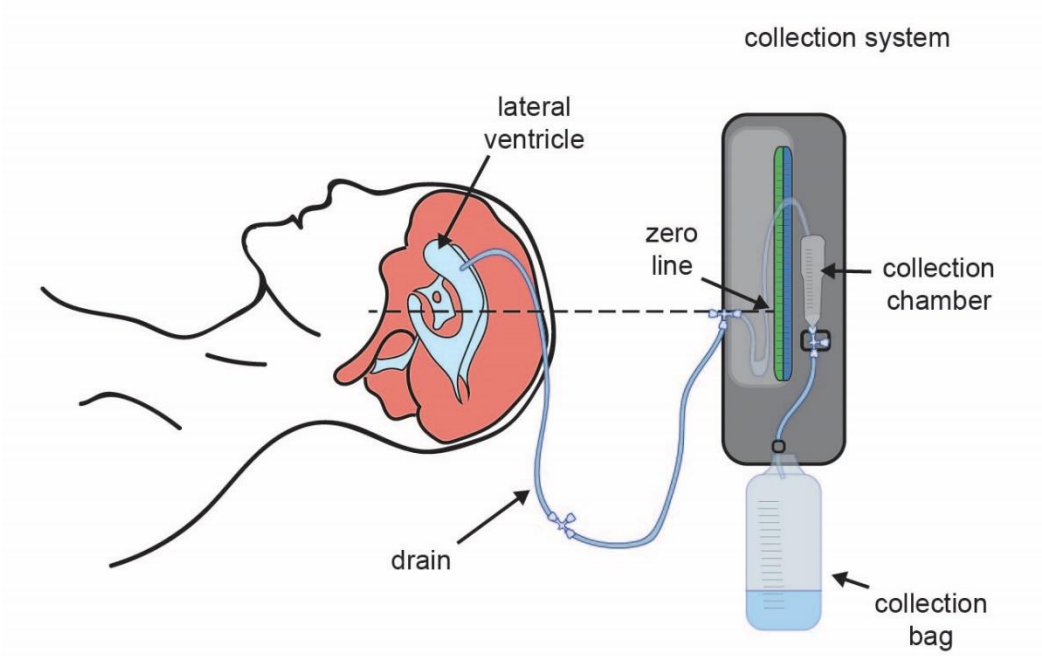

Figure 2. **External ventricular drainage (EVD) system.** An EVD is a medical device used for monitoring and relieving elevated ICP by draining cerebrospinal fluid (CSF) from the brain's ventricles. A catheter is inserted into the lateral ventricle and connected to the collection system outside the skull, allowing for drainage of CSF driven by gravity. The zero line is aligned with the patient's ear, and the collection chamber is placed at the prescribed position above that zero line.

In efforts to find more therapies that would enhance recovery from TBI, significant scientific developments have expanded the knowledge of the intricate pathophysiological mechanisms connected to TBI over the last two decades. Many experimental therapies have been demonstrated to be neuroprotective in animal

models, including various *N*-methyl-D-aspartate receptor antagonists, glutamate agonists, calcium channel antagonists, erythropoietin and immune system modulators. Regretfully, none so far has been identified as beneficial in clinical trials [7,27,30]. Due to generalized failure in providing novel treatments and clinical protocols, biomarkers have been actively explored as a potential evaluation and prognostic tool for monitoring treatment response in TBI patients. One promising source of such biomarkers are extracellular vesicles, cell-derived nanoparticles involved in intercellular communication and transport of bioactive molecules between distant cells and tissues which makes them a promising candidate for TBI biomarker research [27,31].

1.2. Extracellular Vesicles

1.2.1. A Brief History of Extracellular Vesicles – from „Garbage Bags“ to Intercellular Messengers

The term extracellular vesicles (EVs) refers to a group of membrane-bound nanoparticles released by cells into the extracellular space. The discovery of these particles that are now known to be present in all multicellular organisms has unfolded gradually over the past several decades, as researchers began to recognize the role of these small, cell-derived particles in intercellular communication and various biological processes. The earliest observation of EVs dates back to 1946, when Chargaff and West discovered a distinctive “particulate fraction” with procoagulant properties while working on high-speed centrifugation protocol for the isolation of blood-coagulating protein from plasma [32]. Over 20 years will pass until 1967, when Peter Wolf [33] obtained electron microscopy images of said particles, and described them as “platelet dust” shed by platelets in human plasma. In 1974, Nunez et al. reported structures which would later be termed multivesicular bodies (MVB), opening the pathway for the identification of a subtype of small EVs that originate from the inward budding of MVB membranes [34].

The early 1980s marked the beginning of focused EV research with two papers, Harding et al. and Pan and Johnstone, simultaneously discovering reticulocytes release transferrin receptor-associated evenly sized vesicles into the extracellular space [35,36]. In fact, Harding et al. demonstrated that these vesicles originated from

MVBs fused with the plasma membrane and are externalised outside the cell, revealing a novel EV secretion pathway [35]. The term "exosome" was first coined in 1981 to describe EVs shed from the cell surface. It gained traction after Johnstone et al. in 1987 defined them as vesicles released from MVBs [37]. However, in the early days of EV research, it was hypothesised that these newly discovered vesicles primarily function as a cellular garbage disposal system for discarding metabolic waste [38,39].

It wasn't until the 1990s that the functional role and importance of exosomes started to be recognised by the academic community. Observations of altered numbers of EVs in numerous diseases and demonstration of their enzymatic activity led to speculations of their possible involvement in different pathological processes. However, the revelation that EVs excreted from B lymphocytes can bear MHC-II molecules, present antigens to T lymphocytes and initiate T cell response showed that EVs can actively participate in intercellular signalling and be involved in various physiological processes.

Entering the 21st century, EV research has rapidly advanced, evolving from a niche interest to a major field of study. The expanding body of research began delving further into EVs characteristics, examining the lipidome and proteome of EVs derived from different cell types. A seminal paper from 2007 revealed that exosomes can carry RNA, including microRNAs and mRNAs, and deliver them to recipient cells, thereby altering gene expression in those cells and further corroborating the significance of EVs as important messengers in cell-to-cell communication [40]. With the growing knowledge of EV role as intercellular messengers, the role of EVs is being increasingly explored in various pathological processes, such as, among others, infectious diseases, cancer and neurodegenerative disorders. Since EVs have been shown to carry disease-specific molecules and are readily accessible from bodily fluids, they present an appealing potential source of diagnostic and prognostic biomarkers for non-invasive diagnostics and disease monitoring. Other possible utilisations, namely their use as biocompatible nanocarriers in the treatment of cancers and neurodegenerative diseases, are also being actively explored [41,42].

1.2.2. Classification and Biogenesis of Extracellular Vesicles

EVs represent a heterogeneous group of nanoparticles secreted by cells and defined by the lipid bilayer encapsulating their cargo. These particles can carry a diverse array of biologically active molecules including nucleic acids, proteins, lipids and metabolites that can elicit signalling pathways in the recipient cells and modify their behaviour in both homeostatic and pathologic conditions. For years, terms like “exosomes”, “microvesicles”, and “microparticles” were used interchangeably to describe these vesicular entities of different sizes and origins. However, in an attempt to bring order into this growing field, the International Society for Extracellular Vesicles (ISEV) suggested the term extracellular as an umbrella term for all cell-derived, non-replicating, lipid bilayer-delimited structures [38,43,44].

Due to substantial diversity among EVs, multiple classification systems have been proposed to define specific subtypes of these vesicles. According to current Minimal information for studies of extracellular vesicles (MISEV) guidelines from 2023, the ISEV endorses classification based on EV size, dividing them into small (< 200 nm) and large EVs (> 200 nm). Another classification commonly used in literature is based on EV biogenesis [43]. Three main modes of different EV biogenesis pathways have been widely accepted, dividing EVs into exosomes, microvesicles and apoptotic bodies, as depicted in Figure 3. Some newer findings suggest the addition of another specific type of EVs, called autophagic EVs, into the existing terminology. However, autophagic EVs are still considered more as a conceptual framework that reflects the overlap between the autophagy pathway and EV secretion, rather than a distinctive and formally accepted EV classification category [43,45–47].

Exosomes are a subtype of small EVs, ranging from 30 to 200 nm in diameter, with an average size of approximately 100 nm [45,48,49]. The biogenesis of these small EVs is an intricate multistep process that unfolds within membranous compartments of the endosomal system. The endosomal system comprises a dynamic network of sorting organelles that facilitate the intracellular transport of molecules endocytosed from the cell surface via endocytic vesicles. Endocytosed cargo is initially transferred to early endosomes, which function as a sorting hub for directing internalized molecules for recycling, degradation or secretion. Molecules designated for recycling get routed back to the cell surface or transferred to the trans-Golgi network

through the process of retrograde trafficking. The remaining cargo sorted for degradation or secretion undergo an endosomal maturation pathway and formation of late endosomes/MVBs, accompanied by invagination and inward budding of endosomal limiting membranes and formation of intraluminal vesicles (ILVs). Once matured, MVBs can either undergo degradation by merging with lysosomes, or fuse with the plasma membrane, leading to the secretion of ILVs into the extracellular environment where they become exosomes [45,48,50].

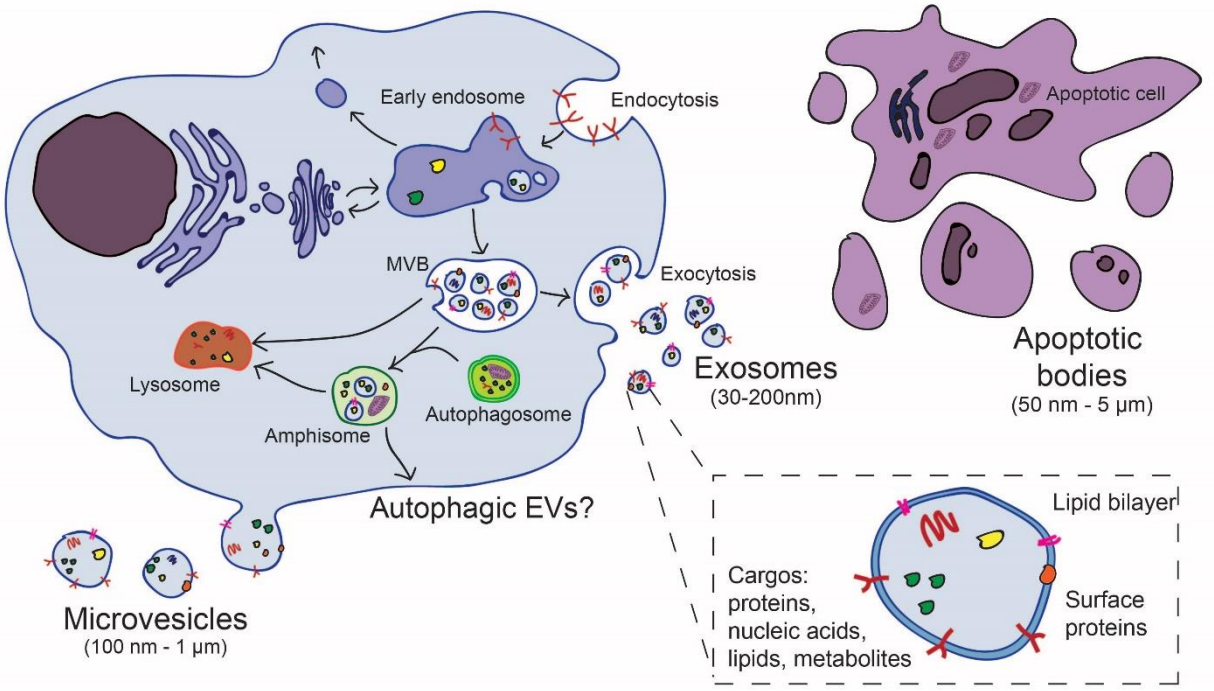

Figure 3. Extracellular vesicles (EVs) biogenesis pathways. Based on their biogenesis and subcellular origin, EVs can be broadly classified into three major subtypes: exosomes, microvesicles and apoptotic bodies. Exosome biogenesis originates from the endocytic pathway. During the process of maturation of early endosomes, endocytosed molecules are packed within intraluminal vesicles (ILVs), forming multivesicular bodies (MVBs). When MVBs fuse with the plasma membrane, ILVs are secreted as exosomes in the extracellular space. Microvesicles arise from direct budding from the plasma membrane mediated by lipid reorganization and cytoskeletal remodelling. Apoptotic bodies are generated by dying cells in the late stage of apoptosis as a product of membrane blebbing and fragmentation of the cell. Autophagic EVs present an additional EV subpopulation that originates from amphisomes, hybrid organelles formed through the fusion of MVBs and autophagosomes. Autophagic EVs are secreted through a pathway related to secretory autophagy. However, the mechanism of autophagic EV secretion is not yet fully elucidated.

Despite still not being completely elucidated, it seems evident that the cargo sorting and packing into exosomes is a tightly regulated process involving multiple pathways. The cargo sorting and formation of ILVs is mostly driven by the endosomal sorting complex required for transport (ESCRT) machinery and its accessory proteins such as ALG-2-interacting protein X (Alix). Multiple tetraspanins, members of integral membrane protein family characterised by their four transmembrane domains and two extracellular loops, also contribute to exosome formation by organizing membrane microdomains and participate in cargo selection. Tetraspanins CD9, CD63 and CD81 are commonly used as markers for exosome identification [48,50]. Furthermore, cellular signals and environmental stimuli can modulate exosome biogenesis and secretion, ensuring that exosomes carry specific cargo for functions like cell signalling and immune response [49,51]. Dysregulation in exosome packaging or secretion is linked to various pathologies, changing both the quantity of secreted exosomes as well as their content. For instance, in Alzheimer's disease, exosomes have been shown to propagate toxic β-amyloid oligomers between neurons, contributing to the disease progression [52].

Microvesicles, also referred to as ectosomes, are a subtype of EVs considerably larger than exosomes, with a diameter typically ranging between 100 nm and 1 µm. However, an increasing number of researchers report a much wider span of sizes observed in different types of microvesicles, indicating that they can range down to approximately 50 nm, and, on the other side of the scale, range up to several micrometres in diameter [45,53,54]. This diverse group of microparticles is connected by a distinctive biogenesis pathway, characterised by outward budding or blebbing of the plasma membrane, resulting in specific regions of the plasma membrane forming bulges that eventually pinch off and create microvesicles. This coordinated process involves localized changes in plasma membrane protein and lipid content, influencing membrane curvature and rigidity. Changes in cytoskeletal remodelling and actin-myosin interactions, regulated by ADP ribosylation factor 6 (ARF6) signalling axis, generate contractile forces necessary for pushing the membrane outwards and pinching off the newly generated microvesicle from the plasma membrane. Furthermore, the presence of cholesterol, and rearrangement of specific lipids, such

as phosphatidylserine, from the inner to the outer leaflet of the plasma membrane, are identified as key factors in the microvesicle biogenesis pathway [53–55].

The release of microvesicles is heavily influenced by environmental conditions, and the occurrence of cellular stress and inflammation has been linked with an increased release of microvesicles carrying stress-related signals. Hence, it's not surprising that increased microvesicle production has been observed in various pathophysiological states. Much of the research has focused on their role in diseases, particularly cancer, where a specific type of microvesicles called oncosomes is shed from tumour cells that can promote tumour growth, angiogenesis, metastasis and immune suppression [46,53].

Apoptotic bodies are a specific subtype of EVs released by the cells undergoing programmed cell death. They are typically larger than other EV subtypes, with sizes ranging between 50 nm and 5 µm, with most apoptotic bodies belonging to the bigger end of the spectrum [56–58]. As a cell undergoes apoptosis, it goes through a characteristic series of morphological changes, including cell shrinkage condensation of the nucleus and chromatin and membrane blebbing. Apoptotic bodies arise from these membrane blebs that pinch off from the dying cell in the later stages of apoptosis when the cell breaks into multiple parts containing nuclear fragments, organelles, chromatin, and other cellular components [58,59]. The process of generating apoptotic bodies as well as the apoptosis itself is highly organised and controlled by caspase activation and multiple downstream protein kinases, such as Rho-associated protein kinase 1 (ROCK1) and LIM kinase 1 (LIMK1), which are known to facilitate and promote membrane blebbing [57–59].

Once formed, quick clearance of apoptotic bodies is necessary to protect the surrounding tissue from harmful exposure to harmful intercellular contents of the dying cells. Thus, apoptotic bodies exhibit "eat-me" signals that promote quick recruitment of phagocytes that provide efficient clearance of apoptotic cell remnants [57,59]. In addition to their primary purpose of removal of dying cells, recent reports indicate that apoptotic bodies also participate in intercellular communication. Although the process is still poorly understood, emerging evidence suggests that apoptotic bodies can promote processes like immunomodulation, tissue regeneration and vascular protection [56].

Lastly, autophagic EVs present an unofficial, yet increasingly recognised subpopulation of EVs associated with the process of autophagy. During autophagy, damaged organelles and proteins are bound into double-membrane structures called autophagosomes, which typically fuse with lysosomes for degradation. In certain cases, autophagosomes can fuse with MVBs to form amphisomes. These amphisomes may then fuse with the plasma membrane, releasing autophagic material as autophagic EVs. These vesicles can contain double membrane like autophagosomes, and often carry specific autophagy markers such as ubiquitin-binding protein p62 and microtubule-associated proteins 1A/1B light chain 3B (LC3) [46,60,61]. A growing amount of evidence suggests that autophagy-related EVs have implications in various pathologies, particularly those with altered autophagy pathways like neurodegenerative disorders, TBI and stroke [62]. Still, autophagic EVs often exhibit characteristics of exosomes and microvesicles, hence they are seen more as a specific functional category of existing EV types.

1.2.3. Extracellular Vesicles as Potential Biomarkers in TBI

The complexity of TBI and the limited understanding of its pathology pose great challenges in the development of effective treatment strategies which would provide better long-term outcomes for TBI patients. This issue has driven a need for improving the diagnosis, monitoring and treatment of TBI. By reflecting the underlying biological processes, clinical use of biomarkers can help guide clinical decisions, identify patients at risk for poor recovery and long-term complications and personalise therapeutic strategies for TBI patients.

Due to their unique ability to provide a snapshot of the state of the originating cells and tissues, EVs became a major area of interest in TBI biomarker discovery. EVs are secreted by all cell types found in the central nervous system (CNS) and facilitate intercellular communication with adjacent cells, or travel through CSF and blood to physically distant cells and tissues [63]. Furthermore, EVs can protect cargo molecules from degradation and denaturation in the extracellular environment and are comparatively stable under a range of physiological conditions. They have been isolated from various biological fluids, including blood, urine, saliva and CSF. Coupled with their ability to bidirectionally cross the blood-brain barrier, EVs present a promising

source of potential TBI biomarkers that could enable detection of brain-specific biomarkers in peripheral blood samples, allowing non-invasive, real-time detection and monitoring of disease progression and treatment response [31,41].

The evaluation of levels and phenotypical characterisation of EVs in biofluids after TBI are vital for improving our comprehension of the molecular mechanisms underlying the pathophysiological processes that accompany TBI and open the possibility for utilisation of EV biomarker potential. Several studies reported changes in EV concentration, particularly elevated concentration of circulating EVs following severe TBI [64,65]. Observation made by our group revealed elevated concentrations of CSF EVs, as well as changes in their size and protein composition within several days after severe TBI [66].

Most studies on biomarkers in TBI primarily focused on the detection of plasma and serum levels of neuroglial proteins, namely glial fibrillary acidic protein (GFAP), neurofilament light chain (NfL) and ubiquitin carboxyl-terminal hydrolase isozyme L1 (UCH-L1), as markers of tissue damage in the nervous system. In a study that evaluated temporal profiles of circulating exosomal proteins associated with brain injury following moderate-to-severe TBI, elevated levels of exosomal NfL and GFAP have been reported in patients with diffuse injuries, while acutely elevated UCH-L1 with secondary steep rise was associated with early mortality [67]. In another study, Flynn et al. revealed that elevated exosomal GFAP and NfL levels one year post severe TBI correlated with poorer clinical outcomes, while Lei et al. reported high serum levels of GFAP during the first 5 days post-injury were a strong predictor for poor prognosis and death [68,69].

As neuroinflammation presents one of the main drivers of secondary injury, considerable efforts have been made to provide a better understanding of the role of EVs in a neuroinflammatory response post TBI. Current evidence suggests that EVs can actively participate in neuroinflammation and that they can carry signals that can modulate the inflammatory process in both pro- and anti-inflammatory fashion. A recent study performed on a mouse model of TBI revealed that microglia-derived EVs found in blood post-injury contain high levels of pro-inflammatory molecules, including interleukin-1β and miR-155, thereby increasing neuroinflammatory response [70]. Conversely, multiple studies on mouse and rat models identified increased levels of miR-124 in microglia-derived EVs, connected with suppression of neuronal

inflammation and promotion of neurite outgrowth, demonstrating the dual role of EVs after TBI [71,72].

Despite numerous findings on EV role in pathophysiological response to TBI and several promising biomarker candidates, there is no widely acknowledged and validated biomarker routinely used in the clinical setting. The lack of progress in EV research involving TBI is partially due to the complexity of TBI pathophysiology, high heterogeneity in clinical presentation, and a substantial number of unreported cases. However, significant hindrances in the clinical translation of EV-based diagnostics and other applications are attributable to the considerable inconsistencies between EV studies regarding the lack of standardised protocols, as well as technical challenges in isolation and characterisation techniques [31,41].

Challenges in EV research are probably best described through the L1 cell adhesion molecule (L1CAM) example. For years, transmembrane protein L1CAM was used as a biomarker of neuron-derived EVs (NDEVs) used in immunocapturing NDEVs from biofluids for further protein and RNA analyses in various disorders. Recent findings from Norman et al., however, brought into question its utilisation as an NDEV marker by showing that upon isolating human CSF and plasma EVs by size-exclusion chromatography, the majority of L1CAM co-eluted with soluble proteins instead of EV fractions. Further examination revealed that L1CAM in plasma and CSF is predominantly expressed in the form of a soluble protein, generated by proteolytic cleaving or alternative splicing [73]. A successive L1CAM literature review by Gomes and Witwer revealed that around 40% of articles reported no physical characterisation of EVs after isolation, indicating that these results should be taken with caution, but also emphasising the urgent need for standardisation in this emerging field [74].

1.3. Methods of Extracellular Vesicles Isolation

The field of EV research is burdened by the use of inconsistent isolation methods, conflicting nomenclature, and the absence of standardised data acquisition and analysis protocols, all of which hinder the ability to interpret the findings from EV studies accurately. Accordingly, the selection of an ideal EV isolation method from body fluids with sufficient yield and purity remains a major matter of debate in the EV field. Their small size (< 1 μm), large heterogeneity and rather fragile nature all

contribute to EV analysis being a technically highly challenging task with several unresolved issues [75,76].

Most widely utilised methods of EV isolation include ultracentrifugation (UC), ultrafiltration (UF), polymer-based precipitation, immunoaffinity (IA) capture and size-exclusion chromatography (SEC), with each of them owing inherent advantages and disadvantages (Figure 4). Since the isolation method significantly affects both the quantity and purity of isolated EVs, the nature and complexity of the sample itself should be taken into consideration in order to obtain high-quality EVs, which is essential for any downstream functional EV analysis [76–78].

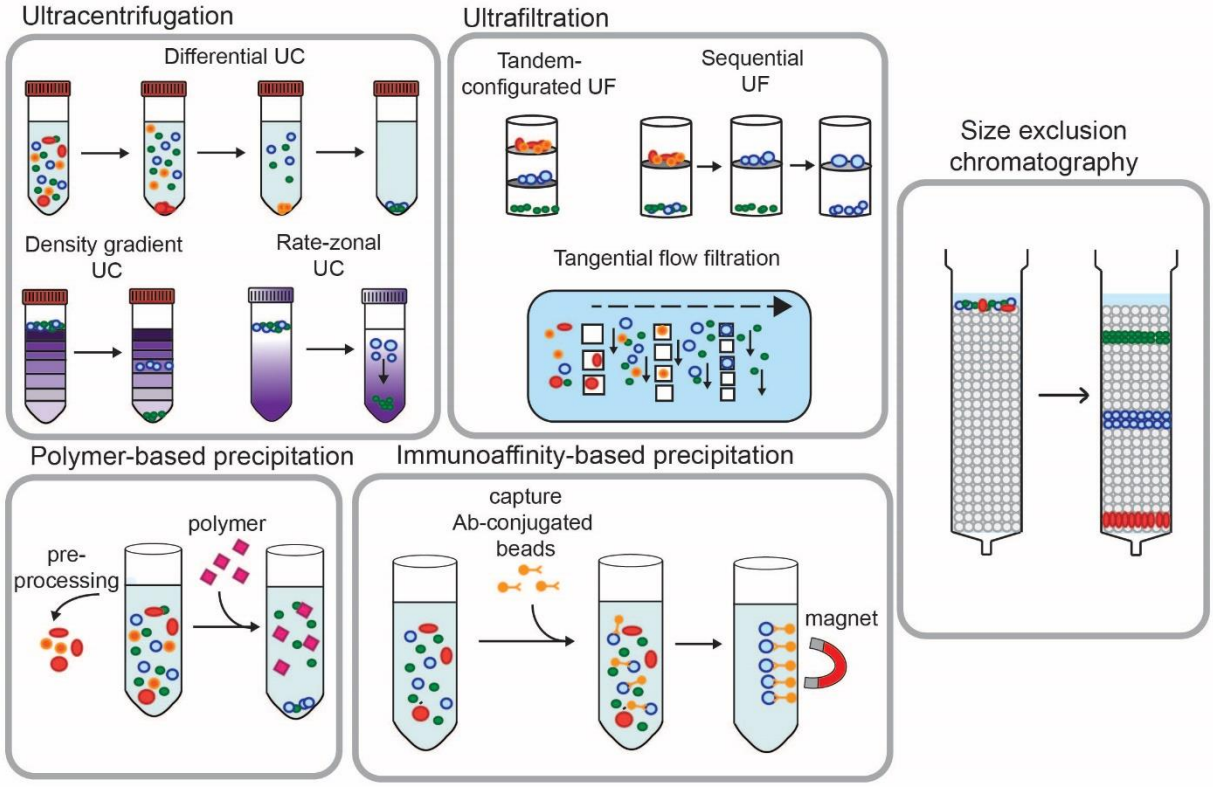

Figure 4. An illustrated summary of commonly used EV isolation methods: ultracentrifugation (UC), ultrafiltration (UF), polymer-based precipitation, immunoaffinity (IA)-based precipitation and size-exclusion chromatography (SEC). EV isolation methods rely on different physical and biological principles for EV isolation based on their size (differential UC, rate-zonal UC, UF, SEC), density (density gradient UC), affinity (IA-based precipitation) and solubility (polymer-based precipitation).

1.3.1. Ultracentrifugation

UC-based methods are the most widely used methods of EV isolation from biofluid samples. The isolation is accomplished by applying high centrifugal forces that provide separation based on particle size and density. Different types of UC have been utilised for EV isolation, specifically differential UC (dUC), density gradient centrifugation and rate-zonal centrifugation [76,79]. In dUC, the sample is subjected to progressively increasing centrifugal forces. Although applied protocols differ in the number of centrifugation steps and applied centrifugation speeds, they can roughly be described in two main stages. In the initial stage, larger particles with high density, such as cells, cellular debris, apoptotic bodies and biopolymer aggregates, are removed by centrifugation at low speeds, typically in multiple steps at 300-10,000 x g. In the following stage, EVs are sedimented from the remaining supernatant by UC at 100,000-200,000 x g, and the EV-containing pellet is resuspended in a suitable buffer for further analysis [76,79,80]. The main advantages of this method are that it typically yields a large quantity of EVs and can process large sample volumes. However, high contamination of isolated EVs with soluble proteins, lipoproteins and other particles similar in size and density to EVs, as well as shear damage, fusion of EV membranes and EV aggregate formation under the influence of high centrifugal forces present serious drawbacks of dUC EV isolation methodology [78,81].

To overcome these disadvantages, different variations of UC protocols have been utilised. Unlike dUC which separated EVs from non-EV particles based on size alone, separation with density gradient centrifugation is achieved by centrifugation of the sample layered on a density gradient medium, allowing separation based on their buoyant density. Although this method provides purer EVs, it is very time-consuming and leads to a substantial loss of EVs throughout the process [76,79]. On the other hand, rate-zonal centrifugation also applies a density gradient, but the separation is based on particle size and sedimentation rate. As the sample particles travel over a gradient with increasing density toward the bottom of the ultracentrifuge tube, they will divide into distinct zones according to their rate of sedimentation. Unlike density gradient centrifugation where particles remain suspended when they reach their isopycnic point in the gradient, in rate-zonal centrifugation particles are separated by the speed at which they move through the gradient, and centrifugation must be stopped before all particles pellet out [45,79]. This variation of UC provides faster separation

than the density gradient and allows the separation of different-sized particles in the same medium. However, it is very time-sensitive and less effective in separating particles of similar size or density [45]. Granting these variations of UC protocols provide some improvements to dUC, they are still plagued with the same issues associated with damaging EV membranes due to high centrifugal forces applied for isolation.

1.3.2. Ultrafiltration

Another commonly utilised size-based method for isolating EVs is UF, which may be employed either as a stand-alone technique, or in conjunction with other isolation methods. The separation of EVs from non-EV particles is achieved by sifting the sample through membrane filters with specific pore sizes, called molecular weight cut-off (MWCO), by employing centrifugation, pressure or vacuum. By using filters with different MCWO values, only the particles of the selected size range are present in the final filtrate [45,77].

The most used approaches for UF-based EV isolation are tandem-configurated UF, sequential UF and tangential-flow filtration. In tandem-configurated UF, usually performed with a pre-made isolation kit, a sample is passed through a syringe equipped with two membranes, which define the upper and lower size limit of the retained particles that stay “trapped” on the second membrane. In sequential filtration, the sample is passed through a series of micro- and ultrafiltration membranes, where microfiltration membranes are used for filtering out larger debris like cells and apoptotic bodies, and ultrafiltration membranes are applied for retaining EVs and depletion of free proteins and nucleic acids from the EV isolate [76,82]. Such protocols are usually more rapid compared to UC-based methods. Still, these techniques often result in low yield, EV damage and high protein contamination. Studies have shown that EV isolates from human biofluids obtained by UF can contain large amounts of non-EV proteins, including albumin and α-1-antitrypsin. Additionally, these two approaches have a common flaw, which is the formation of filter “cake” and frequent plugging of the membrane typical for dead-end filtration, hence complicating the isolation procedure and limiting the sample volume that can be processed [76,78,83]. Tangential flow filtration is intended to overcome this issue by allowing fluid to flow tangentially across

the filter surfaces, thus minimising clogging and fouling and leading to higher efficiency in particle separation. However, the use of pumps to drive fluid tangentially over the membrane surface can subject EVs to shear stress and damage fragile EVs in the process. Moreover, this method requires specialised equipment and operating them is more complex than operating dead-end filtration systems [84].

Although UF-based methods provide a quick and relatively simple EV isolation tactic that enables concentrating EVs from more diluted samples, there are common limitations to these techniques. Firstly, EVs tend to get damaged through the filtering process leading to poor biological activity of isolated EVs, which can affect downstream functional analyses. Secondly, the choice of upper and lower cut-off values leads to the inevitable loss of EV subtypes that could potentially be of biological significance. Finally, high protein contamination results in low purity of obtained isolates, thus requiring additional steps to acquire cleaner preparations [76,77].

1.3.3. Precipitation-Based Methods

Precipitation-based techniques have become an increasingly popular choice for EV isolation because of their general ease of use, simplicity (i.e. not requiring specialised equipment) and low cost and time consumption. Precipitation-based methods involve the addition of chemical or polymeric reagents to the sample that reduce the solubility of sample components and cause them to precipitate out of the solution. These methods include precipitation with hydrophilic polymers, sodium acetate and protamine [76,82].

The precipitation with hydrophilic polymers, namely polyethylene glycol (PEG), is the second most used method for EV isolation after UC [76]. It is based on a principle of alternating the solubility of EVs by hydrophilic water-excluding polymer, which ties up water molecules and creates a hydrophobic microenvironment around EVs, resulting in their precipitation. The isolation procedure itself is very straightforward – the sample is mixed with PEG solution, and after incubation, the solution is centrifuged at low speed to pellet the EVs [76,85]. Current polymer-based techniques for EV precipitation typically utilise PEG with molecular weights ranging from 6000 to 20,000 Da. Moreover, numerous commercially available kits based on PEG have been developed, including Total Exosome Isolation Reagent (Invitrogen, USA), ExoQuick

(System Biosciences, USA), ExoPrep (HansaBioMed, Estonia), miRCURY Exosome Isolation Kit (Exiqon, Denmark) and Exosome Purification Kit (Norgen Biotek, Canada).

Along with speed and low cost, polymer-based precipitation is easily scalable, provides high yield, does not require specialised equipment and, notably, does not cause deformations and damage to EVs. However, one major drawback is that high yield comes at the cost of purity due to high levels of contamination with co-precipitating non-EV proteins. In addition, the retention of polymer can further reduce the purity of isolated EVs. Therefore, by itself, it is deemed unsuitable for descriptive or functional downstream analysis of EVs [76,82,85].

Precipitation with sodium acetate or protamine also works on a similar principle, except these compounds partially depend on charge interactions. Using sodium acetate for EV precipitation causes EV aggregation through hydrophobic interactions by adjusting the ionic environment and breaking the hydration shell around EVs. On the other hand, protamine sulphate, a polycationic peptide, works by directly modifying EVs' surfaces by binding and neutralising the negatively charged EVs, promoting their aggregation through electrostatic repulsion. While both methods are relatively simple and cost-effective, they come with purity concerns because, similarly to polymer-based precipitation, both suffer from high levels of contamination in the samples and would require the application of additional purification methods to obtain cleaner EV samples [76,86].

1.3.4. Immunoaffinity-Based Isolation

Unlike previously described EV isolation methods that rely on EV size, density, solubility and charge, IA based isolation allows for highly selective and specific isolation of EVs by employing antibodies against proteins found on the EV surface. Antibodies against EV markers, most commonly tetraspanins CD9, CD63 and CD81, are immobilised to the solid matrix that allows for selective isolation of EVs expressing chosen surface marker protein [77,85]. After the preparation of the solid matrix, i.e. beads, for EV capture, the sample is incubated with antibody-coated beads, followed by washing to remove the unbound material and elution of EVs from the antibody-coated solid matrix. Antibody-coated magnetic beads are a frequent choice of the fixed phase, but other solid materials like agarose beads, plastic plates, cellulose filters,

monolithic columns and various types of microfluidic devices have also been employed for that purpose [76,80,85].

IA capture provides isolation of specific subtypes of EVs with high purity and medium yield and is probably the most effective method for obtaining a distinct specific subpopulation of EVs from a heterogeneous sample. This property could be useful in specific cases, like isolating EVs of specific origin, as described in a paper by Rupp et al., where they used an antibody against EpCAM, which is overly expressed in tumour-derived EVs, to isolate EVs that originate from tumour cells from different biological samples [87]. However, this quality simultaneously presents the biggest disadvantage of IA-based methods. Not all EVs express the same EV markers, meaning that by selecting a subset of markers that will be used for IA capture, all EVs that do not express those markers will be lost, leading to a lower overall yield [82,85].

Theoretically, IA capture should only result in EVs expressing the desired protein marker. Nevertheless, IA-based methods are as selective as the selected antibodies, meaning that if antibodies do not exclusively bind to desired EV subpopulations, contamination with non-targeted EVs and other cellular debris will be present in the sample. An additional issue with IA methods is that they can suffer from non-specific interactions between the antibodies and other components in complex biological samples, such as plasma, which can result in lower recovery rates and reduced specificity compared to other isolation techniques. Furthermore, elution buffers necessary for separating EVs from capture antibodies can damage isolated EVs and cause irreversible loss of their biological function. Although denatured EVs are typically acceptable in the scope of diagnostics, such samples would not be suitable for functional studies [76,78,82,85]. In conclusion, while immunoaffinity-based methods provide a powerful tool for isolating specific EV subpopulations, challenges related to specificity, cost, biological variability, and potential sample alteration must be carefully managed to ensure reliable outcomes in research and clinical applications.

1.3.5. Size-Exclusion Chromatography

SEC is a widely recognized technique for separation of macromolecules, namely biopolymers, according to their molecular size or volume they occupy in a solution, also known as hydrodynamic radius. More recently, it was also employed for

EV isolation and is becoming a method of choice for isolating physically unaltered and biologically active EVs from complex biological samples [82,84,85]. SEC is performed in a column packed with a porous gel matrix that acts as a stationary phase. When the sample is loaded in the SEC column, molecules are sieved through the matrix, and depending on their size, travel different paths to elution. Smaller molecules penetrate the pores of the matrix, which results in longer elution times, while bigger molecules get excluded from those pores and travel faster, as shown in Figure 5. The sample is flown through the column either by gravity or using a pump, with gravity being preferable since lower flow rates improve column efficiency and are generally gentler to EVs [77,82,88].

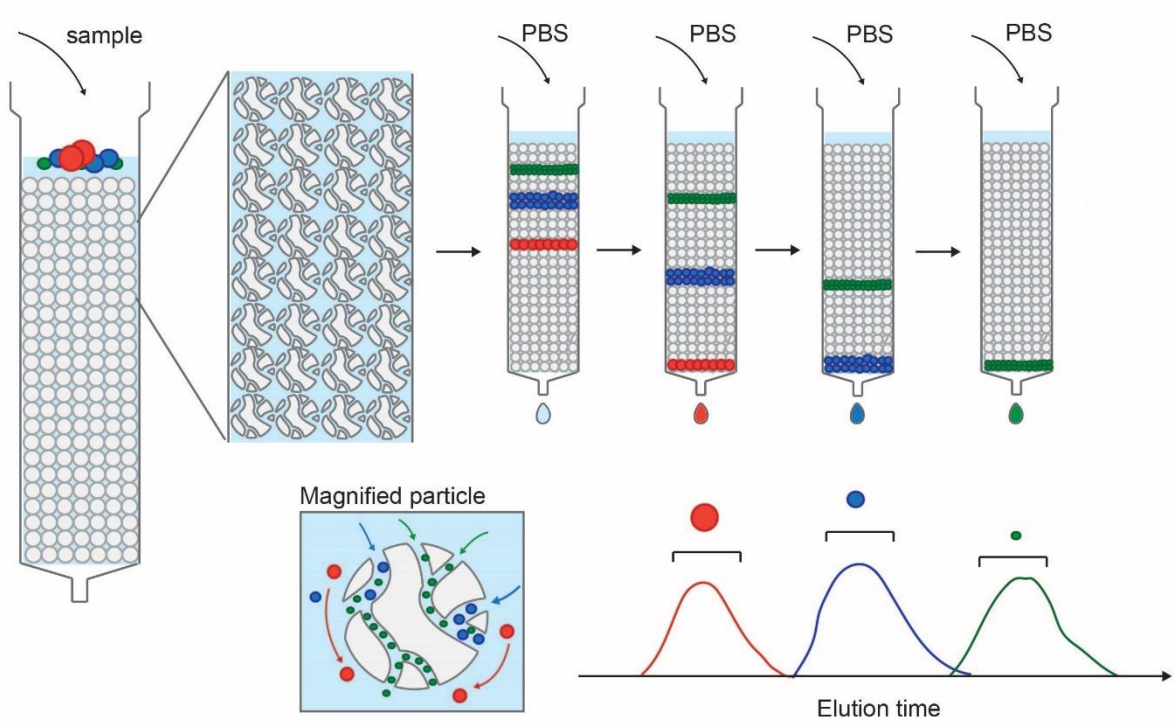

Figure 5. Principle of size-exclusion chromatography-based EV isolation. SEC separation is achieved by passing a sample through a column packed with a porous resin, which acts as a molecular sieve and separates the particles based on their hydrodynamic radius. Depending on their size, molecules transverse through the column in different paths, with smaller molecules travelling a longer path than the bigger ones.

The first use of SEC for EV isolation was reported by Böing et al. in 2014, who developed a straightforward, one-step method using Sepharose CL-2B resin for isolating EVs from human plasma samples [89]. This method laid the groundwork for

subsequent isolations using other SEC materials, such as Sepharose CL-6B and Sephacryl S-400, which were later employed for isolating EVs from human serum and plasma samples [90–92]. These materials are utilised as either in-house prepared gravity-flow columns or as pre-packed columns suited for use with pressure-based chromatography systems. A growing number of commercial ready-to-use EV isolation columns are gaining popularity since they present a more straightforward alternative for rapid and simple EV isolation and have been successfully utilised for the enrichment of EVs from human biofluid samples [92–94].

SEC provides multiple advantages compared to other common EV isolation techniques in both the purity and functionality of isolated EVs. SEC effectively separates EVs from proteins and other contaminants based on their size, allowing for the isolation of relatively pure EV populations. It provides gentle elution of vesicles, especially if performed under gravity flow conditions, which reduces the risk of deformation or rupture of EV membranes and ensures the preservation of EV's morphology and functionality. Thus, the use of SEC for EV isolation provides biologically active and functional EVs suitable for any downstream analysis [77,78,95,96]. Additionally, SEC can handle larger sample volumes, it does not require complex specialised equipment, it is cost-effective and does not require additional sample preparation steps.

However, several limitations of SEC EV isolation must be addressed. The main concern is potential contamination with particles of similar sizes to EVs like plasma lipoproteins, namely chylomicrons, low-density lipoproteins (LDL) and very-low-density lipoproteins (VLDL) [93,97]. Additionally, as a trade-off for good purity, the overall yield is lower compared to some other methods like UC and precipitation methods that are more efficient in terms of total recovery of EVs in the sample and can additionally dilute the samples. This poses a problem when working with samples with overall low concentrations of EVs [77,78]. Finally, the quality and effectiveness of SEC EVs isolation heavily depends on the type of column used for isolation, as well as the quality, sustainability and effectiveness of resin in the column. Hence, good design of SEC set-up is imperative for obtaining quality EV samples. Previous reports on SEC utilisation for EV isolation from biofluids were mainly performed on plasma, serum and urine [77,93,95,98]. However, working with CSF samples is somewhat more intricate due to invasive relatively low protein and nanoparticle concentration in comparison to

other biofluids. Additionally, low availability of CSF samples due to the invasive nature of the procedure required to access CSF presents an additional research challenge [78,88]. Consequently, only a few studies so far reported on the application of SEC for EV isolation from CSF with no comprehensive comparison of SEC designs to identify the most effective method for CSF-EV isolation.

1.4. Techniques for EV Characterisation and Analysis

Characterisation of obtained EVs presents an essential step following every EV isolation to verify their presence in the isolate, estimate their quantity and evaluate the possible contamination with non-EV components in the sample. However, this characterisation process faces several challenges, including their small size, vast molecular diversity and the absence of universal identification methods. Additionally, many techniques lack EV specificity, meaning that no single measurement of method can provide all insights necessary for comprehensive EV characterisation. Hence, ISEV advises employing multiple complementary methods that use different measurement principles for assessing the EV attributes to assess the quality of the obtained isolates [43,99].

1.4.1. Methods for Measuring EV Concentration and Size

Commonly employed methods for measuring EV concentration and size include nanoparticle tracking analysis (NTA), dynamic light scattering (DLS), flow cytometry and tunable resistive pulse sensing (TRPS) [45,100]. Each of them possesses certain trade-offs between precision, throughput, and sensitivity, and the limitations of each method should be considered in the interpretation of obtained data. Additionally, transmission electron microscopy (TEM) also enables size measurements of EVs. However, TEM is not suitable for determining EV concentration and will here be considered primarily as a method for visualisation and morphology analysis, further explained in the later section [100,101].

NTA is a widely employed technique for measuring the concentration and size of EVs based on tracking the Brownian motion of particles in a suspension. The

suspension of particles is illuminated by a laser beam, and a camera captures the scattered light, allowing tracking of the individual particles. The captured video is then analysed by the software to translate the collected data into the vesicle's diffusion rates, which is inversely related to their diameter. NTA detects particles ranging from 30 to 1000 nm in diameter and simultaneously measures the size distribution and concentration of EVs in a sample [45,101,102]. Additionally, it shows good reproducibility, and it is not as technically demanding as some of the other methods. However, NTA requires relatively high concentrations (at least 10^8 particles/mL) of EVs and large sample volumes (~0.5 mL), which can be a limiting factor when working with samples with low concentrations of EVs and limited accessibility like CSF [101,102]. Another drawback of this method is that particles with low refractive indices, like EVs, may scatter light less, making the detection of smaller vesicles more challenging. Furthermore, the composition of the cargo molecules can also affect the refractive indices of the vesicles, causing additional variability in measurements [43]. Finally, the presence of contaminants or other particles in the sample may affect the accuracy of size and concentration measurements [101].

DLS is another frequently used method for EV characterisation that relies on the principle of light scattering to measure particle size. In the DLS method, the fluctuations of the scattering light intensity are analysed to determine the size of the particles based on their Brownian motion [100,102]. DLS can generally handle a wider range of concentrations and provides rapid and reproducible measurements. It can also detect a very wide range of particle sizes, ranging from 1 nm to 6 μm [102]. However, unlike NTA which provides single-particle analysis, DLS measures particles in bulk and is very sensitive to sample polydispersity, meaning that the presence of larger particles can obscure the scattering signals from smaller particles, leading to inaccurate size distributions. This limitation makes it challenging to analyse biological samples due to the high heterogeneity of EV populations and can lead to the underrepresentation of smaller particles in the analysis [102,103].

Flow cytometry is another powerful tool used for single-particle EV analysis based on light scattering. The laser beam is directed to the stream of fluid containing suspended particles, and the scattered light is captured by photodetectors to provide information on the size and granularity of the particles in the sample. Flow cytometry also enables fluorescent labelling of EV markers which can be measured

simultaneously with light scattering, therefore allowing for multi-parameter EV analysis and the identification and quantification of different populations of EVs present in the sample [101,102]. Although flow cytometry offers invaluable insights into EV characterisation, conventional flow cytometers lack sensitivity in the detection of particles smaller than 200 nm, leading to a substantial number of particles going undetected. An additional issue that may occur is when multiple particles pass through the laser beam at the same time, causing a “swarming” effect which leads to multiple EVs being counted as a single event and inaccuracies in measuring EV concentration [102,104]. Additionally, a low refractive index of EVs and challenges related to fluorescent labelling can also affect the analysis results. Some of these problems are being addressed by introducing a new generation of flow cytometers with improved sensitivity and resolution for detecting smaller particles, with emerging nano-flow cytometry technology enabling measurement of particles down to 40 nm in diameter [80,105]. Although this technology is not yet widely available and suffers some inherent drawbacks related to refractive index dependence and fluorescent labelling challenges, ongoing advancements in technology and methodologies offer new opportunities in EV research.

Unlike previous methods that rely on using laser beams for EV analysis, TRPS enables single-particle analysis by employing the Coulter principle, measuring transient changes in ionic current as particles pass through a non-conductive size-tunable nanopore (Figure 6a). By detecting these brief resistive pulses caused by passing particles, TRPS enables measurements of size, concentration and zeta potential of colloidal particles suspended in an electrolyte solution [102,105,106]. Measurement occurs in a fluid cell, which consists of an upper and lower fluid chamber, divided by a non-conductive nanopore. As negatively charged particles transverse the nanopore driven by a combination of pressure and voltage, they cause transient changes in the ionic current flowing through the pore, known as “blockage events” (Figure 6b). The characteristics of these blockage events, specifically their magnitude and duration (Figure 6c), are directly linked to the size and charge of the particles in the solution. The magnitude of the blockage is proportional to the particle’s volume, allowing for accurate size determination when calibrated against standard reference particles. The concentration of particles is derived from the frequency of these

blockages, while the duration of each blockage correlates to their zeta potential [100,106].

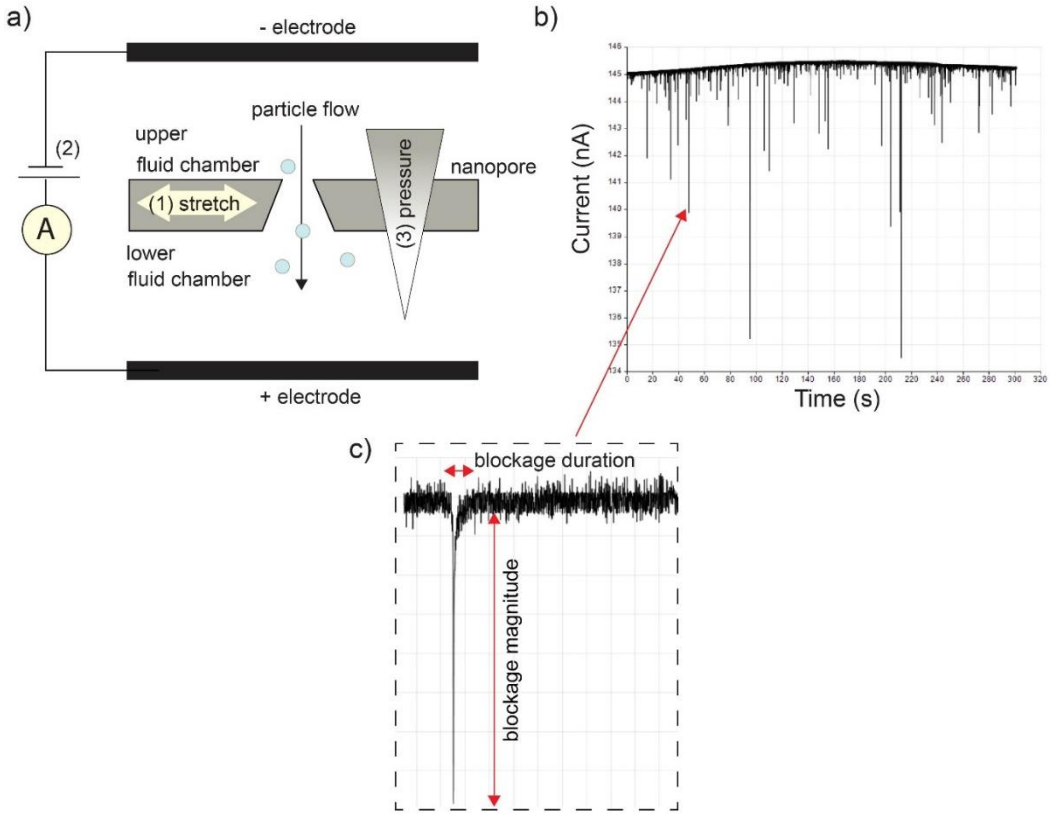

Figure 6. Principle of tunable resistive pulse sensing (TRPS) measurements. (a) The sample containing EVs is placed in the upper fluid chamber, and once the fluid cell is exposed to voltage and pressure, negatively charged EVs start moving towards the lower fluid chamber through the nanopore. As they transverse through the nanopore, they cause transient drops in ionic current. The magnitude and duration of these drops, which are in direct correlation with the size and charge of the nanoparticles, are used for determining size distributions, concentration and zeta potential of detected EVs. Tunable parameters that need to be optimised for each measurement are (1) stretch of the nanopore, (2) applied voltage and (3) pressure. (b) Signal trace of raw data obtained during TRPS measurement of EV-containing sample, with a (c) zoomed-in “blockage event” with denoted blockage magnitude and duration.

Simultaneous determination of size, concentration and surface charge, as well as “tunability” of the system to measure particles of a broad size range and independence of optical properties present the main advantages of TRPS for EV analysis. In addition, TRPS requires a very small volume of undiluted sample (<35 µL), making it suitable for studies where sample availability is limited [105,107].

Nevertheless, TRPS cannot differentiate different types of particles, such as EVs and lipoproteins, which can lead to misinterpretation of results if mixed populations are present in the sample [106]. Furthermore, measuring very small particles can require additional sample preparation to avoid any aggregation and contamination, which can lead to losses of EV populations in the process. Lastly, careful optimisation of parameters such as pore size, voltage and pressure, and proper system operation are essential for obtaining reproducible quality data and require an additional level of expertise, making it less user-friendly than some other commonly employed EV analysis methods [108].

1.4.2. Methods for Analysing EV Protein Composition

Analysis and quantification of EV cargo proteins are frequently done using more conventional and easily available methods, like western blotting and enzyme-linked immunosorbent assays, but complex techniques like mass spectrometry can also be employed for this purpose [45,109]. Whilst the detection of EV cargo proteins does not present such methodological issue as measuring EV size and concentration, problems regarding sample purity and contamination, low overall protein abundance and limited sensitivity of detection methods can present challenges in EV protein analysis. However, the main challenge in characterising EV protein composition again lies with EV heterogeneity. As stated earlier, there is still no universal EV marker, meaning that multiple markers must be used to confirm EV presence in the sample[43,45].

MISEV, first introduced in 2014 and subsequently updated in 2018 and 2023, presents guidelines for general characterisation and validation of the presence of EVs in the sample [43,99,110]. According to the latest MISEV2023, each EV research report should show the presence of the following: at least three positive EV markers, with at least one transmembrane or membrane-associated protein, such as tetraspanins CD9 or CD81, and one cytosolic protein with membrane-binding ability, like Alix and flotillins. Additionally, at least one marker of major components of non-EV structures that can co-isolate with EVs should be analysed as a purity control, including lipoprotein markers and albumin [43]. These pre-requirements should always be met before any further EV analysis.

1.4.3. Methods of EV Visualisation and Morphology Analysis

Along with quantification, size measurements and detection of EV markers, visualisation of EVs is a necessary step for definitive confirmation of their presence in the sample [43]. Visualisation techniques allow morphological analysis of the obtained EVs, help assess the purity of EV preparations and can facilitate quantitative assessments of EV populations. Frequently employed direct imaging methods include electron microscopy (EM) techniques, including scanning electron microscopy (SEM) and transmission electron microscopy (TEM), and scanning probe microscopy techniques, namely atom force microscopy (AFM) [78].

Although both EM techniques employ beams of electrons for visualisation, TEM generates an image by using transmitted electrons to reveal internal structures, while SEM analyses utilise scattered electrons to examine surface features [101]. Both TEM and SEM can achieve resolution as fine as 1 nm, thus overpassing the requirements needed for EV visualisation. However, TEM's high resolution is compromised by the need for sample fixation and dehydration, which can distort EV morphology, often resulting in a cup-shaped appearance instead of the round forms detected by SEM, which requires less complex sample preparation [78,101]. To avoid this issue, cryo-TEM offers a solution by preserving samples in vitreous ice at liquid nitrogen temperatures, thus avoiding the fixation and dehydration steps that lead to deformation. While this method produces low-resolution images, it captures the natural state of individual vesicles, allowing for more accurate visualisation of EVs [100,101]. Although TEM and SEM remain essential for assessing EV morphology and can provide size information, manual selection of imaging locations can introduce bias, making it difficult to estimate the overall population accurately, and are generally not suited for routine concentration assessments [101].

On the other hand, AFM offers imaging of the topography of EVs with nanometre resolution by employing a probe that interacts with the sample’s surface. As the probe deforms in response to morphological changes, the laser beam focused on the probe reflects its motion to the position-sensitive photodiode, allowing precise measurements of the surface topography. Beyond just imaging, AFM can assess biomechanical properties such as adhesion, elasticity, and stiffness of EVs, thus providing valuable information for evaluating their functional roles in biological processes [78,101,105].

Several AFM modes can be used, with contact and tapping modes being most prevalently utilised. In contact mode, the tip of the probe stays in continuous contact with the sample surface, while in tapping mode, the probe oscillates across the sample surface and only intermittently touches the sample. Even though contact mode provides the fastest measurements, the probe can damage the EVs. Thus, tapping modes are favoured for acquiring images of EVs in their unaltered state. Additionally, AFM can be performed in both air and liquid environments. Although imaging in the air requires less optimisation, it can lead to shrinking and deforming of EVs during sample preparation. Contrarily, imaging in liquid does not require drying of the sample and enables the visualisation of EVs in their native state. The sample is simply placed on a substrate, usually mica, previously functionalised with a coating like poly-L-lysine or nickel (II) chloride, which ensures a positively charged surface that binds negatively charged EVs. Hence, AFM in a liquid environment is considered a preferred method for visualising native EV morphology [78,101]. Still, AFM is a low-throughput technique requiring skilled operation and complex set-up, and provides limited ability to visualise internal structures, but can provide valuable information when used in conjunction with other methods.

2. RESEARCH GOAL

The research of EVs is evolving into a rapidly growing field, with many potential areas of application ranging from basic research to patient care. Due to their unique ability to reflect the condition of the originating cells and tissues, the search for EV-derived biomarkers is attracting a lot of attention in the research. EV's role in the central nervous system is particularly interesting since exosomes, a class of small EVs, can pass the blood-brain-barrier, meaning that CNS-derived exosomes could be detected in blood samples, providing input on the condition of the brain in a non-invasive manner. Such property could be of particular use in the diagnostics and treatment of various CNS disorders, including traumatic brain injury. However, the translation of basic findings is hindered due to major inconsistencies in the field and lack of standardisation in exosome isolation, purification and characterisation. Moreover, working with CSF presents an additional challenge due to low exosome and protein concentrations as well as small sample volumes available for analysis.

The research hypothesis was that SEC can be successfully employed to isolate morphologically unaltered exosomes from CSF with sufficient purity, concentration, and total amount necessary for further molecular analysis. Since there are no available methods for such isolation, the specific objectives are to:

1. create a biobank of CSF samples from TBI patients;
2. detect and compare exosome protein markers in collected CSFs;
3. establish several different SEC for isolation of exosomes from CSF;
4. introduce the TRPS method for concentration measurement of isolated exosomes
5. characterize the molecular content of isolated exosomes and confirm their presence in the sample by TEM;
6. compare and suggest the most effective SEC method for the isolation of exosomes from CSFs

3. PATIENTS, MATERIALS AND METHODS

3.1. Patients

The research enrolled three adult patients suffering from severe TBI treated at the intensive care unit of the Clinical Hospital Centre Rijeka and Pula General Hospital in Croatia, who underwent ventriculostomy as part of their treatment for monitoring and managing their ICP levels. The study received approval from the Ethics Committee of the Clinical Hospital Centre Rijeka (Class: 003-05/19-1/57, Registry No.: 2170-29-02/1-19-2), the Ethics Committee of Pula General Hospital (Registry No.: 4943/19-1), and the Ethics Committee for Biomedical Research at the Faculty of Medicine, University of Rijeka (Class: 007-08/22-01/61, Registry No.: 2170-24-04-3/1-22-3).

Given the patient's altered state of consciousness and the use of analgosedation during intensive care a family member or the patient's legal representative provided informed consent. A member of the study team thoroughly explained the research objectives, the sampling procedure, and any potential risks associated with the study prior to obtaining consent. Eligible patients were aged between 18 and 80 years and did not have any prior immunological, malignant, or chronic inflammatory diseases. The research adhered to the principles outlined in the Declaration of Helsinki as well as local laws and regulations.

3.2. Materials

3.2.1. Chemicals

All chemicals used in this study are listed in Table 2.

Table 2. Chemicals used in this study.

Chemical	Producer
2-mercaptoethanol	Sigma-Aldrich, St. Louis, MS, USA
Acetic acid	Kemika, Zagreb, Croatia
Acrylamide/Bisacrylamide 29:1, 30%	Alfa Aesar, Ward Hill, MA, USA

Ammonium persulfate	Sigma-Aldrich, St. Louis, MS, USA
Bovine serum albumin (BSA)	Roche Diagnostics, Mannheim, Germany
Bromphenol blue	Sigma-Aldrich, St. Louis, MS, USA
Ethanol 96-100%	Sigma-Aldrich, St. Louis, MS, USA
Glutaraldehyde (GA), 25% aqueous solution	Spi Chem, West Chester, PA, USA
Glycerol	Sigma-Aldrich, St. Louis, MS, USA
Glycine	Carl Roth, Karlsruhe, Germany
Hydrochloric acid (HCl)	Kemika, Zagreb, Croatia
Methanol	Kemika, Zagreb, Croatia
N, N, N', N'-Tetramethyl ethylenediamine (TEMED)	Sigma Aldrich, St. Louis, MS, USA
Paraformaldehyde (PFA), 32% aqueous solution	Electron Microscopy Sciences, Hatfield, PA, USA
Ponceau S	Sigma-Aldrich, St. Louis, MS, USA
Sodium chloride	Kemika, Zagreb, Croatia
Sodium dodecyl sulfate (SDS)	Sigma-Aldrich, St. Louis, MS, USA
Tris base	Sigma-Aldrich, St. Louis, MS, USA
Tween 20 (Polysorbate 20)	Sigma-Aldrich, St. Louis, MS, USA
Uranyl acetate	Spi Chem, West Chester, PA, USA
Water, HPLC grade	VWR, Radnor, PA, USA

3.2.2. Solutions

5× Laemmli buffer

1M Tris HCl pH 6.8, 50% glycerol (v/v), 10% SDS (w/v), 0.05% bromophenol blue (w/v), 2-mercaptoethanol

1× Running buffer

25 mM Tris, 192 mM glycine and 0.1% SDS (w/v), pH 8.3

1x Transfer buffer

25 mM Tris, 192 mM Glycine, 20% methanol (v/v)

10% and 12% SDS-PAGE separating gel solution

10% or 12% Acrylamide/Bisacrylamide (v/v), 375 mM Tris (pH 8.8), 0.1% SDS (v/v), 0.1% APS (v/v), 0.05% TEMED (v/v)

SDS-PAGE stacking gel solution

5% Acrylamide/Bisacrylamide (v/v), 126 mM Tris (pH 6.8), 0.1% SDS (v/v), 0.1% APS (v/v), 0.05% TEMED (v/v)

Ponceau S staining solution

0.1% Ponceau S (w/v) in 5% acetic acid (v/v)

Tris-buffered saline (TBS)

20 mM Tris and 150 mM NaCl

TBS-T

0.1% Tween20 (v/v) in TBS

Blocking buffer

5% nonfat dry milk (w/v) in TBS

Antibody dilution buffer

5% BSA (w/v) in 1x TBS-T

PFA solution

6% PFA (v/v) in PBS

GA solution

3% GA (v/v) in PBS

Uranyl acetate solution

0.5% uranyl acetate (w/v) in redistilled water

3.2.3. Reagents and Materials

All reagents and materials used in this study are listed in Table 3.

Table 3. Reagents and materials used in this study.

Reagent	Producer	Catalogue number
Acrylamide/Bisacrylamide 29:1, 30%	Thermo Scientific Alfa AesarKandel, Germany	15475549
formvar/carbon-coated, 200-mesh copper grid	Ted Pella, Redding, CA, USA	NC0205992
Bio-Rad column	Bio-Rad Laboratories, Hercules, CA, USA	7374155
Bio-rad flow adaptors	Bio-Rad Laboratories, Hercules, CA, USA	7380016
Blotting Grade Blocker Nonfat dry milk	Santa Cruz, Dallas, USA	SC-2325
Carboxylated polystyrene beads, 200 nm	Izon Science, Christchurch, New Zealand	CPC200
Carboxylated polystyrene beads, 350 nm	Izon Science, Christchurch, New Zealand	CPC400
Chromafil Xtra RC-20/13 (0.20 µm cellulose syringe filters)	Macherey-Nagel, Düren, Germany	729236
Chromafil Xtra MV-45/25 (0.45 µm cellulose syringe filters)	Macherey-Nagel, Düren, Germany	729204
Nitrocellulose membrane, 0.2	GE Healthcare Life Science, Uppsala, Sweden	1620112
NP200 nanopore	Izon Science, Christchurch, New Zealand	NP200
NP400 nanopore	Izon Science, Christchurch, New Zealand	NP400
Phosphate-buffered saline (PBS), sterile	Gibco, Grand Island, NY, USA	10010031

Protein LoBind Tube (low-protein-binding tubes) 1.5 mL	Eppendorf, Hamburg, Germany	022431081
Protein LoBind Tube (low-protein-binding tubes) 2 mL	Eppendorf, Hamburg, Germany	022431102
Protein standard (PageRuler Prestained Protein Ladder)	Thermo Scientific, Waltham, MA, USA 26616	26616
Sephacryl S-400 HR	Cytiva, Uppsala, Sweden	17-0609-10
Sepharose CL-6B	GE Healthcare, Uppsala, Sweden	17-0160-01
SignalFire Elite ECL	Cell Signaling Technology, Danvers, MA, USA	12757
SignalFire Plus ECL	Cell Signaling Technology, Danvers, MA, USA	12630
Superose 6 Prep Grade	Cytiva, Uppsala, Sweden	17-0489-01
TRPS reagent kit	Izon Science, Christchurch, New Zealand	RK3
qEV10/70 nm column	Izon Science, Christchurch, New Zealand	IC10-70

3.2.4. Antibodies

All antibodies used in this study are listed in Table 4. All antibodies were purchased from Cell Signaling Technology, Danvers, MA, USA

Table 4. Antibodies used in this study.

Antibody	Catalogue number
mouse monoclonal anti-human apolipoprotein AI	3350
rabbit monoclonal anti-human albumin	4929
rabbit monoclonal anti-human apolipoprotein E	13366
rabbit monoclonal anti-human CD9	13174

rabbit monoclonal anti-human CD81	56039
rabbit monoclonal anti-human Flotillin-1	18634
anti-mouse horseradish peroxidase-linked antibody	7076
anti-rabbit horseradish peroxidase-linked antibody	7074

3.3. Methods

3.3.1. Cerebrospinal Fluid Sampling and Storing

Human CSF samples were collected in accordance with bioethical standards, ensuring the confidentiality of patient data to uphold medical privacy. The study was conducted following the Nuremberg Code, the most recent revision of the Declaration of Helsinki, and other pertinent guidelines, thereby adhering to all relevant ethical and bioethical principles, including beneficence, non-maleficence, autonomy, and justice, along with associated principles such as privacy and trust.

The CSF samples were collected from the collection chamber of the EVD system using 10 mL sterile syringes in aseptic conditions by a qualified physician. Samples were taken every 24 hours for the first three days following the injury, aliquoted into low-protein-binding tubes, transported on ice and stored at −80 °C. The sampling occurred during the years 2020 and 2021, with each sample undergoing no more than two freeze-thaw cycles.

3.3.2. Size-Exclusion Chromatography

Sepharose CL-6B, Sephacryl S-400 HR, and Superose 6 Prep Grade resins were packed into individual glass columns measuring 1.5 × 50 cm, fitted with a 30 µm frit at the bottom of the column and flow adaptors. Each column was packed with approximately 75 mL of resin using distilled water under gravity flow. Columns were subsequently washed with a minimum of three bed volumes of distilled water and equilibrated with two bed volumes of sterile PBS as the running buffer before the initial

SEC run. The commercial qEV10/70 nm column was washed and equilibrated in PBS prior to SEC run according to the manufacturer's guidelines.

To prepare the CSF-pool for SEC, equal volumes from nine CSF samples collected from three patients with severe TBI were combined and aliquoted in 2 mL low-protein-binding tubes. In initial SEC runs required for establishing a protocol for SEC and subsequent nanoparticle and protein analysis, a total volume of 1.4 mL of CSF-pool was loaded on Sephacryl S-400 and Superose 6 PG packed columns using a sterile 5 mL plastic syringe, and 60 1.5 mL fractions were collected in low-protein-binding tubes per each run. The first 15 mL of initial flow through were discarded to eliminate the dead volume effect. For later analysis and SEC comparison, a total volume of 2.8 mL from this CSF pool was loaded onto each of the four columns. Samples were loaded using a sterile 5 mL plastic syringe, and 50 1.5 mL fractions were collected in low-protein-binding tubes for each run. The first 5 mL of initial flow through were discarded.

The running buffer was placed 20 cm above the columns and delivered to the columns by gravity flow. All SEC separations were conducted at room temperature. Between SEC runs, the columns were rinsed with at least two bed volumes of PBS.

3.3.3. Western Blot

Individual CSF samples, the CSF-pool or collected SEC fractions were combined with reducing 5x Laemmli buffer and heated at 95 °C on a thermoblock for 10 min. 25 µL of individual CSF samples and the CSF-pool, or 200 µL from the SEC fractions, were separated on handcast 10% or 12% polyacrylamide gels in 1× running buffer under variable voltage conditions (90-150V). Sodium dodecyl sulfate-polyacrylamide gel electrophoresis (SDS-PAGE) of individual CSF samples was performed on mini-format gels using Mini-PROTEAN Tetra cell system (Bio-Rad, Hercules, CA, USA) in 1x running buffer, while separation of SEC fractions was conducted using on large-format gels using PROTEAN II xi cell system (Bio-Rad, Hercules, CA, USA) in 1x running buffer, with cooling from continuous running of tap water through the system core. Separated proteins were transferred to a 0.2 µm nitrocellulose membrane (Global Life Sciences Solutions Operations UK Ltd., Little Chalfont, UK) under a constant voltage of 20 V for 35 minutes using a semi-dry transfer

unit (Hoefer, San Francisco, CA, USA) or under 70 V for 90 minutes using a wet transfer unit (Bio-Rad, Hercules, CA, USA) with cooling, in 1x transfer buffer.

After transfer, membranes were placed in Ponceau S staining solution and incubated with blocking solution for 10 minutes at room temperature. Membranes were then probed overnight in antibody dilution buffer with primary antibodies (diluted 1:1000). After washing the membranes three times for five minutes in 1x TBS-T on the following day, membranes were incubated with appropriate secondary antibodies diluted in antibody dilution buffer (1:2000) on a shaker for 30 minutes at room temperature. Following additional three 5-minute washes in TBS-T, proteins were visualised using SignalFire Elite ELC Reagent or SignalFire Plus ECL Reagent and captured using imagers ImageQuant LAS 500 (GE Healthcare Bio-Sciences AB, Uppsala, Sweden) and C-Digit Blot Scanner (LI-COR Biosciences, Lincoln, NE, USA).

3.3.4. Slot Blot

Collected SEC fractions were combined with 5x Laemmli buffer without glycerol and heated at 95 °C on a thermoblock for 10 min. The nitrocellulose membrane was immersed in distilled water and applied in a slot blot apparatus (Hoefer Scientific Instruments, San Francisco, CA, USA). 200 µL of each prepared SEC fraction sample was loaded into an appointed slot and transferred to the membrane using a vacuum pump. Once samples had been completely pulled through the membrane, slots were rinsed three times with 1 mL of sterile PBS per slot. Once all of the buffer had been pulled through, the membrane was removed from the slot-blot apparatus and placed in Ponceau S staining solution, followed by incubation in the blocking solution for 10 minutes at room temperature. Membranes probing and signal detection was performed as described previously for the western blot protocol.

3.3.5. Tunable Resistive Pulse Sensing

TRPS measurements of nanoparticle concentrations and size distributions in collected SEC fractions were performed using a qNano Gold Measurement System (Izon Science, Christchurch, New Zealand) (Figure 7), using size-tunable nanopores

NP150 and NP400. The instrument was controlled through Control Suite 3.4 software (Izon Science, Christchurch, New Zealand). For every measurement session, the fluid cell and nanopore had to be prepared and properly set up before calibration and sample measurements. Measuring electrolyte (ME), wetting solution (WS), and coating solution (CS) were bought as a part of the TRPS Reagent Kit and prepared as per the manufacturer's instructions. All solutions were filtered through a 0.22 µl filter before each application and kept at 4 °C for no more than 7 days.

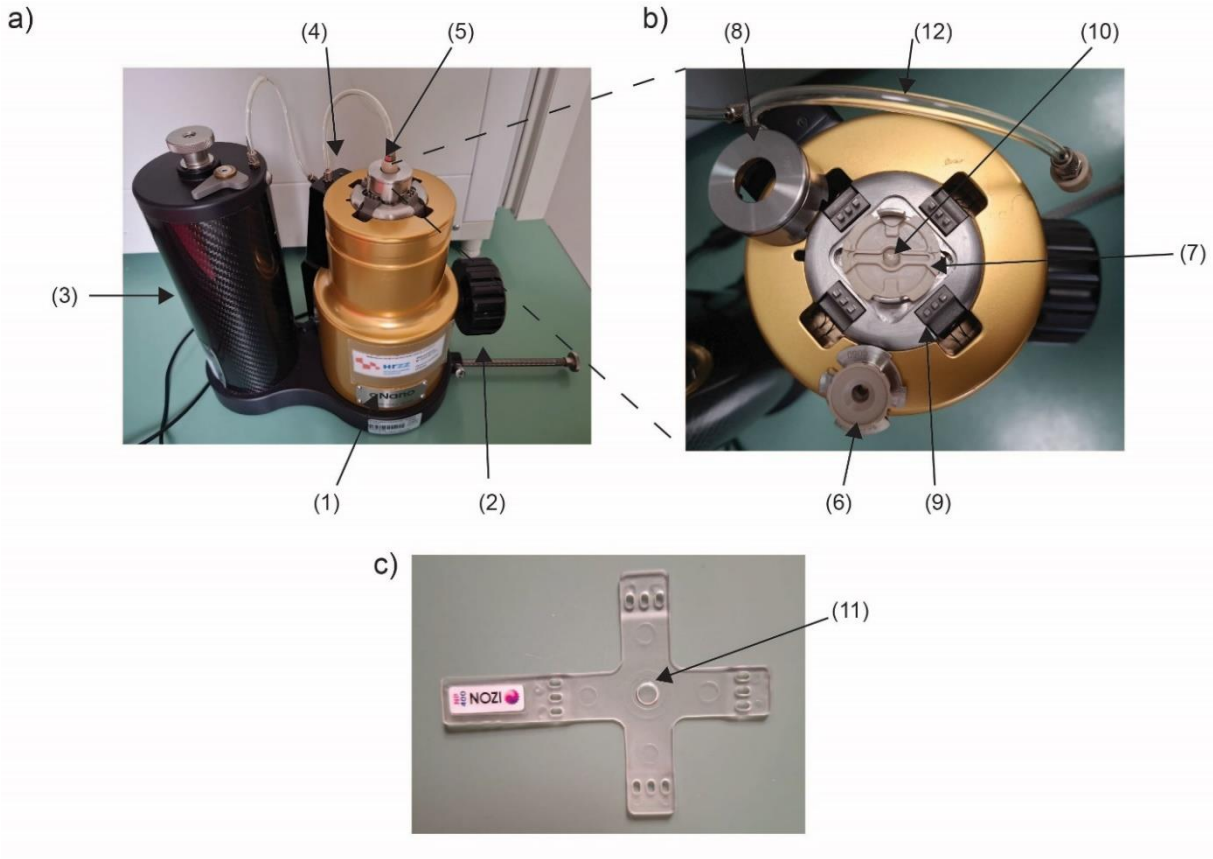

Figure 7. The main elements of Izon's qNano Gold instrument for TRPS measurement. a) The qNano Gold instrument consists of a qNano body (1), which contains electronics and a stretcher unit (2), a variable pressure module (3), a pressure reading module (4), and a fluid cell (5). b) The fluid cell positioned on the top of the qNano body consists of an upper (6) and lower fluid chamber (7), a shielding fluid cell cap (8), and a nanopore stretching arms (9). TRPS measurements are performed on (c) a polyurethane nanopore with a defined pore size range attached to the nanopore stretching arms, with the septum (11) of the nanopore taking place right above electrode paste (10) located in the middle of the lower fluid chamber. The upper fluid chamber is then assembled onto the lower fluid chamber, the shielding fluid cell cap is clicked into place, and the fluid cell is connected to the variable pressure unit by polymer tubing (12).

For the preparation of the fluid cell, both the upper and lower fluid chambers were rinsed with deionised water, dried with compressed air, and wiped with lint-free wipes. The lower fluid cell was loaded with 75 µl of 70% ethanol for 30 seconds and then displaced with 75 µl of ME. ME was pipetted out of the lower fluid cell before the nanopore was then fitted on the instrument and stretched to 47.0 mm. Once properly fitted, the nanopore was wetted using a WS by adding it to both the lower (75 µl) and upper chamber (35 µl) of the fluid cell and applying maximal pressure (20 mbar) for 2 minutes. If at the end of this step stable baseline current of at least 50 nA and low RMS noise (<15 pA) was achieved, the next step was proceeded with. If these conditions were not met, the procedure was repeated at a higher stretch.

In the next step, nanopores were coated using CS to prevent non-specific binding of proteins to the nanopore, which is a necessary step when performing measurements on biological samples. After rinsing and drying the upper fluid chamber from WS with deionised water, CS was applied in both the upper (35 µl) and lower chamber (75 µl) of the fluid cell, and maximal pressure was applied for 10 minutes. Finally, after another rinsing and drying, ME was applied in both chambers of the fluid cell to equilibrate the nanopore under maximal pressure for 10 minutes. If the achieved baseline current was satisfactory, the calibration of the nanopore and sample measurements followed.

For calibration, 100 nm and 350 nm carboxylated polystyrene beads (CPC100 and CPC400) were used, diluted 1:1000 in ME. Calibration beads were thoroughly vortexed before measurements. Calibration runs were performed under pressure conditions of 6 mbar and 3 mbar. Nanopore stretch and applied voltage were then optimised to ensure the same resolution range of 185-740 nm and a current of approximately 135 nA was used at all times, allowing comparability between different measurements. The exception were measurements performed with NP150 nanopore, when the resolution range was set to 70-280 nm. The fluid chamber was then rinsed with both deionised water and ME to ensure no contamination with calibration particles before introducing the samples. After confirming that the obtained rate plots were linear, with measurements performed at higher pressure exhibiting higher rate, sample were measured.

For sample measurements, analysed SEC fractions were suspended in ME in a 1:1 ratio. For each measurement, 35 µl of diluted sample was placed in the upper

fluid chamber, the shielding cap was clicked in place and the fluid cell was connected to the variable pressure module. SEC samples were then measured for 5 minutes at higher pressure (6 mbar) under identical system settings as calibration measurements. If particle count exceeded 500 in 5-minute measurement, an additional measurement was conducted at lower pressure of 3 mbar for another 5 minutes. Between each sample changeover, the nanopore was flushed with ME at least three times at the maximal pressure to prevent cross-contamination. ME from the lower fluid chamber was also replaced between sample changes. The same concentration fraction of 185 to 740 nm was applied for all measurements before any data analysis, meaning that only the nanoparticles within that range would be counted in the calculation, while the outliers will be excluded. Particle concentration and size distribution were calculated only for TRPS-positive fractions that recorded at least 500 nanoparticles under both pressure conditions during 5-minute recordings. Measurements yielding fewer than 500 nanoparticles in that time frame were classified as negative, and the corresponding fractions were labelled as TRPS-negative. All measurements were performed in duplicate for each set of SEC samples.

3.3.6. Zeta Potential Measurement

The zeta potential measurements were also performed using qNano Gold instrument. Only TRPS-positive fractions (described in the 3.3.5. section) were included for zeta potential analysis. Fluid cell and nanopore preparation followed the same protocol described earlier in 3.3.5. section. Measurements were conducted on NP400 nanopore, and initial calibration was performed using CPC400 calibration beads at pressure setting of 0 mbar and three applied voltages, producing a corresponding baseline current of approximately 85, 110 and 140 nA. Additional measurement was then performed at the second pressure setting of 0.5 mbar using the highest voltage from the previous step. Sample measurements were carried out at the maximum calibration voltage and pressure. The recording was stopped when the particle count exceeded 500 particles for each measurement.

3.3.7. Transmission Electron Microscopy

To prepare the samples for transmission electron microscopy (TEM), chosen TRPS-positive SEC fractions were suspended and fixed in an equal volume of PFA solution in GA solution for 15 min at room temperature. A 10 µL drop of the resulting fixed sample (in 3% PFA/1.5%GA) was then loaded to formvar/carbon-coated 200-mesh copper grid placed on parafilm in a Petri dish for 60 min, incubated on ice in a humidified atmosphere. Following the incubation, excess liquid was blotted off using filter paper. The grids were then briefly stained with uranyl acetate solution to enhance contrast. Next, the grids were rinsed three times in 200 µL drops of distilled water and allowed to air dry. Once dried, the grids were examined using a 120-kV transmission electron microscope (JEM-2100 EXII, JEOL, Tokyo, Japan).

3.3.8. Statistical and data analysis

Quantification of chemiluminescent signals from western blot and slot blot were performed using ImageQuantTL v10.2 software (GE Healthcare Bio-Sciences AB, Uppsala, Sweden) and Image Studio Digits software (LI-COR Biosciences, Lincoln, NE, USA). Arbitrary units obtained by quantification of a single membrane were normalised against the highest value and plotted as percentages. Ponceau S staining was quantified using ImageJ open-source image processing programme. Processing raw data from TRPS measurements was done using Control Suite 3.4 software (Izon Science, Christchurch, New Zealand).

Statistical analysis was conducted with GraphPad Prism 8 (version 8.0.1, GraphPad Software Inc., San Diego, CA, USA). The Shapiro–Wilk test was employed to evaluate the normality of data distributions, followed by one-way ANOVA with a post-hoc Tukey test. The statistical significance level was established at $p < 0.05$.

Graphs were generated using GraphPad software (version 8.0.1, GraphPad Software Inc., San Diego, CA, USA). All figures were prepared using Adobe Illustrator CC 2015 (Adobe Systems Inc., San Jose, CA).

4. RESULTS

4.1. Clinical Features of Severe Traumatic Brain Injury Patients

Three patients with severe TBI, 2 males and 1 female, who required the placement of EVD as part of their treatment for ICP monitoring and management in the intensive care unit were included in this study. The clinical diagnosis was determined through physical examination, neuroradiological assessments and GCS score. Patients median age was 44 years, with an age range between 42 and 49 years. GCS score at admission ranged from 3 to 5, and a Glasgow outcome scale (GOS) score of 4 was assessed three months after discharge (Table 5).

Table 5. Clinical presentation of patients suffering from severe traumatic brain injury included in the study.

Patient	Age	Gender	Mechanism of injury	GCS[1] at admission	GCS[1] at discharge	GOS[2] three months after discharge	Intracranial pathology
1	44	M	Fall from height	3	14	4	Epidural haematoma
2	49	F	Motor vehicle accident	5	14	4	Intracerebral haematoma, traumatic subarachnoid haemorrhage
3	42	M	Motor vehicle accident	3	14	4	Traumatic subarachnoid haemorrhage, concussion foci, frontal, temporal, occipital

[1]GCS – Glasgow Coma Scale, [2]GOS – Glasgow Outcome Scale

One patient sustained severe TBI from a fall from height, and the other two as a result of motor vehicle accidents. The pathoanatomical features and structural alterations were identified using neuroradiological procedures. Traumatic subarachnoid haemorrhage was observed in two patients. One of them also suffered an intracerebral haematoma, and the other sustained a concussion with damage to frontal, temporal and occipital lobes. The third patient was diagnosed with isolated epidural haematoma.

4.2. Extracellular Vesicles and Lipoproteins Are Found in Intracranial Cerebrospinal Fluid Three Days After Traumatic Brain Injury

As a part of an initial assessment of the collected samples and the CSF pool, both individual CSF samples and the generated CSF-pool were analysed for the presence of exosomes, lipoproteins, and albumin as a blood contamination indicator in the samples by western blot analyses. A CSF-pool was created by combining nine CSF samples collected during the first three days after the injury. Specifically, samples were screened for exosome markers CD9 and CD81, apolipoproteins AI and E, and blood content was assessed by detected albumin levels (Figure 8).

The analysis of individual samples revealed that albumin was the most abundantly present out of the tested proteins in the samples. Following were lipoprotein markers ApoAI and ApoE, which were detected in comparable levels, and exosomal markers CD9 and CD81 displayed the lowest expression levels. When comparing patients based on protein kinetics, albumin was consistently detected in high levels across all three days in all three patients, with only Patient 2 (Pt2) exhibiting a lower amount in the day (d) 3 sample. In contrast, fluctuations in ApoE kinetics were much more prominent between patients. Pt1 exhibited intermediate ApoE expression levels on d1, which decreased on d2 and 3. Meanwhile, strong ApoE signal was observed in samples from both Pt2 and Pt3 on d1 and 2, but it became barely detectable on d3. Low to moderate levels of ApoAI were observed in all individual CSF samples. Exosome protein markers CD81 and CD9 were generally present at similar levels in all three patients over the three-day period, apart from the sample from Pt2 on d3, where no signal was detected for CD9.

Lastly, the analysis of the CSF-pool generated from individual samples revealed detectable levels of all analysed proteins, confirming the presence of free proteins, lipoproteins and exosomes in the pooled sample.

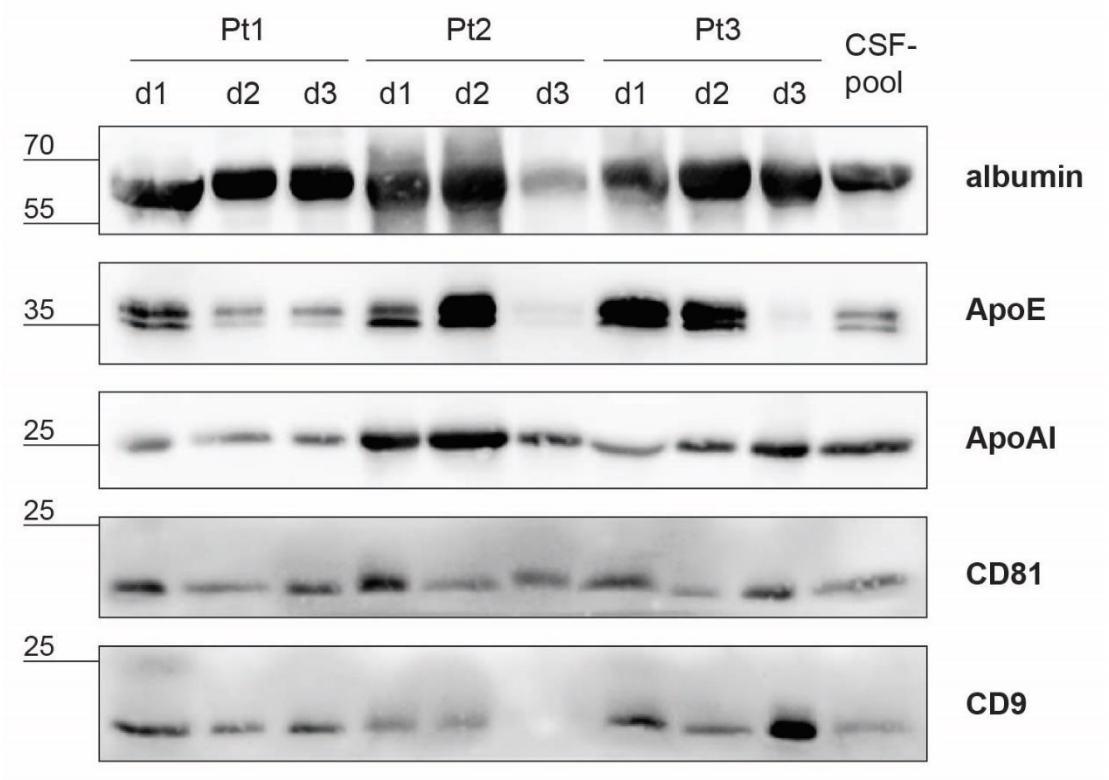

Figure 8. Western blot analysis of intracranial cerebrospinal fluid (CSF) collected during the first three days after severe traumatic brain injury (sTBI) revealed the presence of exosomes, albumin and lipoproteins in CSF. To create a CSF sample for further exosome isolation by size-exclusion chromatography (SEC), individual CSF samples collected from three patients (Pt) in the course of the first three days (d) after sTBI were combined in equal volumes. Western blot of individual samples and CSF-pool, equalled by volume, were probed with antibodies against albumin, lipoprotein markers ApoE and ApoAI and exosome markers CD81 and CD9. The molecular weights of the detected bands are shown in kilodaltons (kDa).

4.3. Establishing In-House Protocols for Size-Exclusion Chromatography and Nanoparticle Quantification

The initial phase of the study involved developing an in-house protocol for exosome isolation by SEC and a protocol for quantifying nanoparticles by TRPS in SEC fractions. A key decision in this development process was adopting a gravity-flow system. This approach was selected to mitigate the potential risks of exosomal damage associated with pressure-driven flow in conventional liquid chromatography instruments, ensuring the integrity of isolated exosomes. Opting for a gravity-flow system necessitated the use of an empty column but also enabled the choice of a resin for column packing since a number of SEC resins were not commercially available in prepacked columns. Furthermore, SEC resins broadly differ in their properties and are primarily developed for protein separation, while only some were tested for exosome isolation from human biofluids. Therefore, suitable candidates for SEC resin were selected based on published studies describing exosome isolation from human body fluid samples and their commercial availability, taking into consideration appropriate features, including resin particle size, fraction range and exclusion limits (Table 6). Based on published data and the conducted comparison of resin characteristics, Sepharose CL-6B, Sephacryl S-400 and Superose 6 PG SEC resins, as well as the commercial ready-to-use qEV10/70 nm column, were selected for exosome isolation.

Table 6. Properties of different size exclusion chromatography (SEC) resin candidates for exosome isolation. The literature search was performed on October 10th, 2020, and only studies performed on human samples until that date were considered. Highlighted in grey are the resins selected for this study.

Resin/ column	Polymer type	Particle size[1] [µm]	Fractionation range (Mr)[2] [kDa]	Exclusion limit[3] [nm]	Previously employed for SEC isolation from:
Sepharose CL-6B	6% cross-linked agarose	40 – 165	10 – 4 000	24	none

Sephacryl S-400	Cross-linked allyl dextran and N,N'-methylene bisacrylamide	25 – 75	20 – 8 000	31	Plasma [90]
Superose 6 PG	Cross-linked agarose	30 – 40	5 – 5000	29	none
qEV10//70 nm	Polysaccharide resin	n/a	n/a	n/a	CSF [111], serum [112], urine [113], saliva [114] milk [115]
Sepharose 2B	2% agarose	60 – 200	70 – 40 000	n/a	Plasma [90,116]
Sepharose CL-2B	2% cross-linked agarose	60 – 200	70 – 40 000	75	Plasma [89,117], serum [118], urine [98,98,119]
Sepharose CL-4B	4% cross-linked agarose	45 – 165	60 – 30 000	42	Plasma [90], urine [120]
Sepharose S-500	Cross-linked allyl dextran and N, N'-methylene bisacrylamide	25 – 75	n/a, for DNA and dextrans	42	Synovial fluid [121], milk [122]

[1] diameter of resin particles
[2] molecular weights for globular proteins
[1,2] values from data sheets provided by manufacturers
[3] resin pore size according to [95]

After selecting a suitable SEC resin, the next step involved choosing an appropriate empty column for packing. A glass column was chosen for this purpose, with a length exceeding the standard dimensions of most commercially prepacked columns, as well as the majority of prepacked columns designed for liquid chromatography instruments.

The extended column length was selected to optimize the path of the SEC separation, as column length plays a critical role in defining the separation process and significantly influences the resolution and overall quality of the separation (Figure 9).

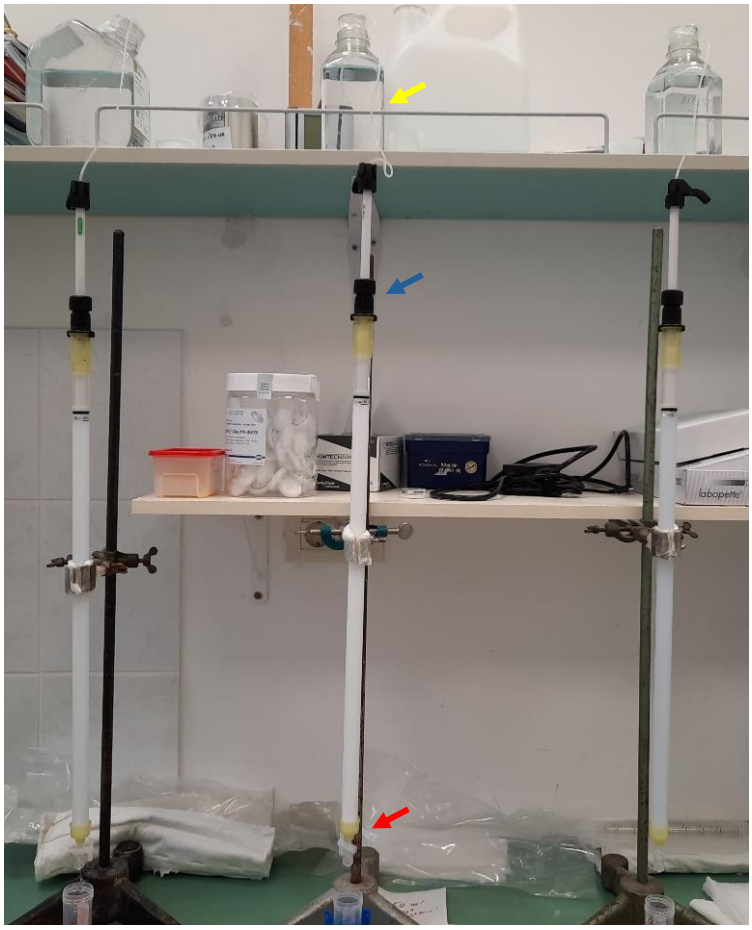

Figure 9. Display of in-house size-exclusion chromatography (SEC) set-up for exosome isolation. SEC was performed on glass chromatography columns equipped with porous polymer bed support at the bottom of the columns (red arrow) and packed with Sepharose CL-6B, Superose 6PG. and Sephacryl S-400. Elution was driven by gravity flow, and the eluent was delivered continuously from the mobile phase reservoir (yellow arrow) to the column through a tube connected by an adaptor (blue arrow).

In the next phase of SEC setup, the parameters for SEC were systematically determined, including the sample loading volume ranging from 1.4 – 2.8 mL, and the total elution volume ranging from 50 – 60 SEC fractions of 1.5 ml to be collected. A slot blot protocol was also established, specifying the SEC fraction volume to be loaded on the nitrocellulose membrane, whereby 50 µL was sufficient for the Ponceau S staining. However, immunodetection of exosome and lipoprotein markers required a larger

volume of SEC fraction to be loaded on the nitrocellulose membrane. Therefore, detection methods were optimized using Ponceau S staining for total protein visualization and immunodetection for exosome markers CD9 and CD81 (Figure 10).

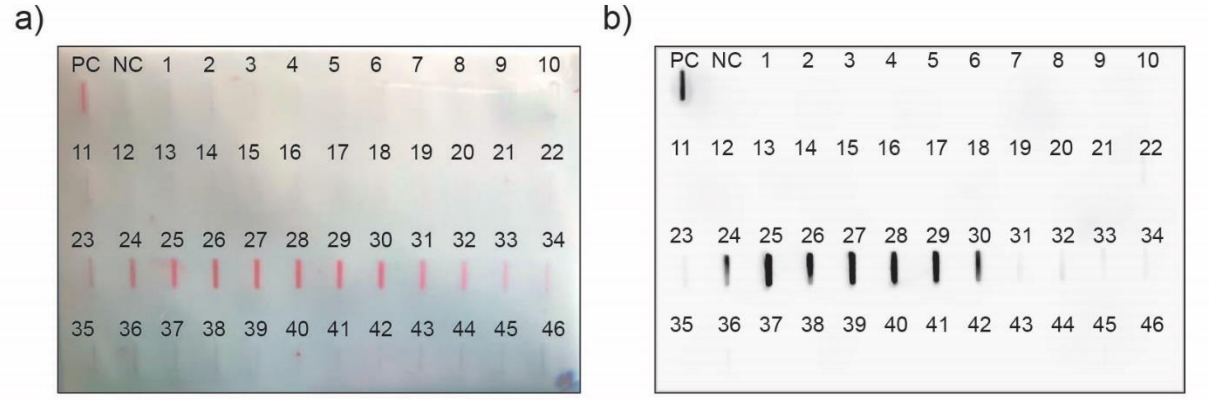

Figure 10. Free proteins and albumin co-elute in the same fractions after size-exclusive chromatography separation of the cerebrospinal fluid sample. Pooled CSF sample was separated using Sephacryl S-400 column, and collected fractions were analysed by slot blot. Shown are images of (a) Ponceau S staining (b) immunodetection of albumin. CSF-pool and PBS (SEC mobile phase) were used as positive (PC) and negative (NC) control.

To establishing a protocol for detection of nanoparticle-enriched fractions, we decided to employ TRPS. However, TRPS requires careful optimisation to ensure accurate and reproducible exosome analysis. Key to this is the selection of the appropriate TRPS nanopore, which must match the size range of the nanoparticles present in the analysed sample to provide optimal resolution and sensitivity, since the pore size determines the detectable size range while minimising the interference from smaller particles or aggregates. Additionally, tunable elements, including applied voltage, pressure and stretch of the nanopore, need to be fine-tuned according to the sample to ensure the system maintains stability, reduce noise and improve signal clarity.

To determine which TRPS nanopore and measurement conditions would be suitable for our exosome detection protocol, two TRPS nanopores weretested , NP400 and NP150, tuned for detection of nanoparticles ranging from 70 – 280 nm and 185 – 740 nm, respectively. For the initial testings, 1.4 mL of CSF-pool sample was separated using the Superose 6 PG column. Since exosomes are expected to elute prior to soluble proteins in SEC, collected SEC fractions were screened by slot blot and

immunodetection of albumin to determine the range of fractions that will be tested by TRPS. Albumin signal was detected from fraction 24 onwards (Figure 11), and the initial 23 fractions were subjected to TRPS analysis. During the screening, fractions were recorded in two pressure conditions for two minutes, and an admissible particle count of >100 particles/min was observed in only 1 matching fraction for both TRPS nanopores, thus confirming peak nanoparticle SEC fraction using both tested nanopores.

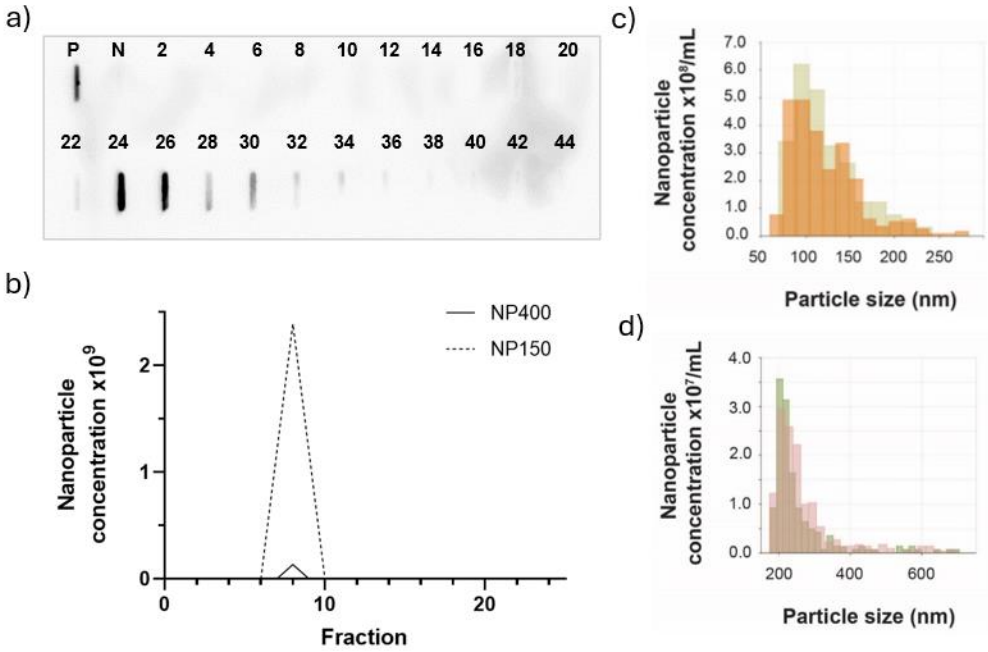

Figure 11. Nanoparticle-peak fraction is successfully detected by tunable resistive pulse sensing (TRPS) using both tested nanopores. Pooled CSF sample was separated using Superose 6 PG column and collected SEC fractions were analysed by slot blot and TRPS. SEC fractions that eluted prior to albumin were screen-tested with two TRPS nanopores detecting different-sized nanoparticles. A fraction was considered TRPS-positive if the particle count exceeded 100 particles/min detected during the 5-minute measurement. Fractions with a lower rate of nanoparticle detection by TRPS, and thus with less than 500 nanoparticles detected, were categorised as TRPS-negative. Shown is (a) immunodetection of albumin on evenly numbered SEC fractions, (b) a plot of the nanoparticle concentration measured by TRPS using NP150 (70 – 280nm size range) and NP400 (185-280 nm size range) nanopore and size distributions of nanoparticles in TRPS-peak fractions measured on (c) NP150 and (d) NP400 nanopore.

Measured concentrations of nanoparticles in TRPS-positive fraction were 2,48 x 10^9 for particles in the size range 70 – 280 nm, and 1.35 x 10^8 for particles in the size range 185 – 740 nm. The mean and mode diameters of isolated nanoparticles detected in TRPS peak fraction were 124.5 ± 4.9 nm and 93.5 ± 4.9 nm for nanoparticles in the size range 70 – 280 nm, and 262.0 ± 9.2 nm and 204.5 ± 3.5 nm for particles in size ranges 185 - 740 nm, respectively. Although TRPS measurement on NP150 nanopore revealed a much larger concentration of nanoparticles in the 70 – 280 nm range, the detection performed with this membrane turned out to be exceptionally challenging due to the constant clogging of the nanopore. Since both membranes successfully identified the matching SEC fraction as a nanoparticle-peak fraction, the succeeding TRPS peak fraction detection were performed using the NP400 nanopore.

4.4. Sepharose CL-6B Outperforms Other Tested Size Exclusion Chromatography Methods in Isolation of Nanoparticles

Upon establishing a protocol for SEC and subsequent TRPS and slot blot analysis, the same volume (2.8 mL) of CSF-pool was separated by all four tested columns to assess their efficiency. The volume was doubled that the one used in initial separation to obtain detectable signals for exosome markers on slot blot. Commercial column qEV10/70nm achieved the most rapid elution, with a flow rate of 3.6 mL/min. In-house columns were significantly slower, with Sephacryl S-400 and Superose 6PG performing at 0.3 mL/min and 0.2 mL/min, while Sepharose CL-6B had the highest flow rate of the three, recorded at 0.6 mL/min. The volume of mobile phase required for elution of nanoparticles (determined by TRPS) and proteins (estimated by Ponceau S staining, depicted in Figure 12a) was comparable for all four SEC methods, equalling 26-28 mL and 68-70 mL, respectively, except for the qEV10/70 nm, which required >74mL for elution of protein fractions (Table 7). The volume required for the elution of nanoparticles varied minimally between replicates (maximum deviation of ±1.5 mL between replicates, equalling ±1 fraction), demonstrating the replicability in column performances.

Table 7. Design and technical characteristics of four analysed gravity flow-based size-exclusion chromatography (SEC) methods used for the separation of cerebrospinal fluid sample from patients with severe traumatic brain injury.

SEC	Column packing required	Flow rate in ml/min	Volume of mobile phase required for the elution of	
			nanoparticles	total proteins
Superose 6 PG	yes	0.2	26 ml	68 ml
Sephacryl S-400	yes	0.3	28 ml	68 ml
Sepharose CL-6B	yes	0.6	25 ml	70 ml
qEV10/70nm	no	3.6	26 ml	>74 ml

TRPS analysis of collected fractions revealed a narrow TRPS nanoparticle peak, mostly extending through 2 fractions positioned between fractions 12 and 17. The highest detected concentrations of nanoparticles in nanoparticle-enriched TRPS-positive fractions were 6.02×10^8 particles/mL for Sepharose CL-6B, 3.72×10^8 particles/mL for Superose 6 PG, 2.60×10^8 particles/mL for Sephacryl S-400 and 1.46×10^8 particles/mL for qEV10/70nm column. The “distance” between the nanoparticle- and protein-enriched fractions differed between compared methods. The greatest distance between the nanoparticle-peak fractions and the protein-enriched fractions was observed for qEV10/70nm and Sephacryl S-400, while Superose 6 PG and Sepharose CL-6B exhibited a slightly smaller gap between nanoparticle-enriched fractions and Ponceau curve. However, none of the analysed methods led to overlapping between the two peaks (Figure 12b).

a)

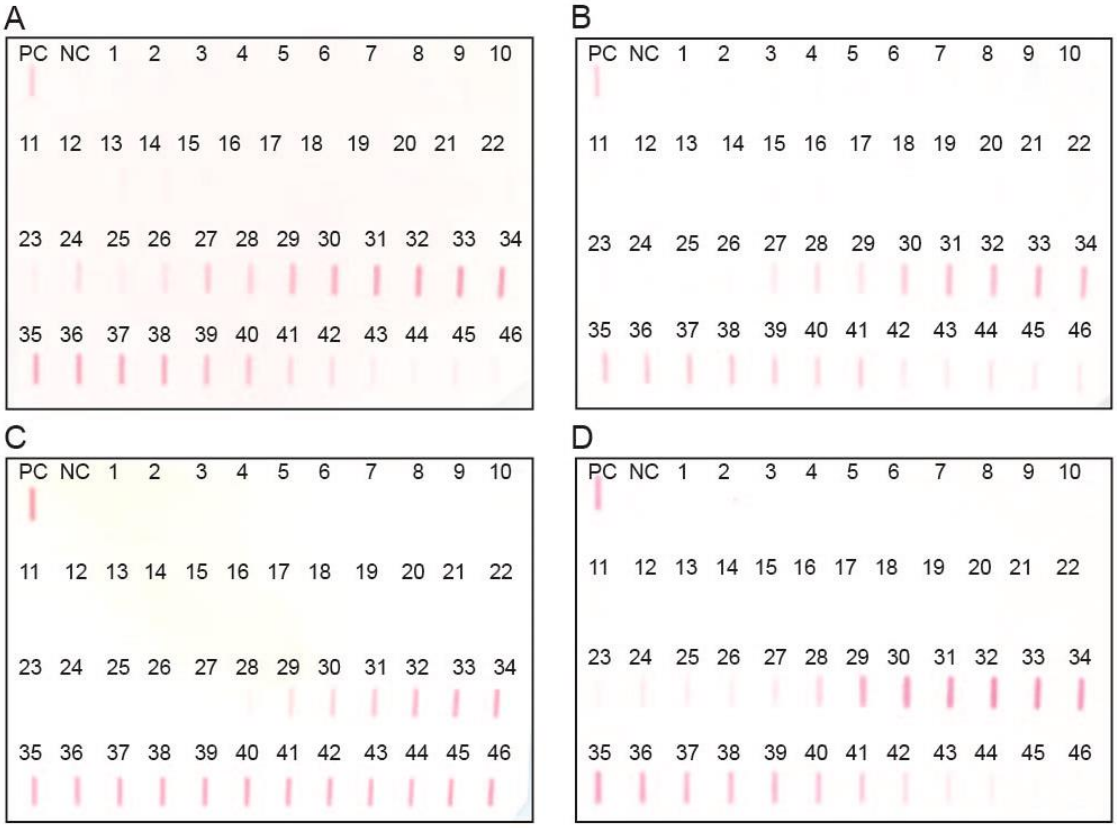
A
PC NC 1 2 3 4 5 6 7 8 9 10
11 12 13 14 15 16 17 18 19 20 21 22
23 24 25 26 27 28 29 30 31 32 33 34
35 36 37 38 39 40 41 42 43 44 45 46
B
PC NC 1 2 3 4 5 6 7 8 9 10
11 12 13 14 15 16 17 18 19 20 21 22
23 24 25 26 27 28 29 30 31 32 33 34
35 36 37 38 39 40 41 42 43 44 45 46
C
PC NC 1 2 3 4 5 6 7 8 9 10
11 12 13 14 15 16 17 18 19 20 21 22
23 24 25 26 27 28 29 30 31 32 33 34
35 36 37 38 39 40 41 42 43 44 45 46
D
PC NC 1 2 3 4 5 6 7 8 9 10
11 12 13 14 15 16 17 18 19 20 21 22
23 24 25 26 27 28 29 30 31 32 33 34
35 36 37 38 39 40 41 42 43 44 45 46

b)

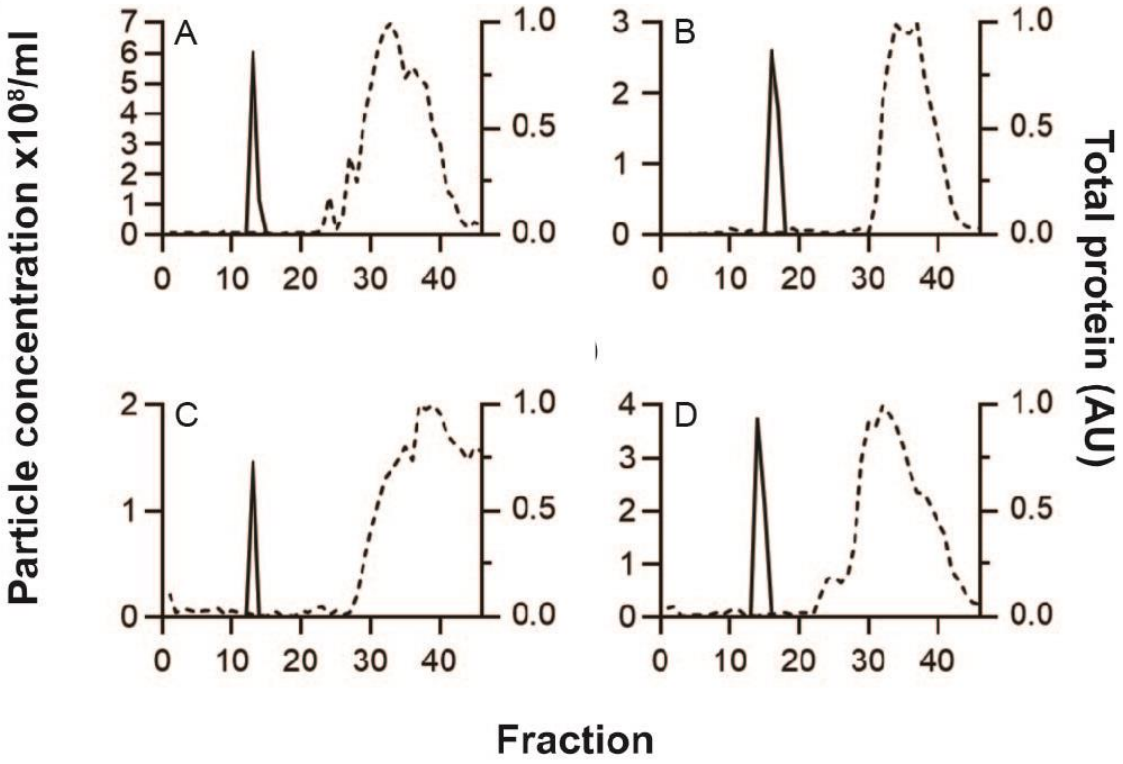
Particle concentration x10⁸/ml
Total protein (AU)
Fraction
A
B
C
D

Figure 12. Four analysed size-exclusion chromatography (SEC) methods efficiently separate nanoparticles from soluble proteins in cerebrospinal fluid (CSF) sample. Samples of intracranial CSF from severe traumatic brain injuries were pooled, and the same volume of the resulting CSF-pool was separated using (A) Sepharose 6B-CL, (B) Sephacryl S-400, (C) qEV10/70nm or (D) Superose 6 PG filled chromatographic columns. A total of 46 fractions of approximately 1.5 mL were collected for each SEC run. (a) An equal volume of fractions collected after each SEC method was applied on the nitrocellulose membrane by slot blot, followed by Ponceau S staining. Initial CSF-pool was used as positive (PC) and SEC mobile phase as negative control (NC). Numbers denote sequentially collected fractions. Displayed images of Ponceau S-stained membranes are representative of three separate experiments conducted for each SEC method. (b) Collected fractions were analysed by tunable resistive pulse sensing (TRPS) to identify nanoparticle-enriched fractions and measure nanoparticle concentration (solid line) and by slot blot to estimate the total protein content (dashed line), represented in arbitrary units of the quantified image of Ponceau-stained membranes. The graphs displayed are representative of three separate experiments conducted for each SEC method.

Lastly, the comparison of the total number of isolated nanoparticles, calculated as the sum of nanoparticles in TRPS peak fractions, revealed significant differences between the compared SEC methods. The highest number of total isolated nanoparticles was observed in Sepharose CL-6B, which yielded $(1.08 \pm 0.08) \times 10^9$ nanoparticles, followed by Superose 6 PG with $(8.74 \pm 0.83) \times 10^8$, Sephacryl S-400 with $(5.71 \pm 0.51) \times 10^8$, and finally qEV10/70nm with $(2.47 \pm 1.01) \times 10^8$ of particles (Figure 13).

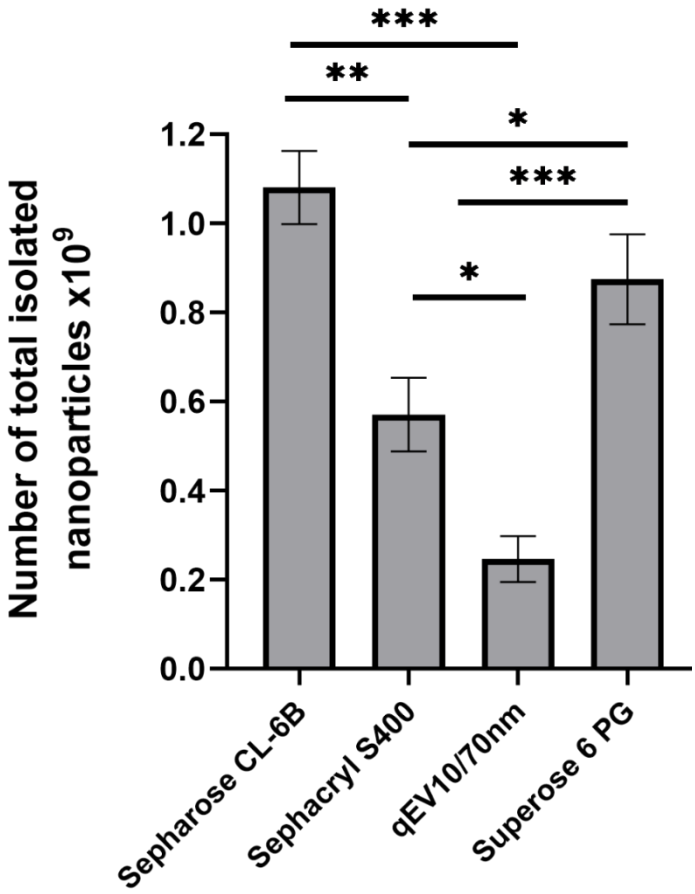

Figure 13. The highest yield of total isolated nanoparticles was achieved using the Sepharose CL-6B filled size-exclusion chromatography (SEC) column. The number of total isolated nanoparticles was calculated by adding up nanoparticle number from nanoparticle-enriched TRPS-positive fractions. The graph shows mean values with standard deviation from three separate experiments for each analysed SEC method. ***p<0.001 Sepharose CL-6B vs. qEV10/70nm, ***p<0.001 Superose 6 PG vs qEV10/70nm, **p=0.002 Sepharose CL-6B vs. Sephacryl S400, **p=0.003 Sephacryl S400 vs. qEV10/70nm, *p=0.048 Sephacryl S400 vs. qEV10/70nm, one-way ANOVA with Tukey's post-hoc test.

4.5. Nanoparticles of Comparable Size and Negative Charge Are Isolated in Similar Proportions by the Applied SEC Methods

Given that the applied SEC methods demonstrated varying efficacy in the separation of nanoparticles from free proteins present in intracranial CSF, a more thorough characterisation of nanoparticles isolated in TRPS-positive fractions was

conducted. TRPS size measurement on peak-nanoparticle fractions revealed that all SEC isolation methods resulted in the enrichment of similar-sized nanoparticles.

All TRPS measurements displayed left-skewed size distributions, with most of the detected particles measuring between 200 and 250 nm in diameter. To summarise the central tendency across three independent experiments, calculated was the arithmetic mean of their median values measured in nanoparticle-peak fractions, resulting in 254.0 nm, 244.7 nm, 272.3 nm and 261.3 nmfor Sepharose CL-6B, Sephacryl S-400, qEV10/70nm and Superose 6 PG, respectively. The size range of nanoparticles was somewhat larger for qEV10/70 nm and Superose 6PG than the ones observed in Sepharose CL-6B and Sephacryl S-400 isolated nanoparticles (Figure 14b). However, no significant difference was observed when comparing the calculated median diameters of isolated nanoparticles.

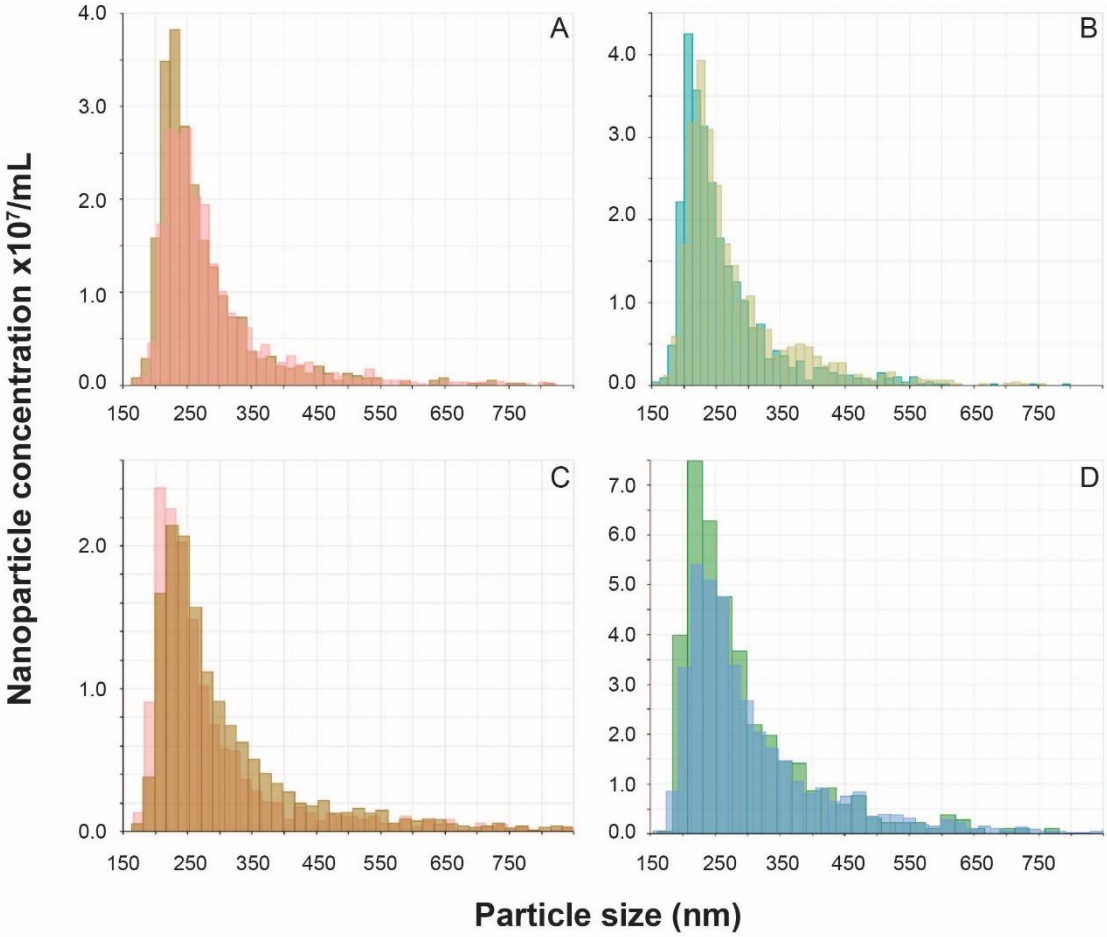

a)

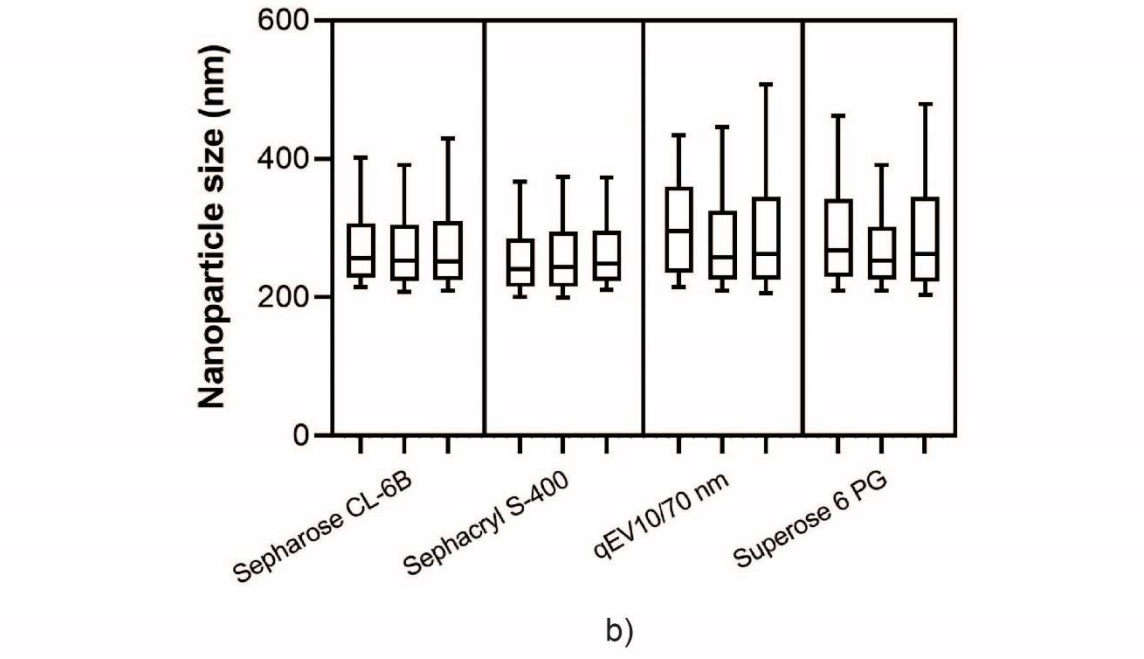

Figure 14. **Nanoparticles of similar size are isolated by all applied SEC methods.** (a) Shown are size distributions of nanoparticles detected by TRPS in nanoparticle-peak fractions isolated using (A) Sepharose CL-6B, (B) Sephacryl S-400, (C) qEV10/70 nm and (D) Superose 6 PG. (b) A plot showing the mean particle diameter in nanometers (nm) of nanoparticles isolated by all four SEC methods. Nanoparticles in the nanoparticle-peak fraction from each SEC replicate (n=3) are represented by one box-and-whiskers plot. The line across the middle of the box shows the median, the upper and lower extremities of the box show the 25th and 75th percentiles of the data set, and the upper and lower whiskers show the 10th and 90th percentiles. No statistically significant difference in median sizes was observed between groups.

To inspect whether the choice of column resins affects the electrical properties of isolated nanoparticles, zeta potential measurements were performed on TRPS-positive fractions. Measurements of zeta potential, otherwise known as surface charge of nanoparticles in a solution, revealed a similar pattern of nanoparticle zeta potential in peak-nanoparticle fractions in samples obtained by all SEC methods, with the majority of SEC-isolated nanoparticles being negatively charged (Figure 15a).

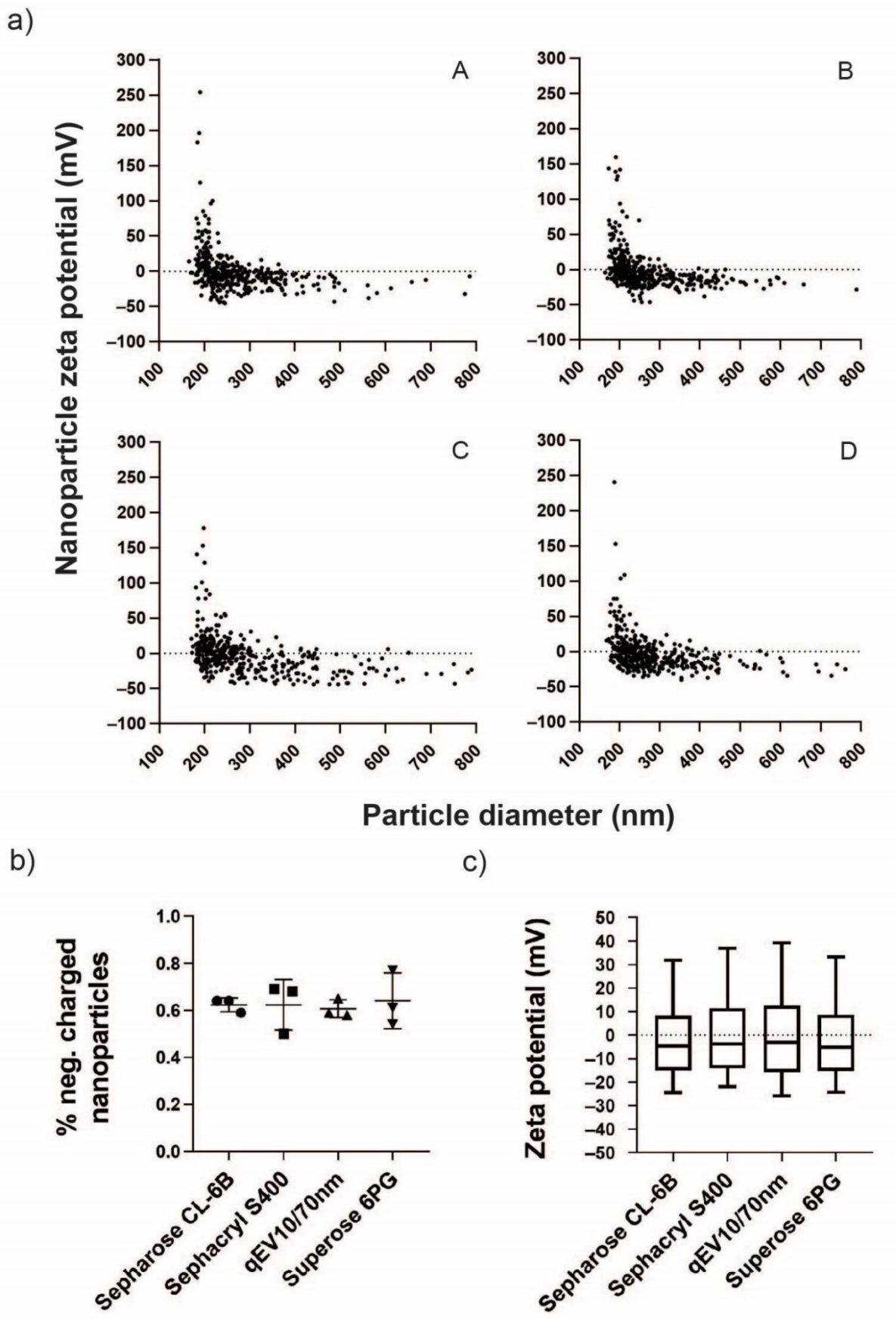
a)
A
B
C
D
Nanoparticle zeta potential (mV)
Particle diameter (nm)
b)
% neg. charged nanoparticles
Sepharose CL-6B
Sephacryl S400
qEV10/70nm
Superose 6PG
c)
Zeta potential (mV)
Sepharose CL-6B
Sephacryl S400
qEV10/70nm
Superose 6PG

Figure 15. The majority of SEC-isolated nanoparticles are negatively charged. a) Measurements of zeta potential were performed on TRPS-positive fractions obtained by SEC separation of CSF-pool sample with (A) Sepharose 6B-CL, (B) Sephacryl S-400, (C) qEV10/70nm and (D) Superose 6PG. Displayed are distributions of nanoparticle zeta potential measured in millivolts (mV) and nanoparticle diameter measured in nanometres (nm) representative of three separate experiments conducted for each SEC method. b) The percentage of negatively charged nanoparticles determined by TRPS zeta potential measurements are displayed as mean values with standard deviation. c) Shown are median values with interquartile ranges (boxes) and 10-90 percentile ranges (whiskers) of zeta potential, measured in millivolts (mV). Both graphs were made based on the results obtained from three experiments for each SEC method.

Median zeta potentials were −4.67 mV (interquartile range (IQR): −15.00 - 8.17) with 61.69% of negatively charged particles for Sepharose CL-6B, −3.67 mV (IQR: −14.00 - 1.33) with 62.39% of negatively charged particles for Sephacryl S-400, −3.00 mV (IQR: −15.67 - 12.67) and 60.58% of negatively charged particles for qEV10/70nm, and −5.00 mV (IQR: −15.25 - 8.67), with 61.18% of negatively charged nanoparticles Superose 6PG (Figure 15b and 15c). These results did not reveal differences in nanoparticles isolated with four tested SEC methods.

4.6. Sepharose CL-6B Separates Exosomes from Lipoproteins and Free Proteins

After identifying Sepharose CL-6B as the best of the four analysed SEC-based methods for the separation of nanoparticles from proteins in human CSF, the next objective was to characterise and identify the isolated nanoparticles. Considering that both exosomes and lipoproteins were found in the starting CSF-pool used for SEC separation, are of similar size, and cannot be differentiated using TRPS, immune-based analysis were applied for their identification.

Hence, immunodetection of exosome protein markers and lipoprotein markers was performed on individual fractions collected after SEC separation of CSF-pool with Sepharose CL-6B (Figure 16a). The exosome markers CD81 and CD9 were readily detected on slot blot in an array of consecutive fractions. CD81 was strongly detected in fractions 13–15, with fraction 16 also exhibiting a weaker but clear signal. The

strongest CD9 signal was detected in fraction 14, while the weaker signal also extended over surrounding fractions 13-18. Occasional and faint CD81 signals were also observed among fractions in the 23–32 range. Lipoprotein markers ApoE and ApoAI were found in an overlapping range of fractions, ApoE extending from fractions 24-31, and ApoAI signal encompassing fractions 25-30. Albumin was detected in a continuous range of fractions 27-37, and additionally in fractions 39 and 40.

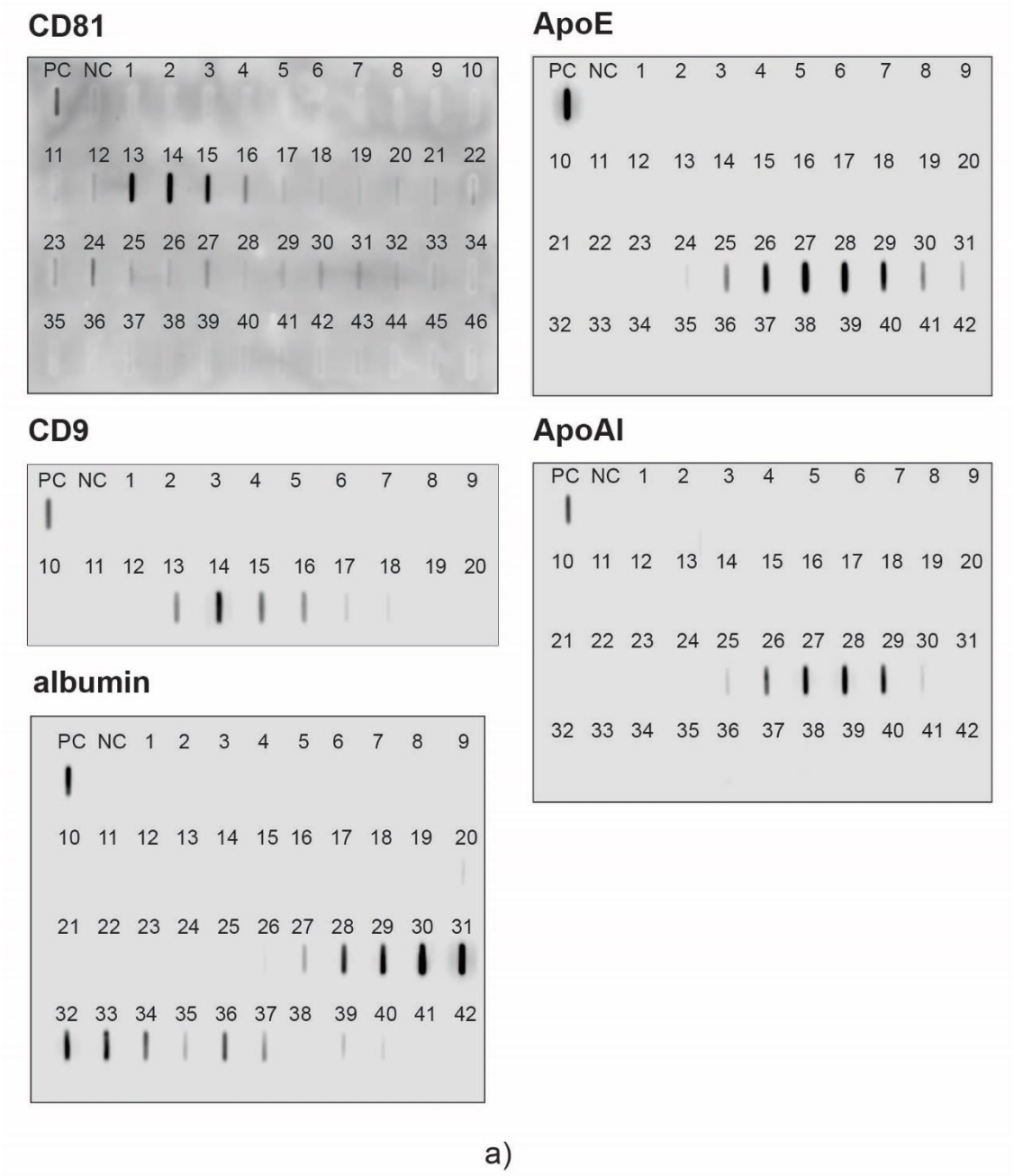

a)

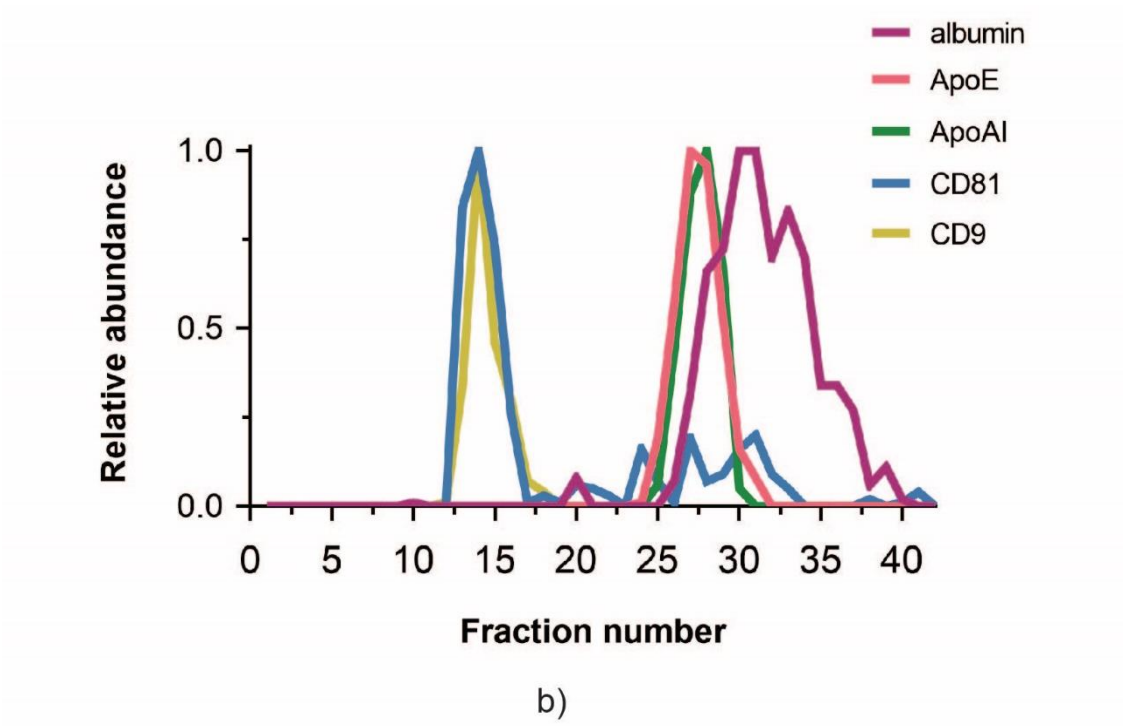

Figure 16. Exosome protein markers CD81 and CD9 are detected in nanoparticle-peak fraction, separate from lipoprotein markers and albumin. (a) CSF-pool generated by samples from severe TBI patients was separated by Sepharose CL-6B-packed gravity flow SEC column. Consecutively collected fractions were loaded on nitrocellulose membrane using slot blot, and CD81, CD9, ApoAI, ApoE and albumin proteins were immunodetected by corresponding antibodies. CSF-pool was loaded as positive, and the SEC mobile phase as negative control (NC). Shown are representative immunoblots after chemiluminescence. (b) Relative protein abundances for CD81, CD9, ApoAI, ApoE and albumin in SEC fractions, calculated by quantification of chemiluminescence signal immunodetected on slot blots.

To offer a clearer representation of protein levels across the individual fractions collected using Sepharose CL-6B, the signals for each protein detected on the slot blot were quantified and plotted the data on the same graph (Figure 16b). The curves for exosome markers CD81 and CD9, and lipoprotein ApoAI, and ApoE were sharp and symmetrical, while the albumin curve was broader and less uniform. Additionally, the CD81 and CD9 curves were completely overlapping, as were the ApoAI and ApoE curves. Both ApoAI and ApoE curves overlapped with the first segment of the albumin curve.

To verify the specificity of immunodetection following slot blot analysis of SEC fractions, further examination of selected fractions was performed by electrophoresis followed by western blotting (Figure 17a). According to the data shown in Figure 17 and previous TRPS measurements, fractions 9, 14 and 20 were selected to represent points before, during and after the nanoparticle-positive peak. Free-protein peak was represented by fraction 34. Ponceau staining revealed no signal in fractions 9, 14, and 20. However, in both fraction 34 and the CSF-pool, abundant level of proteins was detected around 70 kDa and less than 15 kDa, along with smaller levels of proteins near 35 kDa and 100 kDa mark.

Western blot analysis of selected fractions revealed signals corresponding to the expected sizes for each analysed protein. CD81 and CD9 were detected in nanoparticle-positive peak fraction 14, but absent in fraction 34, while ApoAI and ApoE were present in fraction 34 and absent in fraction 14. Notably, the ratio of CD81 to CD9 signals in the nanoparticle-enriched fraction differed from that observed in the initial CSF pool. Additionally, selected fractions were also tested for exosome marker flotilin-1, which revealed a strong signal in nanoparticle-enriched fraction. However, a faint signal was also present in both post-nanoparticle-peak and protein-enriched fraction. To further confirm the presence of exosome in fraction 14, transmission electron microscopy was performed (Figure 17b), revealing spherical exosomes with diameters of 100–130 nm.

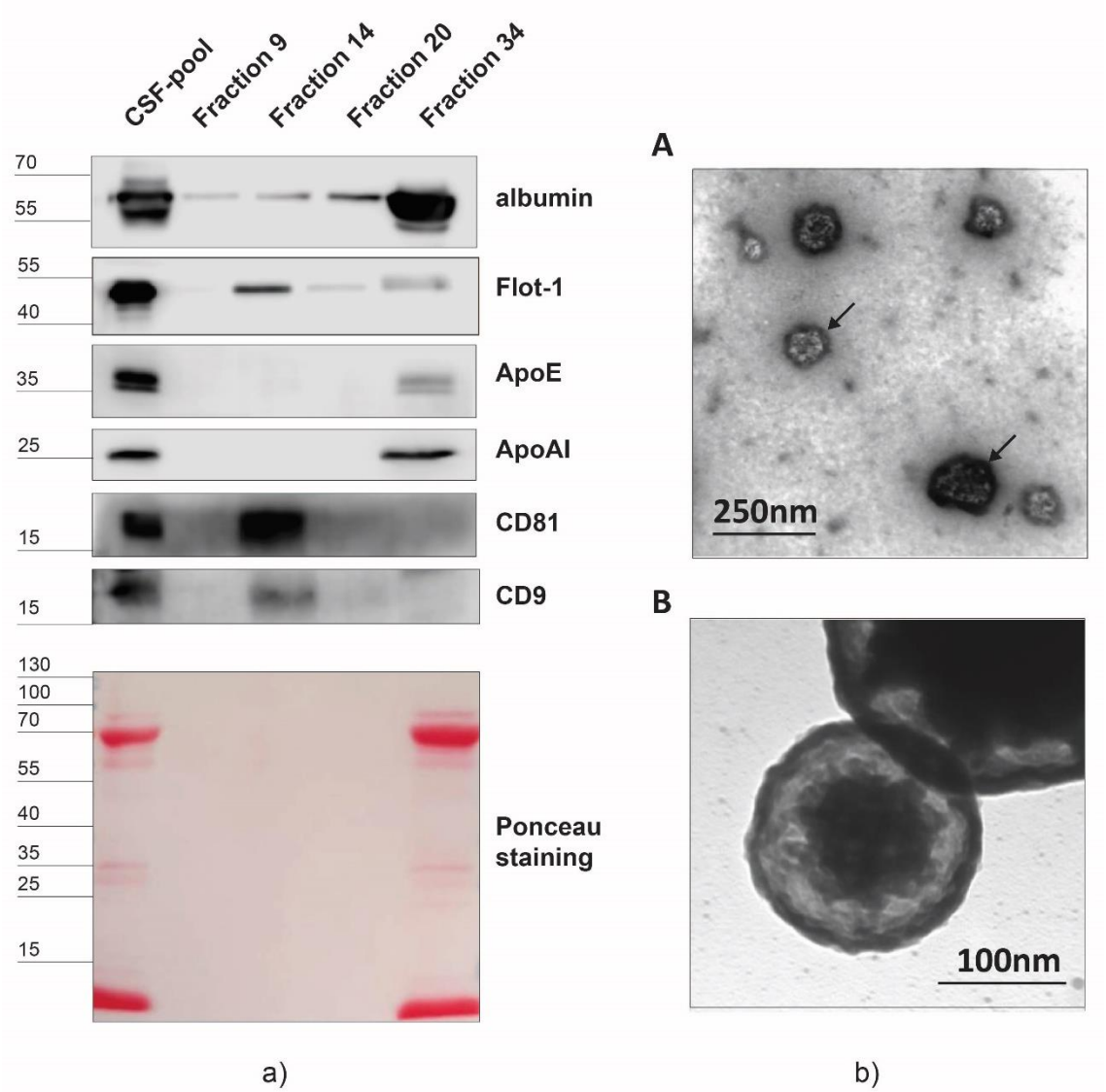

Figure 17. Sepharose CL-6B efficiently separates exosomes from lipoproteins and albumin in cerebrospinal fluid from patients with severe TBI. Fractions corresponding to points before (Fraction 9), amid (Fraction 14), and post nanoparticle-positive peak (Fraction 20), and to free-proteins (Fraction 34) were analysed by western blot after protein separation by SDS-PAGE. Selected fractions and CSF-pool were equalled by volume and probed with antibodies against albumin, lipoprotein markers ApoE and ApoAI and exosome markers CD81, CD9 and flotillin-1. Ponceau S staining of a nitrocellulose membrane after SDS-PAGE is shown below. The molecular weights of the detected bands are shown in kilodaltons (kDa). (b) (A) Transmission electron microscopy micrograph displaying round-shaped exosomes with diameters ranging from 100 to 130 nm, indicated by arrows. (B) Higher magnification of electron micrograph revealing an exosome with double-layer membrane measuring 175 nm.

5. DISCUSSION

Exosomes found in cerebrospinal fluid (CSF) are thought to carry molecular cargo that reflects biochemical changes occurring in the central nervous system. This presents a unique opportunity to use these molecular carriers as biomarker sources in various pathologies, including traumatic brain injury [31,63,66,71]. For successful biomarker detection, it is crucial to isolate exosomes from clinical CSF samples with optimal purity and yield. Generally, due to the large heterogeneity of EVs and incomplete knowledge of different aspects of specific EV subtypes, including exosomes, isolation of total EVs should be a priority. Size exclusion chromatography (SEC), though widely used for protein purification, has not yet become a common or standardised technique for isolating EVs. However, SEC holds a strong advantage compared to other isolation methods, including both purity and heterogeneity of isolated EVs [77,95].

Most exosome isolations using SEC have been conducted on readily accessible samples like serum and urine, while research on CSF has been scarce [77,95]. Working with CSF samples presents numerous challenges due to the invasive procedures required for CSF collection, the small volume of clinical samples, and the relatively low concentrations of proteins and nanoparticles compared to other biological fluids [78,123]. To date, only a limited number of studies have explored the use of SEC for isolating exosomes from CSF, and none have systematically compared different SEC designs to identify the most effective isolation methods [88,111,124]. Our earlier findings indicated that exosomes were present in the intracranial cerebrospinal fluid (CSF) collected in the initial days following injury [66]. In this study, four different SEC methods were compared to evaluate their effectiveness in enriching exosomes from human CSF.

To achieve this goal, an analysis was conducted on CSF samples collected from adult patients with severe TBI who required ventriculostomy for intracranial pressure monitoring and management as part of their urgent care. Analysed samples consisted of intracranial CSF drained within the first three post-injury days . In most individual CSF samples, elevated levels of albumin and apolipoproteins were detected, suggesting the presence of blood, which aligns with the severity of the TBI, as well as the invasive nature of the procedure used to obtain intracranial CSF [125].

The screening on exosome markers CD81 and CD9 in individual CSF samples revealed their presence in all except one individual sample, supporting previous research that has shown these tetraspanins to be commonly detected in clinical CSF samples [66,67]. However, given that CD81 and CD9 are broadly expressed proteins, it is highly probable that some of the CD81+ and CD9+ exosomes originate from the bloodstream. That is evident since relatively high blood levels were present in the samples, which is indicated by detected albumin in all samples [126]. Although immunoblot analyses of individual samples revealed varying levels of albumin, exosome markers, and lipoproteins, moderate levels of analysed proteins were detected in a CSF-pool generated from the nine individual CSF samples from three severe TBI patients (Figure 8). This pooled sample likely reflects the typical composition of CSF samples of TBI patients used for diagnostic and prognostic purposes.

Since various resins have already been utilised with limited information on the differences in their performance for exosome isolation, selection of the best available candidates based on a literature search of materials previously used for SEC isolation of exosome from biofluids was needed. It is well recognised that the pore size and bead diameter can significantly impact the fractionation performance of SEC columns, so these parameters were considered in our selection (Table 6). Cross-linked (CL) agarose beads, commercially available as Sepharose, are most widely used for this purpose and have already been utilised for exosome isolation from many biological samples, including plasma, serum and urine [77]. Variants of Sepharose such as CL-2B, CL-4B and CL-6B differ primarily in their agarose content (2%, 4% and 6%, respectively), but also in their particle and pore size, affecting their fractionation capability. Although Sepharose CL-2B presents a conventional choice, newer findings indicate inferior separation of exosome from human serum samples than separation achieved by Sepharose CL-4B and Sepharose CL-6B resins [91]. In another study, Sepharose CL-4B and Sephacryl S-400 outperformed Sepharose CL-2B in separating exosomes from human plasma samples with comparable efficiency [90]. It has been proposed that smaller pore size may be a contributing factor to improved performance because smaller exosomes do not get retained in the resin, which would explain these results [95]. Hence, Sepharose CL-6B and Sephacryl S-400 were selected as good candidates for comparison of their efficiency. At the time, Superose 6 PG had not yet

been employed for exosome isolation by SEC but was chosen for its small bead size, wide fraction range and similar exclusion limit compared to the other two selected resins. Meanwhile, Superose 6 PG has been utilised for exosome isolation from human blood and serum samples [127,128]. To the best of our knowledge, none of the selected SEC matrices have yet been applied for SEC isolation of exosomes from CSF. Additionally, we wanted to include a widely used, commercially available column advertised to enable SEC isolation of exosome from CSF. The goal was to compare the efficiency of our in-house SEC methods with a ready-to-use qEV10/70nm column.

The equal volume of the CSF-pool was separated using three in-house SEC columns and a commercial column. The direct comparison of the four analysed SEC methods demonstrated that all of them successfully separated nanoparticles measuring around 200 nm in diameter from free proteins, namely albumin. The critical importance of clearly distinguishing exosomes from free proteins was recently highlighted in studies on L1CAM, a neural cell transmembrane protein once considered useful for the immunoisolation of neuron-derived exosomes. In their study, Norman *et al*., demonstrated L1CAM is found in free-protein rather than EV fractions following Sepharose CL-6B SEC and density gradient separation of both CSF and plasma samples [73].

This same research also supports our findings that SEC effectively separates exosomes from lipoproteins (Figures 16 and 17a). Lipoproteins are spherical particles with a core of hydrophobic lipids, surrounded by a single layer of phospholipids, cholesterol, and apolipoproteins. They serve as transport vehicles for hydrophobic lipids throughout the body's aqueous environment and are found to be prevalent in both blood and CSF [129]. Since they share a similar size range with exosomes, it would be expected they could co-isolate with exosomes when using a size-based isolation technique such as SEC. Indeed, studies conducted on plasma-derived exosomes revealed lipoprotein contamination in exosome isolates from all commonly employed purification methods, including commercial SEC column set-ups [93,97]. The results obtained by this study demonstrate that Sepharose CL-6B successfully enriches lipoproteins in later fractions alongside free proteins, making it an effective method for minimizing lipoprotein contamination in exosome preparations. Although it is not yet possible to make concrete conclusions, it can be speculated that the difference in their flexibility could be the reason behind their different elution times.

Since SEC separates particles based on their hydrodynamic volume, both the size and shape of the particles affect their retention time and separation efficiency [77]. Flexible particles can change shape under flow conditions, allowing them to navigate through the gel matrix more efficiently than rigid particles. Hence, it could be possible that the difference in their structural properties and hydrodynamic behaviour could be the reason behind the observed difference in their elution profiles [130]. However, it is not yet clear how the choice of different stationary phases could affect this phenomenon.

Furthermore, a comparison of the analysed SEC methods used in this study demonstrated that the choice of the stationary phase significantly affects the yield of the isolated exosomes. Specifically, Sepharose CL-6B and Superose 6PG yielded markedly higher concentrations of exosomes compared to Sephacryl S400 and qEV10/70 nm, which isolated exosomes in amounts that were two to four times lower (Figure 13). Additionally, Sepharose CL-6B exhibited a flow rate three times greater than that of Superose 6 PG (Table 7). Conversely, the straightforward application and much quicker flow rate of qEV10/70 nm offer certain advantages for the commercially available exosome isolation column. Previous research on exosome isolation has frequently utilized qEV10/70 nm as a representative SEC method, but it proved to be less effective than techniques such as precipitation, membrane affinity, and density gradient methods [131]. Regarding the size and surface charge of the isolated particles, no differences were observed between exosome isolates obtained by four tested SEC methods (Figures 14 and 16). All methods resulted in the isolation of similarly sized nanoparticles exhibiting comparable size distributions in the 185-740 nm size range and indistinguishable zeta potential profiles. However, it should be noted that our choice of TRPS configuration employed by this study did not allow measurements of smaller-sized particles, meaning some differences may be present in nanoparticles of smaller size range.

Although the TRPS method proved to be useful for the detection of exosome-enriched fractions, several downsides of this method severely complicated the measurement process. The main disadvantage is a limited dynamic range of sizes that can be analysed by a single nanopore type. As a result, only nanoparticles in the size range from 185 to 740 nm were measured, thus missing out on information about concentrations of smaller nanoparticles, and possibly discarding additional fractions containing smaller exosomes. Initial measurements performed on the TRPS

membrane which allows measuring smaller nanoparticles revealed a higher concentration of 70-280 nm compared to those found in the size range 185-740 nm (Figure 11) in the same nanoparticle-peak fraction. However, further measurements with this TRPS membrane were abandoned due to constant clogging of the system, making the measurements virtually impossible without prior treatment of the samples, which was avoided in this study for the effect it would have on exosome yield and morphology. Hence, a supplementary method more convenient for measuring <200 nm nanoparticles like nanoparticle tracking analysis (NTA) could be more appropriate for measuring their concentrations.

Data obtained by this study suggests that the efficiency of SEC is heavily influenced by the choice of stationary phase, suggesting that a thorough evaluation of SEC methods requires careful consideration of various factors. While the separation of exosomes from both albumin, serving as a model molecule for free proteins, and lipoproteins represented by ApoAI and ApoE was successfully demonstrated, caution is warranted regarding the purity of the exosome-enriched fractions. In Figure 17a it is notable that, although the majority of albumin signal comes from protein-enriched fraction, a low-but-detectible signal can be seen in exosome-enriched fraction observed even by using western blotting, a method with relatively low sensitivity. Still, it remains unclear whether this albumin is exosome-associated or is it an indicator of contamination by soluble proteins.

Exosomes isolated in this study were analysed following current guidelines for EV studies provided by ISEV, which state that isolated EVs should be characterised by at least three positive protein markers of EVs, including at least one transmembrane/lipid-bound protein, a cytosolic protein, and at least one negative protein marker [43]. In this study, isolated exosomes were CD81, CD9 and Flot-1 positive and negative for ApoAI and ApoE. The additional requirement includes the characterisation of exosome physical properties, specifically their size, morphology, particle concentration and size distribution [43]. For visual confirmation, exosomes isolated in this study were visualised using TEM (Figure 17b), while particle concentration and size distribution were measured using TRPS (Figures 12 and 14), meaning all requirements were met for reliable exosome identification.

A drawback of this study is that SEC may not effectively enrich all types of EVs, leading to the possibility that some EVs go undetected. Specifically, notable

discrepancies in our study were observed in the quantities of isolated exosomes among different SEC methods. This suggests the possibility of the stationary phase interacting with exosomes, leading to these differences. One possible way a stationary phase could be interacting with exosomes is through the binding, and thus inhibiting their movement within the mobile phase and causing retention of certain EV subpopulations within the column. Another potential explanation is that the stationary phase could be affecting the migration of exosomes in such a manner that it causes them to become dispersed throughout a larger volume of the mobile phase, eluting them across multiple fractions and consequently resulting in diluted concentrations. All these considerations must be factored in for future enhancements of exosome isolation using SEC methods. Furthermore, investigating additional exosome markers like Tsg101, Alix, and Rab proteins would provide deeper insights into which specific exosomes are impacted by these potential interactions with the stationary SEC phase.

In summary, this study presents a protocol for gravity-based SEC that can be readily implemented in any laboratory setting. Our findings indicate that Sepharose CL-6B and Superose 6PG are more effective than Sephacryl S400 and qEV10/70 nm for enriching exosomes from clinical CSF samples in SEC eluates. The distribution of exosomes across the fractions is likely influenced by the manual collection process, and the gravity-based columns used in this study may not be suitable for scaling up to processing larger volumes of samples. Increasing the loading volume could result in lower quality of separation of nanoparticles from soluble proteins and other contaminants and should be additionally evaluated and optimised prior to any further exosome analysis. Nevertheless, all SEC stationary phases evaluated were capable of effectively separating exosomes from lipoproteins and free proteins. Further enhancements could be achieved by selecting or developing new stationary phase materials.

6. CONCLUSION

Despite major efforts made over the last 40 years, the field of EV research is still in its infancy, with many unresolved questions and challenges hindering its progress. It is becoming clear that EVs play an important role in many pathophysiological processes including traumatic brain injury. However, several technical challenges continue to impede the translation of EV findings into clinical practice. The lack of standardised isolation methods as well as the small size and large heterogeneity of EVs present the biggest obstacles in the progress of EV research. The goal of this study was to provide an efficient, reproducible, and easily employable protocol for SEC-based exosome isolation and characterisation that provides enrichment of high-quality exosomes from human cerebrospinal fluid samples.

The key findings made in this thesis are:

1. The four tested SEC-based methods successfully separated 200 nm-sized nanoparticles from soluble proteins in severe TBI CSF samples.
2. Sepharose CL-6B outperformed Superose 6 PG, Sephacryl S-400 and qEV10/70 nm in the enrichment of nanoparticles in clinical CSF samples.
3. Tandem TRPS and slot blot approach enables successful detection of exosomes after SEC isolation.
4. Sepharose CL-6B SEC-based isolation successfully separated CD9+/CD81+/Flotillin-1 positive exosomes from most soluble proteins and apoAI+ and apoE+ lipoproteins in CSF samples from severe TBI patients.
5. Transmission electron microscopy visualisation of exosomes isolated using Sepharose CL-6B column revealed 100-200 nm round, double-layer membrane exosomes.

Overall, this study provided a systematic comparison of four SEC-based methods to provide a novel protocol for exosome isolation from human CSF, to lay a foundation for future exosome biomarker research in severe TBI.

7. LITERATURE

1. Capizzi A, Woo J, Verduzco-Gutierrez M. Traumatic Brain Injury: An Overview of Epidemiology, Pathophysiology, and Medical Management. Med Clin North Am. 2020 Mar;104(2):213–38.

2. Majdan M, Plancikova D, Brazinova A, Rusnak M, Nieboer D, Feigin V, et al. Epidemiology of traumatic brain injuries in Europe: a cross-sectional analysis. Lancet Public Health. 2016 Dec;1(2):e76–83.

3. Maas AIR, Stocchetti N, Bullock R. Moderate and severe traumatic brain injury in adults. Lancet Neurol. 2008 Aug;7(8):728–41.

4. Masel BE, DeWitt DS. Traumatic brain injury: a disease process, not an event. J Neurotrauma. 2010 Aug;27(8):1529–40.

5. Stocchetti N, Zanier ER. Chronic impact of traumatic brain injury on outcome and quality of life: a narrative review. Crit Care [Internet]. 2016 [cited 2024 Jul 12];20:148. Available from: https://www.ncbi.nlm.nih.gov/pmc/articles/PMC4915181/

6. Ng SY, Lee AYW. Traumatic Brain Injuries: Pathophysiology and Potential Therapeutic Targets. Front Cell Neurosci. 2019;13:528.

7. Ahmed Z. Current Clinical Trials in Traumatic Brain Injury. Brain Sci [Internet]. 2022 Apr 21 [cited 2024 Aug 21];12(5):527. Available from: https://www.ncbi.nlm.nih.gov/pmc/articles/PMC9138587/

8. Saatman KE, Duhaime AC, Bullock R, Maas AIR, Valadka A, Manley GT. Classification of Traumatic Brain Injury for Targeted Therapies. J Neurotrauma [Internet]. 2008 Jul [cited 2024 Jul 13];25(7):719–38. Available from: https://www.liebertpub.com/doi/full/10.1089/neu.2008.0586

9. GBD 2016 Traumatic Brain Injury and Spinal Cord Injury Collaborators. Global, regional, and national burden of traumatic brain injury and spinal cord injury, 1990-2016: a systematic analysis for the Global Burden of Disease Study 2016. Lancet Neurol. 2019 Jan;18(1):56–87.

10. Leo P, McCrea M. Epidemiology. In: Laskowitz D, Grant G, editors. Translational Research in Traumatic Brain Injury [Internet]. Boca Raton (FL): CRC Press/Taylor and Francis Group; 2016 [cited 2024 Jul 18]. (Frontiers in Neuroscience). Available from: http://www.ncbi.nlm.nih.gov/books/NBK326730/

11. Dewan MC, Rattani A, Gupta S, Baticulon RE, Hung YC, Punchak M, et al. Estimating the global incidence of traumatic brain injury. J Neurosurg. 2018 Apr 27;130(4):1080–97.

12. Roozenbeek B, Maas AIR, Menon DK. Changing patterns in the epidemiology of traumatic brain injury. Nat Rev Neurol. 2013 Apr;9(4):231–6.

13. Frost RB, Farrer TJ, Primosch M, Hedges DW. Prevalence of traumatic brain injury in the general adult population: a meta-analysis. Neuroepidemiology. 2013;40(3):154–9.

14. Thompson HJ, McCormick WC, Kagan SH. Traumatic Brain Injury in Older Adults: Epidemiology, Outcomes, and Future Implications. J Am Geriatr Soc [Internet]. 2006 Oct [cited 2024 Jul 17];54(10):1590. Available from: https://www.ncbi.nlm.nih.gov/pmc/articles/PMC2367127/

15. Taylor CA, Bell JM, Breiding MJ, Xu L. Traumatic Brain Injury-Related Emergency Department Visits, Hospitalizations, and Deaths - United States, 2007 and 2013. Morb Mortal Wkly Rep Surveill Summ Wash DC 2002. 2017 Mar 17;66(9):1–16.

16. Roozenbeek B, Chiu YL, Lingsma HF, Gerber LM, Steyerberg EW, Ghajar J, et al. Predicting 14-day mortality after severe traumatic brain injury: application of the IMPACT models in the brain trauma foundation TBI-trac® New York State database. J Neurotrauma. 2012 May 1;29(7):1306–12.

17. Maas A. Traumatic brain injury: Changing concepts and approaches. Chin J Traumatol Zhonghua Chuang Shang Za Zhi. 2016;19(1):3–6.

18. Hawryluk GWJ, Manley GT. Classification of traumatic brain injury: past, present, and future. Handb Clin Neurol. 2015;127:15–21.

19. The Glasgow Coma Scale at 40 years: standing the test of time - PubMed [Internet]. [cited 2024 Jul 16]. Available from: https://pubmed.ncbi.nlm.nih.gov/25030516/

20. Mckee AC, Daneshvar DH. The neuropathology of traumatic brain injury. Handb Clin Neurol. 2015;127:45–66.

21. Keating CE, Cullen DK. Mechanosensation in traumatic brain injury. Neurobiol Dis. 2021 Jan;148:105210.

22. Kaur P, Sharma S. Recent Advances in Pathophysiology of Traumatic Brain Injury. Curr Neuropharmacol. 2018;16(8):1224–38.

23. McAllister TW. Neurobiological consequences of traumatic brain injury. Dialogues Clin Neurosci. 2011;13(3):287–300.

24. Blennow K, Brody DL, Kochanek PM, Levin H, McKee A, Ribbers GM, et al. Traumatic brain injuries. Nat Rev Dis Primer. 2016 Nov 17;2:16084.

25. Alao T, Munakomi S, Waseem M. Penetrating Head Trauma. In: StatPearls [Internet]. Treasure Island (FL): StatPearls Publishing; 2024 [cited 2024 Jul 26]. Available from: http://www.ncbi.nlm.nih.gov/books/NBK459254/

26. McGinn MJ, Povlishock JT. Pathophysiology of Traumatic Brain Injury. Neurosurg Clin N Am. 2016 Oct;27(4):397–407.

27. Yan A, Torpey A, Morrisroe E, Andraous W, Costa A, Bergese S. Clinical Management in Traumatic Brain Injury. Biomedicines. 2024 Apr 2;12(4):781.

28. Meyfroidt G, Bouzat P, Casaer MP, Chesnut R, Hamada SR, Helbok R, et al. Management of moderate to severe traumatic brain injury: an update for the intensivist. Intensive Care Med. 2022 Jun;48(6):649–66.

29. Carney N, Totten AM, O'Reilly C, Ullman JS, Hawryluk GWJ, Bell MJ, et al. Guidelines for the Management of Severe Traumatic Brain Injury, Fourth Edition. Neurosurgery. 2017 Jan 1;80(1):6–15.

30. Buccilli B, Alan A, Baha' A, Shahzad A, Almealawy YF, Chisvo NS, et al. Neuroprotection strategies in traumatic brain injury: Studying the effectiveness of different clinical approaches. Surg Neurol Int. 2024;15:29.

31. Khan NA, Asim M, El-Menyar A, Biswas KH, Rizoli S, Al-Thani H. The evolving role of extracellular vesicles (exosomes) as biomarkers in traumatic brain injury: Clinical perspectives and therapeutic implications. Front Aging Neurosci. 2022;14:933434.

32. Chargaff E, West R. The biological significance of the thromboplastic protein of blood. J Biol Chem. 1946 Nov;166(1):189–97.

33. Wolf P. The nature and significance of platelet products in human plasma. Br J Haematol. 1967 May;13(3):269–88.

34. Nunez EA, Wallis J, Gershon MD. Secretory processes in follicular cells of the bat thyroid. 3. The occurrence of extracellular vesicles and colloid droplets during arousal from hibernation. Am J Anat. 1974 Oct;141(2):179–201.

35. Harding C, Heuser J, Stahl P. Receptor-mediated endocytosis of transferrin and recycling of the transferrin receptor in rat reticulocytes. J Cell Biol. 1983 Aug;97(2):329–39.

36. Pan BT, Johnstone RM. Fate of the transferrin receptor during maturation of sheep reticulocytes in vitro: selective externalization of the receptor. Cell. 1983 Jul;33(3):967–78.

37. Johnstone RM, Adam M, Hammond JR, Orr L, Turbide C. Vesicle formation during reticulocyte maturation. Association of plasma membrane activities with released vesicles (exosomes). J Biol Chem. 1987 Jul 5;262(19):9412–20.

38. Couch Y, Buzàs EI, Di Vizio D, Gho YS, Harrison P, Hill AF, et al. A brief history of nearly EV-erything - The rise and rise of extracellular vesicles. J Extracell Vesicles. 2021 Dec;10(14):e12144.

39. Vidal M. Exosomes: Revisiting their role as "garbage bags." Traffic Cph Den. 2019 Nov;20(11):815–28.

40. Valadi H, Ekström K, Bossios A, Sjöstrand M, Lee JJ, Lötvall JO. Exosome-mediated transfer of mRNAs and microRNAs is a novel mechanism of genetic exchange between cells. Nat Cell Biol. 2007 Jun;9(6):654–9.

41. Mondello S, Thelin EP, Shaw G, Salzet M, Visalli C, Cizkova D, et al. Extracellular vesicles: pathogenetic, diagnostic and therapeutic value in traumatic brain injury. Expert Rev Proteomics [Internet]. 2018 May 4 [cited 2020 Dec 8];15(5):451–61. Available from: https://doi.org/10.1080/14789450.2018.1464914

42. Kumar MA, Baba SK, Sadida HQ, Marzooqi SA, Jerobin J, Altemani FH, et al. Extracellular vesicles as tools and targets in therapy for diseases. Signal Transduct Target Ther. 2024 Feb 5;9(1):27.

43. Welsh JA, Goberdhan DCI, O'Driscoll L, Buzas EI, Blenkiron C, Bussolati B, et al. Minimal information for studies of extracellular vesicles (MISEV2023): From basic to advanced approaches. J Extracell Vesicles. 2024 Feb;13(2):e12404.

44. Bazzan E, Tinè M, Casara A, Biondini D, Semenzato U, Cocconcelli E, et al. Critical Review of the Evolution of Extracellular Vesicles' Knowledge: From 1946 to Today. Int J Mol Sci. 2021 Jun 15;22(12):6417.

45. Doyle LM, Wang MZ. Overview of Extracellular Vesicles, Their Origin, Composition, Purpose, and Methods for Exosome Isolation and Analysis. Cells [Internet]. 2019 Jul [cited 2020 Apr 15];8(7). Available from: https://www.ncbi.nlm.nih.gov/pmc/articles/PMC6678302/

46. Sheta M, Taha EA, Lu Y, Eguchi T. Extracellular Vesicles: New Classification and Tumor Immunosuppression. Biology. 2023 Jan 10;12(1):110.

47. Jeppesen DK, Zhang Q, Franklin JL, Coffey RJ. Extracellular vesicles and nanoparticles: emerging complexities. Trends Cell Biol. 2023 Aug;33(8):667–81.

48. Gurung S, Perocheau D, Touramanidou L, Baruteau J. The exosome journey: from biogenesis to uptake and intracellular signalling. Cell Commun Signal CCS. 2021 Apr 23;19(1):47.

49. Kalluri R, LeBleu VS. The biology, function, and biomedical applications of exosomes. Science. 2020 Feb 7;367(6478):eaau6977.

50. Krylova SV, Feng D. The Machinery of Exosomes: Biogenesis, Release, and Uptake. Int J Mol Sci. 2023 Jan 10;24(2):1337.

51. Lee YJ, Shin KJ, Chae YC. Regulation of cargo selection in exosome biogenesis and its biomedical applications in cancer. Exp Mol Med. 2024 Apr;56(4):877–89.

52. Sardar Sinha M, Ansell-Schultz A, Civitelli L, Hildesjö C, Larsson M, Lannfelt L, et al. Alzheimer's disease pathology propagation by exosomes containing toxic amyloid-beta oligomers. Acta Neuropathol (Berl). 2018 Jul;136(1):41–56.

53. Clancy JW, Schmidtmann M, D'Souza-Schorey C. The ins and outs of microvesicles. FASEB BioAdvances. 2021 Jun;3(6):399–406.

54. van Niel G, D'Angelo G, Raposo G. Shedding light on the cell biology of extracellular vesicles. Nat Rev Mol Cell Biol. 2018;19(4):213–28.

55. Tricarico C, Clancy J, D'Souza-Schorey C. Biology and biogenesis of shed microvesicles. Small GTPases. 2017 Feb;8(4):220–32.

56. Yu L, Zhu G, Zhang Z, Yu Y, Zeng L, Xu Z, et al. Apoptotic bodies: bioactive treasure left behind by the dying cells with robust diagnostic and therapeutic application potentials. J Nanobiotechnology. 2023 Jul 12;21(1):218.

57. Atkin-Smith GK, Poon IKH. Disassembly of the Dying: Mechanisms and Functions. Trends Cell Biol. 2017 Feb;27(2):151–62.

58. Li M, Liao L, Tian W. Extracellular Vesicles Derived From Apoptotic Cells: An Essential Link Between Death and Regeneration. Front Cell Dev Biol [Internet]. 2020 Oct 2 [cited 2024 Sep 27];8:573511. Available from: https://www.ncbi.nlm.nih.gov/pmc/articles/PMC7561711/

59. Gregory CD, Rimmer MP. Extracellular vesicles arising from apoptosis: forms, functions, and applications. J Pathol. 2023 Aug;260(5):592–608.

60. Jeppesen DK, Fenix AM, Franklin JL, Higginbotham JN, Zhang Q, Zimmerman LJ, et al. Reassessment of Exosome Composition. Cell. 2019 Apr 4;177(2):428-445.e18.

61. Xu J, Camfield R, Gorski SM. The interplay between exosomes and autophagy - partners in crime. J Cell Sci. 2018 Aug 3;131(15):jcs215210.

62. Wei W, Pan Y, Yang X, Chen Z, Heng Y, Yang B, et al. The Emerging Role of the Interaction of Extracellular Vesicle and Autophagy-Novel Insights into Neurological Disorders. J Inflamm Res. 2022;15:3395–407.

63. Filannino FM, Panaro MA, Benameur T, Pizzolorusso I, Porro C. Extracellular Vesicles in the Central Nervous System: A Novel Mechanism of Neuronal Cell Communication. Int J Mol Sci. 2024 Jan 28;25(3):1629.

64. Nekludov M, Mobarrez F, Gryth D, Bellander BM, Wallen H. Formation of microparticles in the injured brain of patients with severe isolated traumatic brain injury. J Neurotrauma. 2014;31(23):1927–33.

65. Hazelton I, Yates A, Dale A, Roodselaar J, Akbar N, Ruitenberg MJ, et al. Exacerbation of Acute Traumatic Brain Injury by Circulating Extracellular Vesicles. J Neurotrauma. 2018 Jan;

66. Kuharić J, Grabušić K, Tokmadžic VS, Štifter S, Tulić K, Shevchuk O, et al. Severe Traumatic Brain Injury Induces Early Changes in the Physical Properties and Protein Composition of Intracranial Extracellular Vesicles. J Neurotrauma. 2019;36(2).

67. Guedes VA, Devoto C, Leete J, Sass D, Acott JD, Mithani S, et al. Extracellular Vesicle Proteins and MicroRNAs as Biomarkers for Traumatic Brain Injury. Front Neurol [Internet]. 2020 Jul 16 [cited 2020 Oct 30];11. Available from: https://www.ncbi.nlm.nih.gov/pmc/articles/PMC7378746/

68. Lei J, Gao G, Feng J, Jin Y, Wang C, Mao Q, et al. Glial fibrillary acidic protein as a biomarker in severe traumatic brain injury patients: a prospective cohort study. Crit Care Lond Engl. 2015 Oct 12;19:362.

69. Flynn S, Leete J, Shahim P, Pattinson C, Guedes VA, Lai C, et al. Extracellular vesicle concentrations of glial fibrillary acidic protein and neurofilament light measured 1 year after traumatic brain injury. Sci Rep. 2021 Feb 16;11(1):3896.

70. Kumar A, Stoica BA, Loane DJ, Yang M, Abulwerdi G, Khan N, et al. Microglial-derived microparticles mediate neuroinflammation after traumatic brain injury. J Neuroinflammation. 2017 Mar 15;14(1):47.

71. Huang S, Ge X, Yu J, Han Z, Yin Z, Li Y, et al. Increased miR-124-3p in microglial exosomes following traumatic brain injury inhibits neuronal inflammation and contributes to neurite outgrowth via their transfer into neurons. FASEB J Off Publ Fed Am Soc Exp Biol. 2018 Jan;32(1):512–28.

72. Yang Y, Ye Y, Kong C, Su X, Zhang X, Bai W, et al. MiR-124 Enriched Exosomes Promoted the M2 Polarization of Microglia and Enhanced Hippocampus Neurogenesis After Traumatic Brain Injury by Inhibiting TLR4 Pathway. Neurochem Res. 2019 Apr;44(4):811–28.

73. Norman M, Ter-Ovanesyan D, Trieu W, Lazarovits R, Kowal EJK, Lee JH, et al. L1CAM is not associated with extracellular vesicles in human cerebrospinal fluid or plasma. Nat Methods [Internet]. 2021 Jun [cited 2021 Nov 2];18(6):631–4. Available from: https://www.nature.com/articles/s41592-021-01174-8

74. Gomes DE, Witwer KW. L1CAM-associated extracellular vesicles: A systematic review of nomenclature, sources, separation, and characterization. J Extracell Biol. 2022 Mar;1(3):e35.

75. Gandham S, Su X, Wood J, Nocera AL, Alli SC, Milane L, et al. Technologies and Standardization in Research on Extracellular Vesicles. Trends Biotechnol. 2020 Oct;38(10):1066–98.

76. Konoshenko MY, Lekchnov EA, Vlassov AV, Laktionov PP. Isolation of Extracellular Vesicles: General Methodologies and Latest Trends. BioMed Res Int. 2018;2018:8545347.

77. Sidhom K, Obi PO, Saleem A. A Review of Exosomal Isolation Methods: Is Size Exclusion Chromatography the Best Option? Int J Mol Sci. 2020 Sep 4;21(18).

78. Malenica M, Vukomanović M, Kurtjak M, Masciotti V, dal Zilio S, Greco S, et al. Perspectives of Microscopy Methods for Morphology Characterisation of Extracellular Vesicles from Human Biofluids. Biomedicines [Internet]. 2021 Jun [cited 2021 Jun 18];9(6):603. Available from: https://www.mdpi.com/2227-9059/9/6/603

79. Akbar A, Malekian F, Baghban N, Kodam SP, Ullah M. Methodologies to Isolate and Purify Clinical Grade Extracellular Vesicles for Medical Applications. Cells. 2022 Jan 6;11(2):186.

80. Dilsiz N. A comprehensive review on recent advances in exosome isolation and characterization: Toward clinical applications. Transl Oncol. 2024 Sep 14;50:102121.

81. Linares R, Tan S, Gounou C, Arraud N, Brisson AR. High-speed centrifugation induces aggregation of extracellular vesicles. J Extracell Vesicles. 2015;4:29509.

82. Liu WZ, Ma ZJ, Kang XW. Current status and outlook of advances in exosome isolation. Anal Bioanal Chem. 2022 Oct;414(24):7123–41.

83. J C, P L, T Z, Z X, X H, R W, et al. Review on Strategies and Technologies for Exosome Isolation and Purification. Front Bioeng Biotechnol [Internet]. 2022 Jan 5 [cited 2024 Oct 8];9. Available from: https://pubmed.ncbi.nlm.nih.gov/35071216/

84. Liangsupree T, Multia E, Riekkola ML. Modern isolation and separation techniques for extracellular vesicles. J Chromatogr A. 2021 Jan 11;1636:461773.

85. Yang D, Zhang W, Zhang H, Zhang F, Chen L, Ma L, et al. Progress, opportunity, and perspective on exosome isolation - efforts for efficient exosome-based theranostics. Theranostics. 2020;10(8):3684–707.

86. Yakubovich EI, Polischouk AG, Evtushenko VI. Principles and Problems of Exosome Isolation from Biological Fluids. Biochem Mosc Suppl Ser Membr Cell Biol. 2022;16(2):115–26.

87. Rupp AK, Rupp C, Keller S, Brase JC, Ehehalt R, Fogel M, et al. Loss of EpCAM expression in breast cancer derived serum exosomes: role of proteolytic cleavage. Gynecol Oncol. 2011 Aug;122(2):437–46.

88. Kangas P, Nyman TA, Metsähonkala L, Burns C, Tempest R, Williams T, et al. Towards optimised extracellular vesicle proteomics from cerebrospinal fluid. Sci Rep. 2023 Jun 12;13(1):9564.

89. Böing AN, van der Pol E, Grootemaat AE, Coumans FAW, Sturk A, Nieuwland R. Single-step isolation of extracellular vesicles by size-exclusion chromatography. J Extracell Vesicles. 2014;3(1):1–11.

90. Baranyai T, Herczeg K, Onódi Z, Voszka I, Módos K, Marton N, et al. Isolation of Exosomes from Blood Plasma: Qualitative and Quantitative Comparison of Ultracentrifugation and Size Exclusion Chromatography Methods. PLoS ONE [Internet]. 2015 Dec 21 [cited 2021 Nov 3];10(12):e0145686. Available from: https://www.ncbi.nlm.nih.gov/pmc/articles/PMC4686892/

91. Guo J, Wu C, Lin X, Zhou J, Zhang J, Zheng W, et al. Establishment of a simplified dichotomic size-exclusion chromatography for isolating extracellular vesicles toward clinical applications. J Extracell Vesicles [Internet]. 2021 [cited 2021 Nov 2];10(11):e12145. Available from: https://onlinelibrary.wiley.com/doi/abs/10.1002/jev2.12145

92. Ter-Ovanesyan D, Norman M, Lazarovits R, Trieu W, Lee JH, Church GM, et al. Framework for rapid comparison of extracellular vesicle isolation methods. eLife. 2021 Nov 16;10:e70725.

93. Brennan K, Martin K, FitzGerald SP, O'Sullivan J, Wu Y, Blanco A, et al. A comparison of methods for the isolation and separation of extracellular vesicles from protein and lipid particles in human serum. Sci Rep. 2020 Jan 23;10(1):1039.

94. Park S, Lee K, Park IB, Kim NH, Cho S, Rhee WJ, et al. The profiles of microRNAs from urinary extracellular vesicles (EVs) prepared by various isolation methods and their correlation with serum EV microRNAs. Diabetes Res Clin Pract. 2020 Feb;160:108010.

95. Monguió-Tortajada M, Gálvez-Montón C, Bayes-Genis A, Roura S, Borràs FE. Extracellular vesicle isolation methods: rising impact of size-exclusion chromatography. Cell Mol Life Sci CMLS. 2019 Jun;76(12):2369–82.

96. Gámez-Valero A, Monguió-Tortajada M, Carreras-Planella L, Franquesa M la, Beyer K, Borràs FE. Size-Exclusion Chromatography-based isolation minimally alters Extracellular Vesicles' characteristics compared to precipitating agents. Sci Rep. 2016 Sep 19;6:33641.

97. Sódar BW, Kittel Á, Pálóczi K, Vukman KV, Osteikoetxea X, Szabó-Taylor K, et al. Low-density lipoprotein mimics blood plasma-derived exosomes and microvesicles during isolation and detection. Sci Rep [Internet]. 2016;6(April):24316. Available from: http://www.nature.com/articles/srep24316

98. Lozano-Ramos I, Bancu I, Oliveira-Tercero A, Armengol MP, Menezes-Neto A, Del Portillo HA, et al. Size-exclusion chromatography-based enrichment of extracellular vesicles from urine samples. J Extracell Vesicles. 2015;4:27369.

99. Théry C, Witwer KW, Aikawa E, Alcaraz MJ, Anderson JD, Andriantsitohaina R, et al. Minimal information for studies of extracellular vesicles 2018 (MISEV2018): a position statement of the International Society for Extracellular Vesicles and update of the MISEV2014 guidelines. J Extracell Vesicles. 2018;7(1):1535750.

100. Bağcı C, Sever-Bahcekapili M, Belder N, Bennett APS, Erdener ŞE, Dalkara T. Overview of extracellular vesicle characterization techniques and introduction to combined reflectance and fluorescence confocal microscopy to distinguish extracellular vesicle subpopulations. Neurophotonics. 2022 Apr;9(2):021903.

101. Zhao Z, Wijerathne H, Godwin AK, Soper SA. Isolation and analysis methods of extracellular vesicles (EVs). Extracell Vesicles Circ Nucleic Acids. 2021;2:80–103.

102. Szatanek R, Baj-Krzyworzeka M, Zimoch J, Lekka M, Siedlar M, Baran J. The Methods of Choice for Extracellular Vesicles (EVs) Characterization. Int J Mol Sci. 2017 May 29;18(6).

103. Filipe V, Hawe A, Jiskoot W. Critical evaluation of Nanoparticle Tracking Analysis (NTA) by NanoSight for the measurement of nanoparticles and protein aggregates. Pharm Res. 2010 May;27(5):796–810.

104. Rupert DLM, Claudio V, Lässer C, Bally M. Methods for the physical characterization and quantification of extracellular vesicles in biological samples. Biochim Biophys Acta Gen Subj. 2017 Jan;1861(1 Pt A):3164–79.

105. Zhu J, Wu F, Li C, Mao J, Wang Y, Zhou X, et al. Application of Single Extracellular Vesicle Analysis Techniques. Int J Nanomedicine. 2023;18:5365–76.

106. Vogel R, Coumans FAW, Maltesen RG, Böing AN, Bonnington KE, Broekman ML, et al. A standardized method to determine the concentration of extracellular vesicles using tunable resistive pulse sensing. J Extracell Vesicles. 2016;5:31242.

107. Gross-Rother J, Blech M, Preis E, Bakowsky U, Garidel P. Particle Detection and Characterization for Biopharmaceutical Applications: Current Principles of Established and Alternative Techniques. Pharmaceutics. 2020 Nov 19;12(11):1112.

108. Maas SLN, de Vrij J, van der Vlist EJ, Geragousian B, van Bloois L, Mastrobattista E, et al. Possibilities and limitations of current technologies for quantification of biological extracellular vesicles and synthetic mimics. J Control Release Off J Control Release Soc. 2015 Feb 28;200:87–96.

109. Davidson SM, Boulanger CM, Aikawa E, Badimon L, Barile L, Binder CJ, et al. Methods for the identification and characterization of extracellular vesicles in cardiovascular studies: from exosomes to microvesicles. Cardiovasc Res. 2023 Mar 17;119(1):45–63.

110. Lötvall J, Hill AF, Hochberg F, Buzás EI, Di Vizio D, Gardiner C, et al. Minimal experimental requirements for definition of extracellular vesicles and their functions: a position statement from the International Society for Extracellular Vesicles. J Extracell Vesicles. 2014;3:26913.

111. Costa J, Pronto-Laborinho A, Pinto S, Gromicho M, Bonucci S, Tranfield E, et al. Investigating LGALS3BP/90 K glycoprotein in the cerebrospinal fluid of patients with neurological diseases. Sci Rep. 2020 Mar 27;10(1):5649.

112. Hermann S, Buschmann D, Kirchner B, Borrmann M, Brandes F, Kotschote S, et al. Transcriptomic profiling of cell-free and vesicular microRNAs from matched arterial and venous sera. J Extracell Vesicles. 2019;8(1):1670935.

113. Oeyen E, Van Mol K, Baggerman G, Willems H, Boonen K, Rolfo C, et al. Ultrafiltration and size exclusion chromatography combined with asymmetrical-flow field-flow fractionation for the isolation and characterisation of extracellular vesicles from urine. J Extracell Vesicles. 2018;7(1):1490143.

114. Aqrawi LA, Galtung HK, Vestad B, Øvstebø R, Thiede B, Rusthen S, et al. Identification of potential saliva and tear biomarkers in primary Sjögren's

syndrome, utilising the extraction of extracellular vesicles and proteomics analysis. Arthritis Res Ther. 2017 Jan 25;19(1):14.

115. Vaswani K, Mitchell MD, Holland OJ, Koh YQ, Hill RJ, Harb T, et al. A Method for the Isolation of Exosomes from Human and Bovine Milk. J Nutr Metab [Internet]. 2019 Dec 3 [cited 2024 Oct 26];2019:5764740. Available from: https://pmc.ncbi.nlm.nih.gov/articles/PMC6914892/

116. Hong CS, Funk S, Muller L, Boyiadzis M, Whiteside TL. Isolation of biologically active and morphologically intact exosomes from plasma of patients with cancer. J Extracell Vesicles. 2016;5:29289.

117. de Menezes-Neto A, Sáez MJF, Lozano-Ramos I, Segui-Barber J, Martin-Jaular L, Ullate JME, et al. Size-exclusion chromatography as a stand-alone methodology identifies novel markers in mass spectrometry analyses of plasma-derived vesicles from healthy individuals. J Extracell Vesicles. 2015;4:27378.

118. Smolarz M, Pietrowska M, Matysiak N, Mielańczyk Ł, Widłak P. Proteome Profiling of Exosomes Purified from a Small Amount of Human Serum: The Problem of Co-Purified Serum Components. Proteomes. 2019 Apr 28;7(2):18.

119. Gheinani AH, Vögeli M, Baumgartner U, Vassella E, Draeger A, Burkhard FC, et al. Improved isolation strategies to increase the yield and purity of human urinary exosomes for biomarker discovery. Sci Rep [Internet]. 2018 Mar 2 [cited 2024 Nov 3];8:3945. Available from: https://pmc.ncbi.nlm.nih.gov/articles/PMC5834546/

120. Wachalska M, Koppers-Lalic D, van Eijndhoven M, Pegtel M, Geldof AA, Lipinska AD, et al. Protein Complexes in Urine Interfere with Extracellular Vesicle Biomarker Studies. J Circ Biomark. 2016;5:4.

121. Foers AD, Chatfield S, Dagley LF, Scicluna BJ, Webb AI, Cheng L, et al. Enrichment of extracellular vesicles from human synovial fluid using size exclusion chromatography. J Extracell Vesicles. 2018;7(1):1490145.

122. Blans K, Hansen MS, Sørensen LV, Hvam ML, Howard KA, Möller A, et al. Pellet-free isolation of human and bovine milk extracellular vesicles by size-exclusion chromatography. J Extracell Vesicles. 2017;6(1):1294340.

123. Soares Martins T, Catita J, Martins Rosa I, A B da Cruz E Silva O, Henriques AG. Exosome isolation from distinct biofluids using precipitation and column-based approaches. PloS One. 2018;13(6):e0198820.

124. Welton JL, Loveless S, Stone T, von Ruhland C, Robertson NP, Clayton A. Cerebrospinal fluid extracellular vesicle enrichment for protein biomarker discovery in neurological disease; multiple sclerosis. J Extracell Vesicles. 2017;6(1):1369805.

125. O'leary RA, Nichol AD. Pathophysiology of severe traumatic brain injury. J Neurosurg Sci. 2018 Oct;62(5):542–8.

126. Charrin S, Jouannet S, Boucheix C, Rubinstein E. Tetraspanins at a glance. J Cell Sci [Internet]. 2014 Sep 1 [cited 2020 Mar 12];127(17):3641–8. Available from: https://jcs.biologists.org/content/127/17/3641

127. Nouvel J, Quevedo GB, Prinz T, Masood R, Daaboul G, Gainey-Schleicher T, et al. Separation of small extracellular vesicles (sEV) from human blood by Superose 6 size exclusion chromatography. J Extracell Vesicles. 2024 Oct;13(10):e70008.

128. Díaz Ludovico I, Powell SM, Many G, Bramer L, Sarkar S, Stratton K, et al. A fast and sensitive size-exclusion chromatography method for plasma extracellular vesicle proteomic analysis. Proteomics. 2024 Aug;24(16):e2400025.

129. Koch S, Donarski N, Goetze K, Kreckel M, Stuerenburg HJ, Buhmann C, et al. Characterization of four lipoprotein classes in human cerebrospinal fluid. J Lipid Res. 2001 Jul;42(7):1143–51.

130. Robertson JD, Rizzello L, Avila-Olias M, Gaitzsch J, Contini C, Magoń MS, et al. Purification of Nanoparticles by Size and Shape. Sci Rep. 2016 Jun 8;6:27494.

131. Veerman RE, Teeuwen L, Czarnewski P, Güclüler Akpinar G, Sandberg A, Cao X, et al. Molecular evaluation of five different isolation methods for extracellular vesicles reveals different clinical applicability and subcellular origin. J Extracell Vesicles. 2021 Jul;10(9):e12128.

ILLUSTRATIONS

LIST OF FIGURES

Figure 1. Typical biophysical mechanisms of traumatic brain injury.....5
Figure 2. External ventricular drainage (EVD) system.....8
Figure 3. Extracellular vesicles (EVs) biogenesis pathways.....12
Figure 4. An illustrated summary of commonly used EV isolation methods .18
Figure 5. Principle of size-exclusion chromatography-based EV isolation. ...24
Figure 6. Principle of tunable resistive pulse sensing (TRPS) measurements. 29
Figure 7. The main elements of Izon's qNano Gold instrument for TRPS measurement. 42
Figure 8. Western blot analysis of intracranial cerebrospinal fluid (CSF) collected during the first three days after severe traumatic brain injury (sTBI) revealed the presence of exosomes, albumin and lipoproteins in CSF. 48
Figure 9. Display of in-house size-exclusion chromatography (SEC) set-up for exosome isolation. 51
Figure 10. Free proteins and albumin co-elute in the same fractions after size-exclusive chromatography separation of the cerebrospinal fluid sample. 52
Figure 11. Nanoparticle-peak fraction is successfully detected by tunable resistive pulse sensing (TRPS) using both tested nanopores. 53
Figure 12. Four analysed size-exclusion chromatography (SEC) methods efficiently separate nanoparticles from soluble proteins in cerebrospinal fluid (CSF) sample. 57
Figure 13. The highest yield of total isolated nanoparticles was achieved using the Sepharose CL-6B filled size-exclusion chromatography (SEC) column. 58
Figure 14. Nanoparticles of similar size are isolated by all applied SEC methods. 60

Figure 15. The majority of SEC-isolated nanoparticles are negatively charged. 62

Figure 16. Exosome protein markers CD81 and CD9 are detected in nanoparticle-peak fraction, separate from lipoprotein markers and albumin. 64

Figure 17. Sepharose CL-6B efficiently separates exosomes from lipoproteins and albumin in cerebrospinal fluid from patients with severe TBI….66

LIST OF TABLES

Table 1. Glasgow coma scale. 4
Table 2. Chemicals used in this study. 34
Table 3. Reagents and materials used in this study. 37
Table 4. Antibodies used in this study. 38
Table 5. Clinical presentation of patients suffering from severe traumatic brain injury included in the study. 46
Table 6. Properties of different size exclusion chromatography (SEC) resin candidates for exosome isolation. 49
Table 7. Design and technical characteristics of four analysed gravity flow-based size-exclusion chromatography (SEC) methods used for the separation of cerebrospinal fluid sample from patients with severe traumatic brain injury. 55

LIST OF ABBREVIATIONS

Alix	ALG-2-interacting protein X
AFM	Atomic force microscopy
ApoAI	Apolipoprotein AI
ApoE	Apolipoprotein E
APS	Ammonium persulfate
ARF6	ADP ribosylation factor 6
CNS	Central nervous system
CS	Coating solution
CSF	Cerebrospinal fluid
CT	Computed tomography
DLS	Dynamic light scattering
dUC	Differential ultracentrifugation
ESCRT	Endosomal sorting complex required for transport
EVD	External ventricular drainage
EVs	Extracellular vesicles
Flot-1	Flotillin 1
GA	Glutaraldehyde
GCS	Glasgow coma scale
GFAP	Glial fibrillary acidic protein
GOS	Glasgow outcome scale
IA	Immunoaffinity
ICP	Intracranial pressure

ILVs	Intraluminal vesicles
ISEV	International Society for Extracellular Vesicles
L1CAM	L1 cell adhesion molecule
LDL	Low-density lipoproteins
LIMK1	LIM kinase 1
NTA	Nanoparticle tracking analysis
MWCO	Molecular weight cut-off
ME	Measuring electrolyte
MISEV	Minimal information for studies of extracellular vesicles
MVB	Multivesicular body
Nfl	Neurofilament light chain
PEG	Polyethylene glycol
PAGE	Polyacrylamide gel electrophoresis
PBS	Phosphate-buffered saline
PFA	Paraformaldehyde
ROCK1	Rho-associated protein kinase 1
SDS	Sodium dodecyl sulfate
SEC	Size exclusion chromatography
SEM	Scanning electron microscopy
TBI	Traumatic brain injury
TBS	Tris-buffered saline
TEM	Transmission elecrton microscopy
TEMED	N, N, N’, N’-Tetramethyl ethylenediamine
TRPS	Tunable resistive pulse sensing

UC	Ultracentrifugation
UCH-L1	Ubiquitin carboxyl-terminal hydrolase isozyme L1
UF	Ultrafiltration
VLDL	Very-low-density lipoproteins
WS	Washing solution

CURRICULUM VITAE

PERSONAL INFORMATION

Vedrana Krušić Alić, mag. biotech in med.

Date and place of birth: January 23rd, 1997, Rijeka, Croatia

Adress: Braće Cetina 2, 51000 Rijeka (Croatia) E-mail adress: vedrana.krusic@uniri.hr

Phone number: +385 91 7520409

WORK EXPERIENCE

[10 Sep 2020 – Current] **Research assistant**

Faculty of Medicine, University of Rijeka

— assistant on Coatian Science Foundation project "Identification of circulating biomarkers for neuro-recovery of brain-injured patients"" at Dpt. of Physiology, Pathophysiology and Immunology, Faculty of Medicine, Univeristy of Rijeka

Address: Braće Branchetta 20, Rijeka, Croatia

EDUCATION

[2020 – Current] **Doctoral study of Biomedicine**

Faculty of Medicine, University of Rijeka

Adress: Braće Branchetta 20, Rijeka, Croatia |

[2018 – 2020] **Master's degree, Biotechnology in medicine (summa cum laude)**

Department of Biotechnology and Drug Development (now Faculty of Biotechnology and Drug Development), University of Rijeka

Adress: Ul. Radmile Matejčić 2, 51000 Rijeka, Croatia |

[2015 – 2018] **Bachelor's degree, Biotechnology and drug research (summa cum laude)**

Department of Biotechnology and Drug Development (now Faculty of Biotechnology and Drug Development), University of Rijeka

Adress: Ul. Radmile Matejčić 2, 51000 Rijeka, Croatia |

[2011 – 2015] **Natural sciences and mathematics programme**

Gymnasium Andrije Mohorovičića Rijeka

Adress: Ulica Frana Kurelca 1, 51000, Rijeka, Croatia |

PUBLICATIONS

Scientific work from doctoral thesis topic:

[2022] **Krušić Alić V,** Malenica M, Biberić M, Zrna S, Valenčić L, Šuput A, Kalagac Fabris L, Wechtersbach K, Kojc N, Kurtjak M, Kučić N, Grabušić K. Extracellular Vesicles from Human Cerebrospinal Fluid Are Effectively Separated by Sepharose CL-6B-Comparison of Four Gravity-Flow Size Exclusion Chromatography Methods. Biomedicines. 2022 Mar 27;10(4):785.

Other original research articles:

[2023] Valenčić Seršić, L*, **Krušić Alić V***, Biberić M, Zrna S, Jagoić T, Tarčuković J, Grabušić K. Real-Time PCR Quantification of 87 miRNAs from Cerebrospinal Fluid: miRNA Dynamics and Association with Extracellular Vesicles after Severe Traumatic Brain Injury. Int J Mol Sci. 2023 Mar 1;24(5):4751.

[2022] Kurtjak M, Kereïche S, Klepac D, Križan H, Perčić M, **Krušić Alić V**, Lavrin T, Lenassi M, Wechtersbach K, Kojc N, Vukomanović M, Zrna S, Biberić M, Domitrović R, Grabušić K, Malenica M. Unveiling the Native Morphology of Extracellular Vesicles from Human Cerebrospinal Fluid by Atomic Force and Cryogenic Electron Microscopy. Biomedicines. 2022 May 27;10(6):1251.

[2021] Malenica M, Vukomanović M, Kurtjak M, Masciotti V, dal Zilio S, Greco S, Lazzarino M, **Krušić V**, Perčić M, Jelovica Badovinac I, Wechtersbach K, Vidović I, Baričević V, Valić S, Lučin P, Kojc N, Grabušić K. Perspectives of Microscopy Methods for Morphology Characterisation of Extracellular Vesicles from Human Biofluids. Biomedicines. 2021 May 26;9(6):603.

Other publications:

[2022] Grabušić K, **Krušić Alić V**. „Priručnik za analizu RNA“, Sveučilište u Rijeci, 2022

CONGRESSES AND MEETINGS

[2023] Zrna S, **Krušić Alić V**, Jagoić T, Biberić M, Tarčuković J, Grabušić K. „Superoxide disumutase mediated response to oxidative stress following severe traumatic brain injury“. June 2023, The European Anaesthesiology Congress: The Euroanaesthesia, Glasgow, Ireland.

[2023] Jagoić T, Zrna S, Valenčić Seršić L, **Krušić Alić V**, Bilić A, Biberić M, Tarčuković J, Grabušić K. „Growth Associated Protein 43 in the acute phase of recovery after severe traumatic brain injury“, 12th Student Congress of Neuroscience – NeuRi 2023. April 2022. Rijeka-Rab, Croatia.

[2022] **Krušić Alić V**, Biberić M, Zrna S, Valenčić L, Malenica M, Kalagac Fabris L, Šuput A, Grabušić K. „Evaluation of four size-exclusion chromatographies to separate extracellular vesicles from human intracranial cerebrospinal fluid“. International Society for Extracellular Vesicles Annual Meeting. May 2022, Lyon, France.

[2022] **Krušić Alić V**, Valenčić L, Zrna S, Biberić M, Jagoić T, Tarčuković J, Grabušić K. „Identification of microRNA cargo of extracellular vesicles“; 3rd Regional Congress of Physiological Societies and 5th Congress of Croatian Physiological Society. September 2022, Plitivička Jezera, Croatia.

[2022] Jagoić T, **Krušić Alić V**, Zrna S, Biberić M, Valenčić L, Grabušić K. „Antioxidative enzymes from cerebrospinal fluid as protein biomarkers of neurorecovery in patients with severe traumatic brain injury“. 11th Student Congress of Neuroscience – NeuRi 2022. April 2022. Rijeka-Rab, Croatia.

[2021] **Krušić V**, Biberić M, Zrna S, Valenčić L, Malenica M, Kalagac Fabris L, Šuput A, Grabušić K. „Size-exclusion chromatography based separation of extracellular vesicles from cerebrospinal fluid of severe traumatic brain injury patients“. 15th Annual Meeting of Croatian Physiological Society with International Participation, October 2021, Zagreb, Croatia.

[2021] Vidović I, Perčić M, **Krušić V**, Grabušić K, Malenica M. Nanotechnology-based quantifications of nanoparticles from human cerebrospinal fluid: comparison of Atomic Force Microscopy and Tunable Resistive Pulse Sensing, 10th Student Congress of Neuroscience – NeuRi 2022April 2021, Rijeka-Rab, Croatia.

[2020] **Krušić V**, Biberić M, Zrna S, Valenčić L, Malenica M, Kalagac Fabris L, Šuput A, Grabušić K. Size-exclusion chromatography based separation of extracellular vesicles from cerebrospinal fluid of severe traumatic brain injury patients, 14th Annual Meeting of Croatian Physiological Society with International Participation, September 2020, “online” MS Teams

COURSES

[Oct 2022] **Course on Transmission electron microscopy**, Faculty of Medicine, University of Rijeka

HONOURS AND AWARDS

University of Rijeka

Rector's award for excellence in academic year 2019/2020

Department of Biotechnology, University of Rijeka

Class of 2017/2018 Undergraduate Valedictorian

University of Rijeka

Scholarship for Excellence in academic years 2015/2016, 2016/2017, 2017/2018, 2018/2019 and 2019/2020

LANGUAGE SKILLS

Mother tongue(s): CROATIAN

Other language(s):

ENGLISH (C1) GERMAN (A2)

VOLONTEERING AND STUDENT ACTIVITIES

[ACADEMIC YEARS 2018/19 AND 2019/2020]

Student demonstrator, Department of Biotechnology, University of Rijeka, course of Physical chemistry

[ACADEMIC YEARS 2017/18 AND 2018/19]

Volunteer on The day of open doors of University of Rijeka, Department of Biotechnology
- Workshop "Šarenilo kemije"

[ACADEMIC YEAR 2017/18]

Student demonstrator, Department of Biotechnology, University of Rijeka, course of Bioactive Components of Mediterranean Diet

[AUG 2016 – DEC 2016]

Active participation in the project "Putujući znanstvenici" of the student association USBRi